

5/16/79 19 Johnston File advg

Chief, Fuel Behavior Research Branch  
Division of Reactor Safety Research  
U.S. Nuclear Regulatory Commission  
Washington, D.C. 20555

NUREG/CR-0220  
PNL-2692

SPECIAL FOURTH CLASS RATE - BOOKS

54-1900-035 (3-78)

at ins qs  
of  
6-12-79.

---

## Manifestations of Nonlinearity in Fuel Center Thermocouple Steady-State and Transient Data: Implications for Data Analysis

D. D. Lanning  
B. O. Barnes  
R. E. Williford

---

January 1979

Prepared for  
the U.S. Nuclear Regulatory Commission

Pacific Northwest Laboratory  
Operated for the U.S. Department of Energy  
by Battelle Memorial Institute

 **Battelle**

PNL-2692

7906020097

NOTICE

This report was prepared as an account of work sponsored by the United States Government. Neither the United States nor the United States Nuclear Regulatory Commission, nor any of their employees, nor any of their contractors, subcontractors, or their employees, makes any warranty, express or implied, or assumes any legal liability or responsibility for the accuracy, completeness or usefulness of any information, apparatus, product or process disclosed, or represents that its use would not infringe privately owned rights.

PACIFIC NORTHWEST LABORATORY  
operated by  
BATTELLE  
for the  
UNITED STATES DEPARTMENT OF ENERGY  
Under Contract EY-76-C-06-1830

Printed in the United States of America  
Available from  
National Technical Information Service  
United States Department of Commerce  
5285 Port Royal Road  
Springfield, Virginia 22151  
Price: Printed Copy \$ \_\_\_\_\*; Microfiche \$3.00

*Pages	NTIS Selling Price
001-025	\$4.00
026-050	\$4.50
051-075	\$5.25
076-100	\$6.00
101-125	\$6.50
126-150	\$7.25
151-175	\$8.00
176-200	\$9.00
201-225	\$9.25
226-250	\$9.50
251-275	\$10.75
276-300	\$11.00

MANIFESTATIONS OF NONLINEARITY IN FUEL CENTER  
THERMOCOUPLE STEADY-STATE AND TRANSIENT DATA:  
IMPLICATIONS FOR DATA ANALYSIS

D. D. Lanning  
B. O. Barnes  
R. E. Williford

Prepared for the  
Nuclear Regulatory Commission

Fin No. B-2043

January 1979

Pacific Northwest Laboratory  
Richland, Washington 99352

### ACKNOWLEDGMENTS

The authors wish to acknowledge support from the Fuel Behavior Research Branch (Division of Reactor Safety Research) Nuclear Regulatory Commission (NRC). The comments from Mr. Harold Scott of that branch were helpful.

Mr. J. A. Christensen and Mr. R. W. Miller, NRC representatives at the Halden Reactor, helped in the collecting of the transient data. We are also grateful to the Halden staff for their cooperation in the production of required power decreases and the recording of data at the required high frequency.

Dr. B. A. Scheffler of the Joint Center for Graduate Study (Richland, WA) reviewed the derivation presented in Appendix A.

## SUMMARY AND RECOMMENDATIONS

This report deals with the interpretation and verification of fuel centerline thermocouple data. Two new concepts are discussed along with their application to in-reactor data from IFA-432, a heavily instrumented six-rod Halden reactor test assembly sponsored by the Nuclear Regulatory Commission.

The main ideas presented in this report are that;

- it is more useful to plot resistance versus power than simply to plot temperature versus power. The resistance is defined as the relative centerline temperature (above coolant) divided by the local power.
- the response of the centerline temperature to a linear power decrease is correlated to the rod's current resistance-vs-power behavior. Thus, the resistance-vs-power measurement can be verified by performing a linear power decrease and by plotting the temperature response.

As explained in the text, plots of resistance vs power magnify the nonlinearities in the relationship between fuel temperature and power. These nonlinearities arise from the temperature dependence of the material properties, and from the temperature-dependent feedback between fuel temperatures and fuel-to-cladding thermal conductance. It is recommended that resistance-vs-power plots be used to make definitive comparisons between fuel temperature data and predictive computer codes. Departures of predicted temperatures from measured temperatures then could be identified, quantified and explained in terms of the code's own parameters.

Further experimental and analytical work must be done to extend and refine the ideas presented here. On the experimental side, temperature-vs-power relationships must be defined with higher densities of data at powers other than 100% of full power. More refinement of the linear power decrease is also desirable. On the analytical side, more detailed exploration into the causes of manifested system nonlinearity will lead to better insight into the true modes of heat transfer within a fuel rod.

## CONTENTS

SUMMARY AND RECOMMENDATIONS . . . . .	iii
LIST OF FIGURES . . . . .	vii
LIST OF TABLES . . . . .	xi
INTRODUCTION . . . . .	1
BASIC IDEAS AND SAMPLE DATA ANALYSIS . . . . .	3
BASIC IDEAS . . . . .	3
EXAMPLE OF DATA ANALYSIS . . . . .	14
DATA ANALYSIS FOR IFA-432 RODS . . . . .	22
DESCRIPTION OF ASSEMBLY . . . . .	22
BEGINNING-OF-LIFE DATA . . . . .	25
LIFE HISTORIES OF THE RODS . . . . .	33
Rod 1 . . . . .	36
Rod 2 . . . . .	43
Rod 3 . . . . .	54
Rod 6 . . . . .	60
APPENDIX A - ANALYTICAL BASIS FOR THE OBSERVED CORRELATION BETWEEN RESISTANCE PLOTS AND TEMPERATURE/POWER SLOPE RATIOS . . . . .	A-1
A1.0 REVIEW OF SOLUTIONS FOR STEADY STATE AND TRANSIENT TEMPERATURES, ASSUMING CONSTANT PROPERTIES AND BOUNDARY CONDITIONS . . . . .	A-3
A2.0 TEMPERATURE/POWER SLOPE BEHAVIOR FOR FIXED CONDUCTANCE AND TEMPERATURE DEPENDENT CONDUCTIVITY . . . . .	A-17
A3.0 TEMPERATURE/POWER SLOPE BEHAVIOR WITH FIXED CONDUCTIVITY AND TEMPERATURE DEPENDENT CONDUCTANCE . . . . .	A-25

A4.0 APPLICATION OF THE CORRELATION TO DETECTING ERRORS IN POWER AND TEMPERATURE ESTIMATES . . . . .	A-35
APPENDIX B - CALCULATIONAL PROCEDURES FOR PRODUCING TEMPERATURE/ POWER SLOPE ESTIMATES FROM CALCULATED R-P CURVES . . . . .	B-1
GENERAL PROCEDURE . . . . .	B-1
THE SOLUTION ROUTINE MWRAM . . . . .	B-2
REFERENCES . . . . .	B-5

## FIGURES

1	Plot of Combinations of Major Variables Which will Result in a Calculated Centerline Temperature of 1320°C at 8.3 KW/ft ( $2.72 \times 10^4$ W/m) for a 0.01068 m Diameter 10% Enriched UO <sub>2</sub> Solid Pellet . . . . .	4
2	(a) Hypothetical Plot of Fuel Temperature vs. Power (b) Same Data in Resistance Form, Showing the Definite Nonlinear Trend . . . . .	5
3	(a) Temperature vs. Power for Two Hypothetical Rods Having Different Gap Conditions but Similar Centerline Temperatures at Full Power (b) The Same Curves Translated to Resistance Form . . . . .	7
4	Components of the Total Centerline-to-Coolant Thermal Resistance for the Two Rods Described in Figure 3 . . . . .	9
5	Temperature vs. Time for a Linear Power Decrease, for the Two Reference Rods . . . . .	11
6	Normalized Temperature and Power vs. Time for a Linear Power Decrease for the Two Reference Rods . . . . .	13
7	Data Scatter for Rod 1, IFA-432 at 14,000 MWd/MTM Burnup, and Various Calculated R vs. P responses Using GAPCON-3 . . . . .	17
8	Normalized Power and Temperature Data from Rod 1, IFA-432 at 14,000 MWd/MTM Rod-Averaged Burnup . . . . .	18
9	Data and Calculated Normalized Temperatures vs. Time for the First 3 Cases in Figure 7 . . . . .	19
10	Data and Calculated Normalized Temperatures for the Last Three Cases in Figure 7 . . . . .	20
11	The Shaded Area Represents the Narrowed Range of Possibilities for Rod 1 at 14,000 MWd/MTM Burnup, Based on R-P and Transient Data Analysis . . . . .	21
12	Schematic of Instrumented Fuel Assembly---IFA-432 . . . . .	23
13	Beginning of Life R-P Data Trends for the Helium-Filled Rods in IFA-432 . . . . .	26
14	Beginning of Life R-P Data Trends for the Upper Thermocouples of Rods 1, 5 and 6 . . . . .	27

15	Beginning-of-Life R-P Data Trends for the Upper and Lower Thermocouples in Rod 4 . . . . .	28
16	Calculated Response of Rods 1, 3, and 4 to a Hypothetical Linear Power Decrease of 0.67%/sec from $\sim 3.0 \times 10^4$ W/m . . . . .	29
17	Response of Rods 1, 2, and 3 to a Beginning-of-Life Linear Power Decrease . . . . .	31
18	Response of Upper and Lower Ends of Rod 4 to Beginning-of-Life Power Decrease . . . . .	32
19	Run 31 Response of Rod 5 . . . . .	34
20	Run 31 Response of Rod 6 . . . . .	35
21	Resistance-Power Data Trends for Rod 1 . . . . .	37
22	Calculated R-P Curves for Rod 1 at 0 Gj/kgU Burnup. . . . .	39
23	Data and Calculated R-P Response for Rod 1 at 121 Gj/kgU . . . . .	39
24	Data and Calculated R-P Response for Rod 1 at 450 Gj/kgU Burnup . . . . .	40
25	Data and Calculated R-P Response for Rod 1 at 690 Gj/kgU . . . . .	40
26	Data and Calculated R-P Responses for Rod 1 at 920 Gj/kgU Burnup . . . . .	41
27	Data and Calculated R-P Response for Rod 1 at 1100 Gj/kgU Burnup . . . . .	41
28	Calculated R-P Responses for Rod 1 at 1200 Gj/kgU Burnup . . . . .	42
29	Estimated Life History for Rod 1 . . . . .	44
30	Resistance vs. Power Data Trends for Rod 2 . . . . .	45
31	R-P Calculated Responses for Rod 2 at 0 Gj/kgU . . . . .	47
32	Data and Calculated R-P Responses for Rod 2 at 121 Gj/kgU . . . . .	48
33	Data and Calculated R-P Responses for Rod 2 at 450 Gj/kgU . . . . .	49
34	Data and Calculated R-P Responses for Rod 2 at 690 Gj/kgU Burnup . . . . .	50

35	Data and Calculated R-P Responses for Rod 2 and 920 Gj/kgU . . . . .	51
36	Data and Calculated R-P Responses for Rod 2 at 1100 Gj/kgU . . . . .	52
37	Data and Calculated R-P Responses for Rod 2 at 1200 Gj/kgU . . . . .	53
38	Estimated Life History of Rod 2, IFA-432. . . . .	55
39	Resistance vs. Burnup for Rod 3, IFA-432. . . . .	56
40	Data for Rod 3, IFA-432 . . . . .	58
41	Data and Calculated R-P Responses for Rod 3 at 0 Gj/kgU . . . . .	59
42	Data and Calculated R-P Responses for Rod 3 at 1200 Gj/kgU Burnup . . . . .	59
43	R-P Data Trends for Rod 6, IFA-432 . . . . .	61
44	Trends of Ex-Reactor Data for Rod 1 and Rod 6 Fuel Conductivity . . . . .	63
45	Data and Calculated R-P Responses for Rod 6, IFA-432 at 0 Gj/kgU Burnup . . . . .	64
46	Data and Calculated R-P Responses for Rod 6 at 0 Gj/kgU Burnup . . . . .	64
47	Data and Calculated R-P Responses for Rod 6 at 121 Gj/kgU . . . . .	65
48	Data and Calculated R-P Responses for Rod 6 at 450 Gj/kgU . . . . .	65
49	Data and Calculated R-P Responses for Rod 6 at 690 Gj/kgU . . . . .	66
50	Data and Calculated R-P Responses for Rod 6 at 900 Gj/kgU . . . . .	67
51	Data and Calculated R-P Responses for Rod 6 and 1100 Gj/kgU . . . . .	68
52	Data and Calculated R-P Responses for Rod 6 at 1200 Gj/kgU . . . . .	69
53	Estimated Life History for Rod 6, IFA-432 . . . . .	70
A-1	Idealized Linear Power Decrease . . . . .	A-3
A-2	Relative Variation of $UO_2$ Heat Capacity and Conductivity . . . . .	A-18
A-3	Plot of $G(0)$ at a Function of Temperature . . . . .	A-24
A-4	Calibration Curve for a W-26% Re/W-5% Re Thermocouple . . . . .	A-36

TABLES

1	Measured and Calculated Temperature/Power Slope Ratios . . . . .	16
2	Description of IFA-432 Rods . . . . .	24
3	Expected Thermocouple Response to to Linear Power Decrease . . . . .	33
4	Power Drop Dates and Identity . . . . .	36
5	Data for Temperature/Power Slope Ratios . . . . .	38
6	Data and Calculations for Temperature/Power Slope Ratio from Linear Power Decreases for Rod 1, Lower Thermocouple . . . . .	43
7	Rod 2 Data for Temperature/Power Slope Ratios . . . . .	54
8	Measured and Calculated Temperature/Power Slope Ratios for Rod 2 . . . . .	55
9	Measured and Calculated Temperature/Power Slope Ratios for Rod 3 . . . . .	58
10	Measured Temperature/Power Slope Ratios for Rod 6 . . . . .	60
11	Calculated Temperature/Power Slope Ratios for Rod 6, Lower Thermocouple . . . . .	66

MANIFESTATIONS OF NONLINEARITY IN FUEL CENTER THERMOCOUPLE  
STEADY-STATE AND TRANSIENT DATA: IMPLICATIONS FOR DATA ANALYSIS

INTRODUCTION

Measurements of in-reactor fuel centerline temperature have been taken in various experimental reactors for many years. These measurements generally have been taken to assess the effect of different design parameters and operating history on the heat transfer within a fuel rod. The data is used to verify fuel modeling computer codes. A problem with comparing computer codes to centerline temperature data is the number of parameters (gap size, gas composition, fuel conductivity, etc.) that can be combined in various ways to explain the same set of power-temperature data. This report shows that the nonlinear character of a fuel rod can be used to reduce the possible combinations.

The nonlinearity arises from the temperature dependence of the thermal properties of the materials in the fuel rod, and from the temperature-dependent feedback between effective gap size and fuel temperature. We have found a certain way of plotting the steady-state centerline temperature data to magnify the manifestation of these nonlinearities. For calculated temperatures these plots become characteristic of the particular combinations of fill gas composition, gap size, etc. that are chosen.

The time-varying thermocouple response to linear power decreases has been plotted; it is used to crosscheck the steady-state data. Calculated transient temperatures, plotted in this way, are at least as sensitive to various combinations of gas composition, gap size, etc. as the steady-state temperatures.

Several examples of actual data taken from the USNRC/PNL Halden reactor six-rod assembly, IFA-432, include rod-to-rod comparisons and data trends throughout the life of individual rods. The transient temperatures confirm the steady-state measurements and trends.

## BASIC IDEAS AND SAMPLE DATA ANALYSIS

This section describes the method and rationale for the form of temperature/power data plots which we have found to be particularly definitive. The basic ideas and sample plots are given for both steady-state and time-varying data. Sample calculations under various assumptions are shown to emphasize the definitive nature of the plots.

### BASIC IDEAS

The fuel rod, from a dynamic analysis viewpoint, is a nonlinear system; that is, the transfer function between temperature (output) and power (input) is itself dependent on the power level. This is actually of great benefit, because the nature of the nonlinearities coupled with the absolute values of the transfer function are characteristic of specific combinations of the three major determinants of centerline temperature at a given power: fuel conductivity, gap gas composition, and effective hot gap size.

The three dimensional plot in Figure 1 emphasizes the need for such discrimination. The axes are:

- The % helium in the fill gas (the remainder being fission gas).
- The gap size (expressed as fuel relocation).
- The fuel conductivity (expressed as % deviation from standard  $UO_2$  conductivity).

The surface in this parameter space represents many simultaneous combinations, all of which could match a given temperature/power target data point in a particular calculational scheme. Figure 1 was prepared using the GAPCON-THERMAL-3<sup>(1)</sup> fuel modeling program; but a similar figure could be produced using any fuel modeling code.

The multitudinous possibilities noted in Figure 1 can be narrowed down somewhat by plotting the steady-state temperature/power data in a certain way. Rather than simply plotting the temperature vs. power, let us plot resistance vs. power. The resistance,  $R$ , is defined as

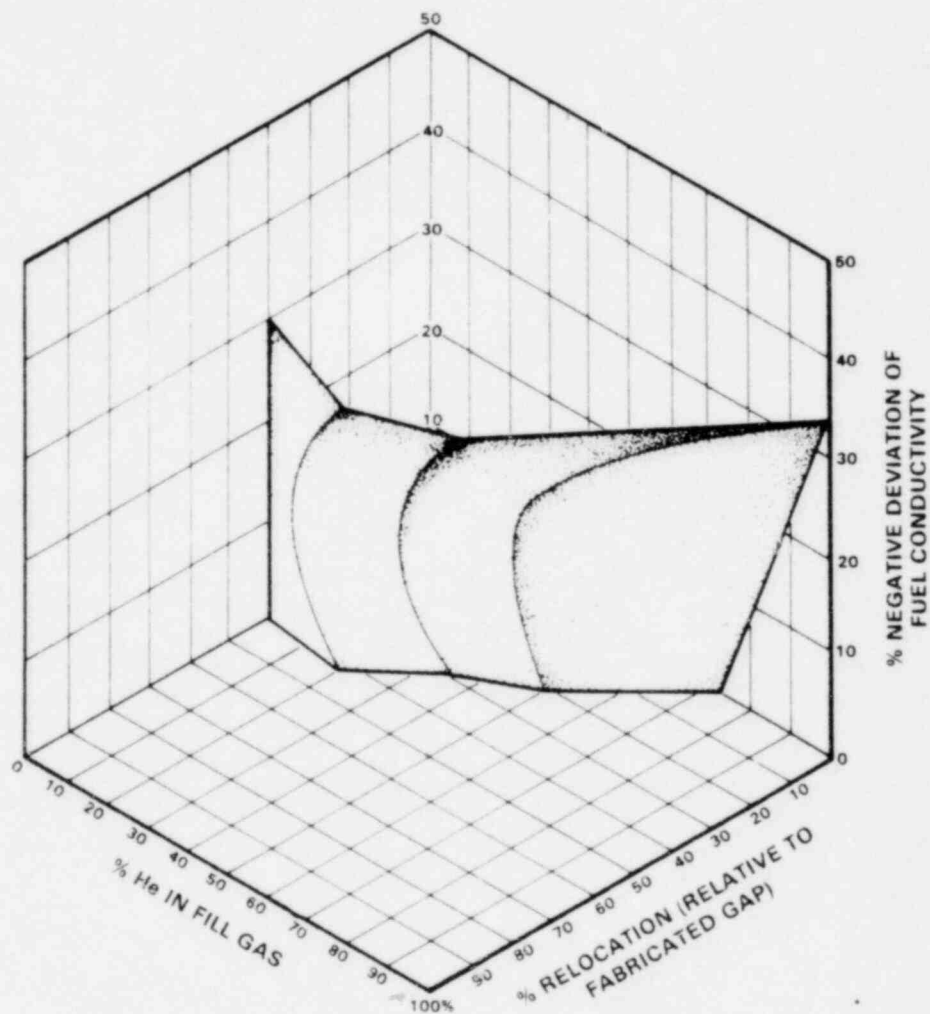


FIGURE 1. Plot of Combinations of Major Variables Which will Result in a Calculated Centerline Temperature of 1320°C at 8.3 KW/ft ( $2.72 \times 10^4$  W/m) for a 0.01068 m Diameter, 10% Enriched UO<sub>2</sub> Solid Pellet. Every point on the surface will hit the target temperature/power point.

$$R = \frac{T_{\text{center}} - T_{\text{coolant}}}{\text{Power}} = T_r/P$$

where  $T_r$  is the relative temperature, i.e., the temperature above coolant.

Figure 2 illustrates the reason for choosing this parameter. In 2a we show scattered points typical of collected temperature and power data. It is not immediately obvious in 2a whether the data is indicating a linear trend of temperature vs. power. In 2b the same data was plotted in resistance form, and it is immediately obvious that the data is showing a non-linear trend; if it were totally linear, the resistance would be constant as a function of power.

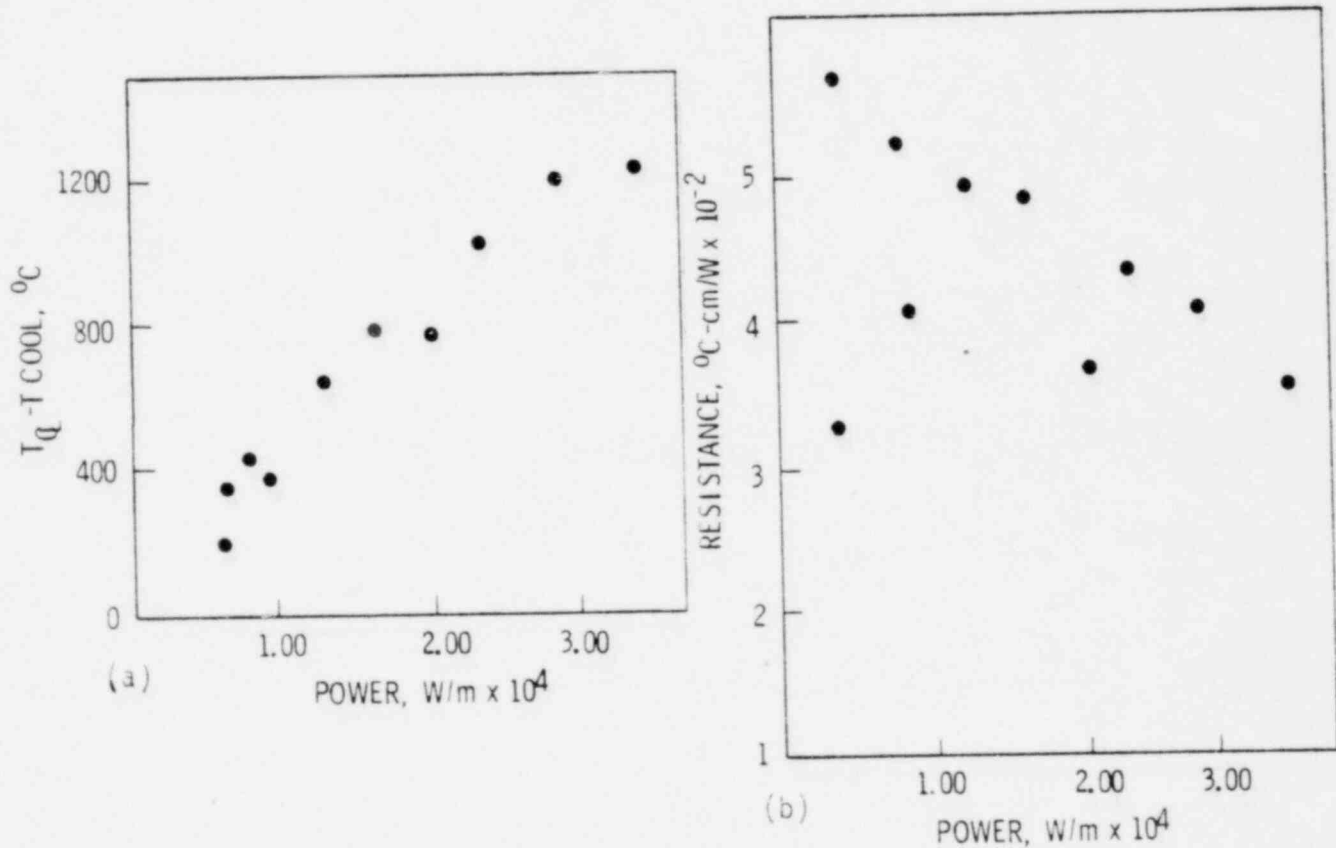


FIGURE 2. (a) Hypothetical Plot of Fuel Temperature vs. Power  
 (b) Same Data in Resistance Form, Showing the Definite Nonlinear Trend

The sensitivity of the resistance to the nonlinear trend of temperature vs. power makes it extremely useful in plotting the sparse and scattered data that is usually available. This sensitivity can be understood analytically by assuming that the power dependence of the relative temperature is the sum of a dominant linear term and a small nonlinear term, e.g.,

$$T_r = aP + bP^2, \text{ where } aP \gg bP^2.$$

Upon dividing by power (P), we have

$$T_r/P = R = a + bP$$

So a plot of R vs. P relegates the linear power dependence of temperature to an intercept and allows the eye to focus on the nonlinear terms.

These nonlinear terms are the ones which are most significant in determining the nature of the fuel rod heat transfer.<sup>(a)</sup> Two extreme cases emphasize this: (1) a small-gap rod with helium plus fission gas in the gap (and thus a degraded gas conductivity with respect to pure helium) and (2) a large-gap rod with pure helium in the gap. Suppose both rods have approximately the same centerline temperature at full power. Figure 3a is a plot of the calculated temperature vs. power; the major GAPCON-3 input variables used for the plot are noted on the figure. In Figure 3b, the same temperatures are plotted in resistance form. The difference between the two situations is distinguishable in the full power range in Figure 3b; but the difference is even more dramatic in Figure 3b. If, instead of calculated curves, we looked at scattered temperature data points, we probably could not say which of the two extreme cases is prevailing, based on a temperature vs. power plot. But the resistance versus power plot would allow us to make some inference about which extreme is more likely.

---

(a) Nonlinear dependence on power arises from the temperature dependence of the thermal properties. The basic heat transfer equations would predict proportionality between relative temperature and power if the conductivities and boundary conditions were not temperature dependent.

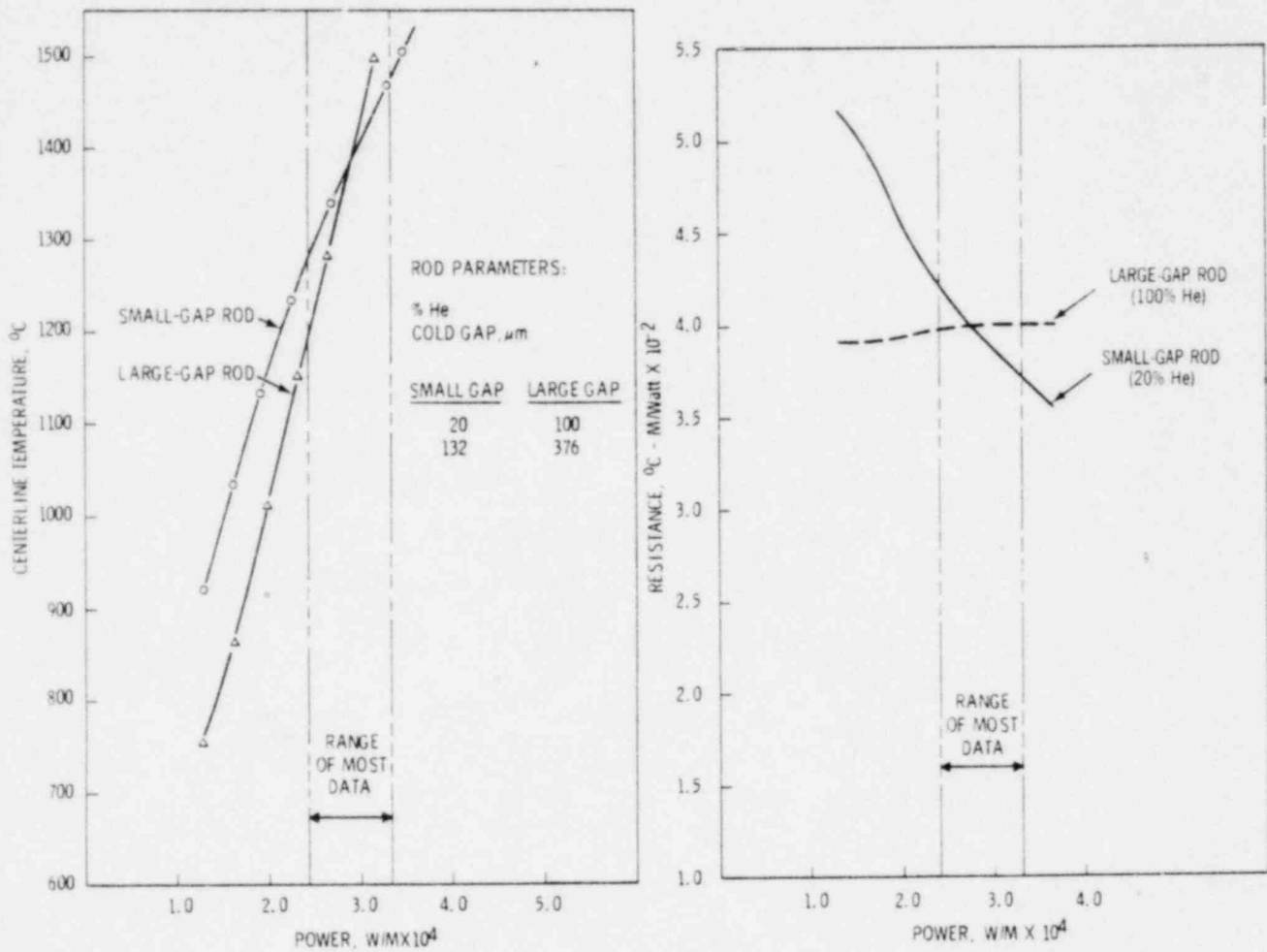


FIGURE 3. (a) Temperature vs. Power for Two Hypothetical Rods Having Different Gap Conditions but Similar Centerline Temperatures at Full Power  
(b) The Same Curves Translated to Resistance Form

The reason for the difference in the resistance curves (Figure 3b) may be understood by taking them apart. The total resistance from centerline to coolant may be thought of as a sum of a series of resistances:

- The resistance from coolant to cladding inner radius (cladding inner temperature minus coolant temperature, divided by power)
- The resistance across the gap (fuel surface temperature minus cladding inner temperature, divided by power)
- The fuel resistance (fuel centerline temperature minus fuel surface temperature, divided by power)

The first of these resistances is small and fairly constant as a function of local power. The gap resistance tends to decrease with power (due to gap closure from differential thermal expansion). The fuel resistance tends to increase with power (due to increasing fuel temperatures, which lower the thermal conductivity.)

The calculated resistance components are shown in Figure 4, for both of the situations discussed previously. The cladding resistance is, of course, identical for both rods; and the fuel resistances are similar since the fuel temperatures are similar. But the gap resistances are markedly different as a function of power. The smaller gap rod has a gap resistance decreasing in absolute value much more rapidly as a function of power, for two reasons: 1) the fractional change in gap size is greater; 2) the absolute value of the gap resistance at lower powers is much greater, owing to the degraded conductivity of the gas in this rod. In the small gap rod, the decrease in gap resistance more than compensates for the increasing fuel resistance, causing the decreasing total resistance observed in Figure 3b. The large-gap, He-filled rod, however, experiences a gap resistance decrease that is *less* than the fuel resistance increase which results in the slight net increase shown in Figure 3b.

Thus, the observation of how total resistance changes as a function of power gives some indication as to the split in total resistance between the fuel and the gap and, thus, some indication as to the gap condition (i.e., effective gap size and gas composition). Of course, to quantify the gap conditions, one must assume a knowledge of the fuel conductivity; but, conversely, if the gap is firmly closed and the gap conductance is considered well known, the R-P plot can yield some inferred values of effective fuel conductivity. For cases where neither the fuel conductivity nor the gap conductance are well known, some ambiguity still exists. As we shall see later, in that case a simultaneous statement of fuel conductivity, fuel relocation, and % He in the gas cannot be made closer than  $\pm 15\%$  for any one of the three. But this is still a considerable improvement over the approximate range of  $\pm 30\%$  that is possible from a simple consideration of temperature (Figure 1).

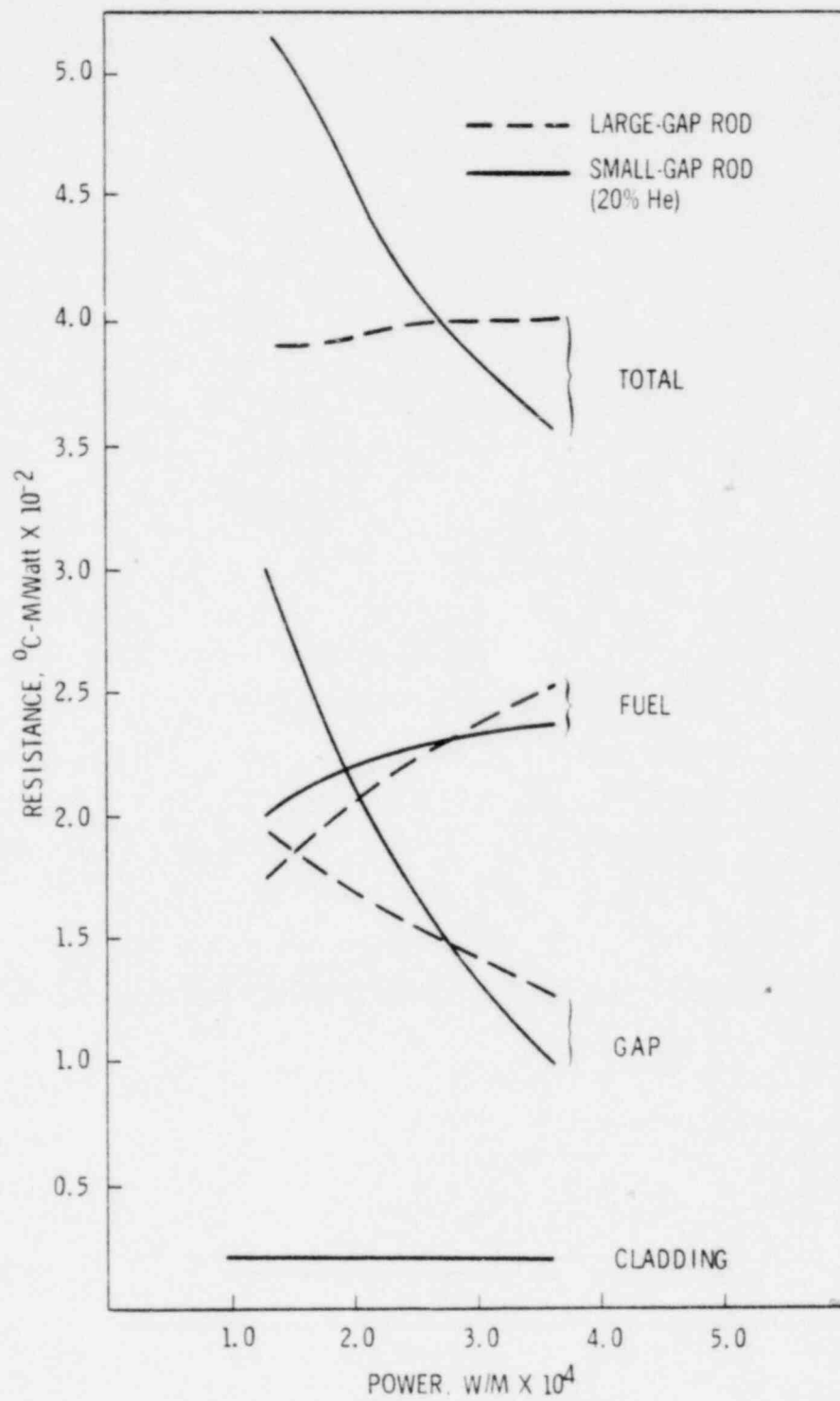


FIGURE 4. Components of the Total Centerline-to-Coolant Thermal Resistance for the Two Rods Described in Figure 3

However, we still have no independent way of knowing whether there is significant absolute bias in the "measured" temperature and power. Significant bias is possible in either the temperature or the power measurement due to several sources.

These sources of uncertainty are discussed in Reference 2, where it was concluded that probable uncertainties for temperature and local power for IFA-431 were 3% and 5.6%, respectively. Although IFA-431 was identical in design to IFA-432, the foregoing uncertainties must be viewed as *minimum* values for IFA-432, primarily because no direct calibration of neutron detector readings and assembly power was possible for IFA-432 (a key valve that would have permitted the calibration, failed). Thus, independent confirmation of the temperature/power data would be quite important.

The thermocouple response to linear power decreases offers an independent crosscheck of the steady-state data trends. As with the steady-state data, a way has been found to plot the transient data which magnifies the manifestations of system nonlinearities, since these are most sensitive to differing divisions of resistance within the fuel rod. Let us return to the previous example of the superficially similar large and small-gap rods. Figure 5 contains calculated transient temperatures vs. time for these rods. The power decreases linearly from 100% to 80% of full power during the first 30 seconds. We see that the transient temperatures appear rather similar for both rods: both assume a linear trend with time (after a few seconds), and both come into a new steady-state level at the cessation of the power decrease. Again, if we were looking at somewhat scattered data points rather than calculated curves, we probably could not distinguish between these two (extremely different) rods, based on this ordinary plot of temperature versus time.

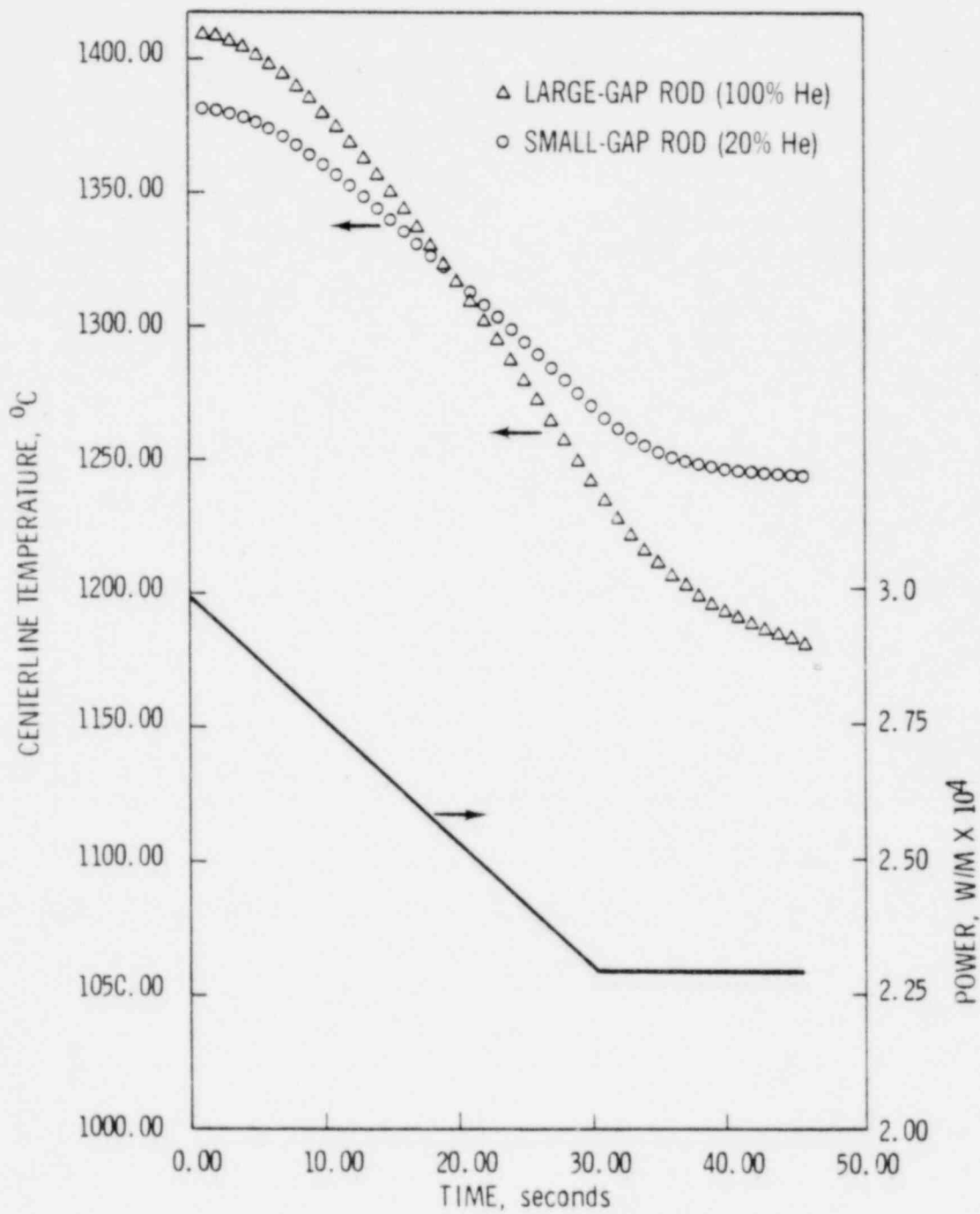


FIGURE 5. Temperature vs. Time for a Linear Power Decrease, for the Two Reference Rods

But now let us normalize both temperature and power to their initial values and replot them. The normalization equations are:

$$T_N = T_r(t)/T_r^i$$

$$P_N = P(t)/P^i$$

where  $T_r$  is relative centerline temperature (above coolant) and the superscript  $i$  refers to initial values. Figure 6 contains plots of the normalized curves. Observe that normalized temperature slopes (in the linear region) are not the same for the two rods. The large-gap rod has a normalized temperature slope very close to that of the normalized power; but the small-gap rod has a slope considerably less than that of the power. This process of comparing normalized temperature/power slope ratios is analogous to converting steady-state data to resistance data, as discussed in Appendix A. The reasons for the slope ratio differences are also discussed in Appendix A. Briefly, as the gap widens with decreasing power, the gap conductance decreases, heat flow is inhibited, and the decrease of temperature slows with time. Both rods "feel" this effect, but the small-gap rod feels it more, since it makes a larger fractional effect on its total resistance. Thus, we see that the ratio of normalized temperature and power slopes is sensitive to different gap conditions, even if these conditions happen to yield the same centerline temperature at full power. We shall see in the example of data analysis, page 14, that the temperature/power slope ratio is *equally* as sensitive to differing gap and fuel conditions as are the steady-state R-P plots. Appendix A indicates the reasons we expect this.

In addition, however, the response to linear power decreases provides an *independent* check on the steady state because the normalized data plots refer to *relative* rather than absolute values. If the percentage changes in normalized temperature do not match transient calculations which are based on R-P plots, then one of three conditions exists:

- the absolute value of initial temperatures is wrong
- the absolute value of initial power is wrong
- the calculational procedure is inadequate

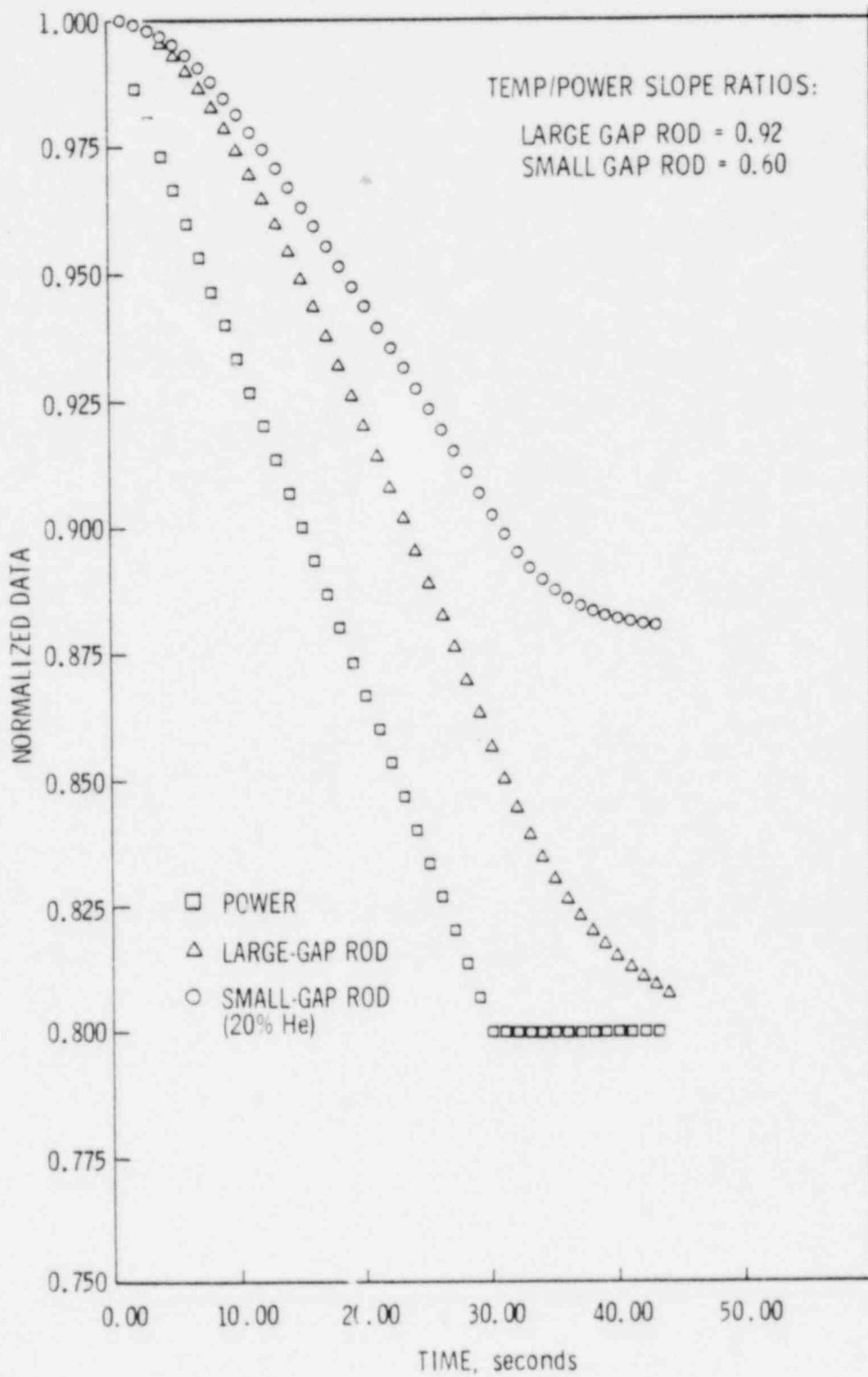


FIGURE 6. Normalized Temperature and Power vs. Time for a Linear Power Decrease for the Two Reference Rods

Close match between data and calculation early in fuel life leads us to believe the calculational procedures discussed in Appendix B are adequate. We, therefore, believe the continued comparison of R-P plots and transient data throughout the life of a fuel rod is a tool to detect significant drift of power/temperature measurements away from true values.

The example which follows demonstrates the definitive nature of the R-P data plots when combined with normalized transient data plots. In the next Section, page 21, this methodology has been applied to analyzing and confirming IFA-432 temperature data, for rod-to-rod comparisons and trends as a function of burnup.

#### EXAMPLE OF DATA ANALYSIS

Let us return to Figure 1, which shows a wide range of combinations of the major variables which will match a target temperature/power data point. We will use the foregoing ideas to narrow down the range of possibilities. The target data point happened to come from IFA-432 Rod 1 at 14,000 MWd/MTM (1200 GJ/kgU) burnup. The rod had a 230  $\mu$ m diametral gap, initially filled with helium at 1 atmosphere of pressure. (Details of design and operation for all the IFA-432 rods are given at the beginning of the next section.) At 14,000 MWd/MTM (2 1/2 years after first startup) the helium was certainly contaminated with fission gas; the fuel was probably relocated; the fuel thermal conductivity may have changed; and the thermocouple may have decalibrated. We will have to analyze more than just a single temperature/power point to assess these possibilities.

The target data point was chosen with some forethought; it represents a steady-state condition just ahead of a rapid linear power decrease, and near several reactor startups. So we will be able to use the data from the startups to prepare an R-P plot which we can use to make a transient calculation to compare with transient data from the rapid linear power drop. The R-P plot will guide us as to the probable values of fuel conductivity gas composition and effective gap size; the normalized transient data will give us a check on the validity of the power-temperature measurements.

Figure 7 shows scatter in an R-P data plot, along with six different cases of GAPCON-3 calculations. The R-P data was taken from an entire month centered around the fast power drop. (A narrower time period might have reduced the scatter, but it would also have reduced the number of highly important data points lying below the full-power range.) In the light of the data scatter, we can estimate the % He to be between 20% and 35%, the relocation to be between 33% and 50%, and the conductivity to be between 85% and 100% of the Lyons<sup>(3)</sup> equation.

Figure 8 shows the normalized data from a contemporaneous rapid power decrease. Although the power variation is rather rough, there is a portion (from 26 to 42 seconds) that is linear enough for our purposes. The power history from Figure 8 and the various initial conditions appropriate to the calculated R-P curves in Figure 7 were combined to produce the calculated temperature curves in Figures 9 and 10. The variable combinations which provided the best R-P data comparison in Figure 7 are even visibly the same as those which provide the best comparison to the transient temperature slope in Figures 9 and 10. Table 1 quantitatively confirms this; it lists the ratios of least-squares fit slopes of normalized power and temperature. The strong agreement between the steady-state and transient data<sup>(a)</sup> in this regard makes it unlikely that there is gross (greater than 10%) discrepancy in either the power or temperature measurements. Given the scatter in the present data, this is the most that can be said.

However, our estimate of the range of possible combinations is considerably less than that indicated in Figure 1. Figure 11 graphically illustrates the reduced range. To narrow down the combinations still further would require a high density of steady-state data points taken, at several power levels, just prior to the linear power decrease to minimize the scatter in the R-P plot. More nearly linear power decreases to confirm the further narrowed range of variables, also would be desirable. Request for operating sequences which will provide such data have been made for future Halden assemblies.

(a) The term "transient" is used rather loosely in this report to refer to the data from rapid linear power decreases. The linear portion of the thermocouple response is technically "quasi-steady-state" data, but this term is both cumbersome and misleading. Because of system nonlinearities, the real fuel rod never attains true quasi-steady-state.

TABLE 1. Measured and Calculated Temperature/Power Slope Ratios

	<u>Source</u>	<u>Temperature/Power Slope Ratio</u> <u>(<math>\pm 2\sigma</math> Uncertainty)</u>
Transient	Data	0.580 $\pm$ 0.036
Gapcon-3	Case 1	0.568 $\pm$ 0.036
Gapcon-3	Case 2	0.567 $\pm$ 0.036
Gapcon-3	Case 3	0.563 $\pm$ 0.036
Gapcon-3	Case 4	0.625 $\pm$ 0.036
Gapcon-3	Case 5	0.698 $\pm$ 0.036
Gapcon-3	Case 6	0.497 $\pm$ 0.036

To summarize, we have shown, for one example, that the R-P plots do indeed narrow the range of possibilities for the fuel rod thermal state at a given point in time. We have also shown that data from rapid linear power decreases tend to confirm the conclusions reached from steady-state R-P data plots. In the next section we will examine data from IFA-432 rods at several points in their lifetimes, and apply these ideas to develop a probable scenario for the thermal history of some of the rods.

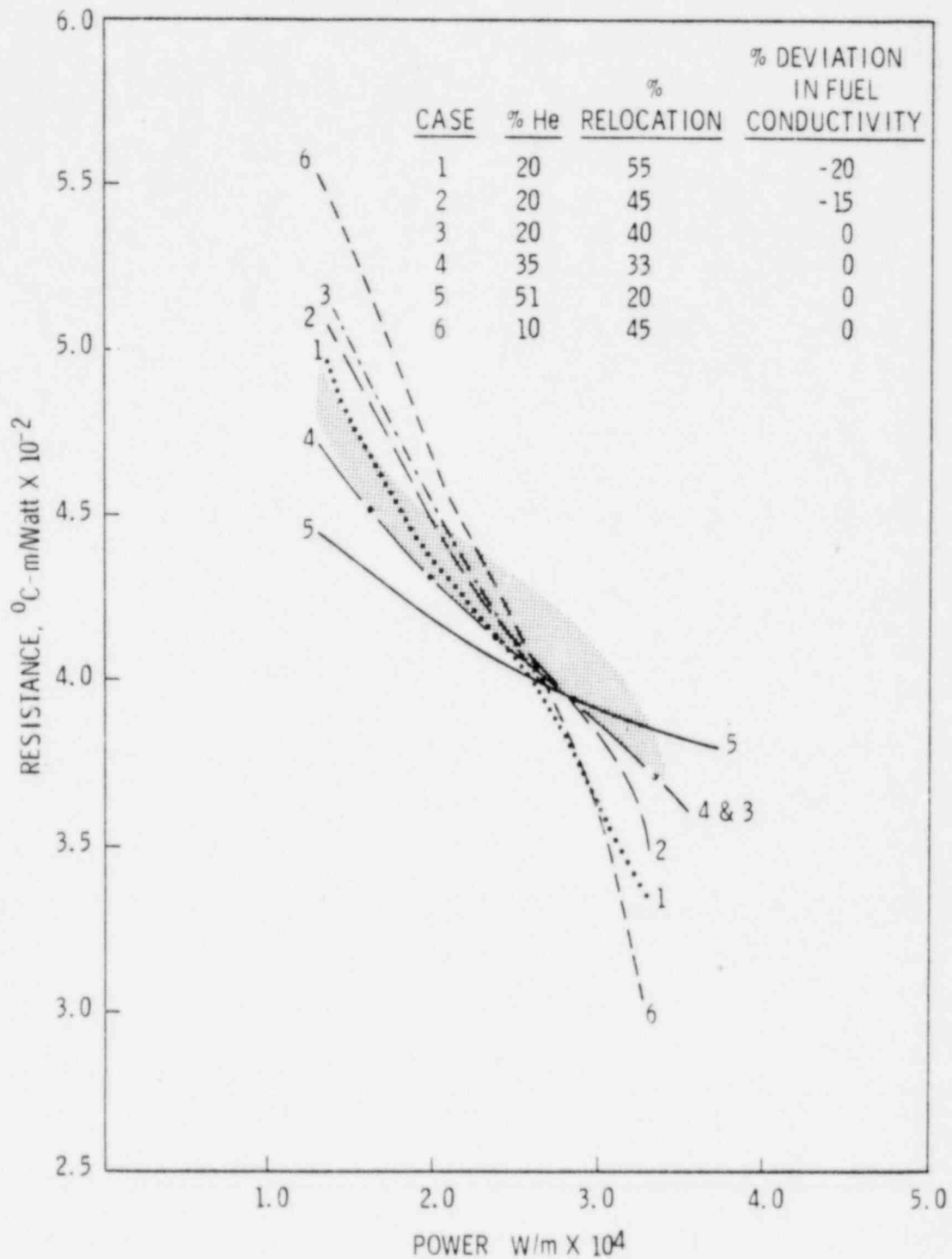


FIGURE 7. Data Scatter for Rod 1 IFA-432 at 14,000 MWd/MTM Burnup, and Various Calculated R vs. P Responses Using GAPCON-3

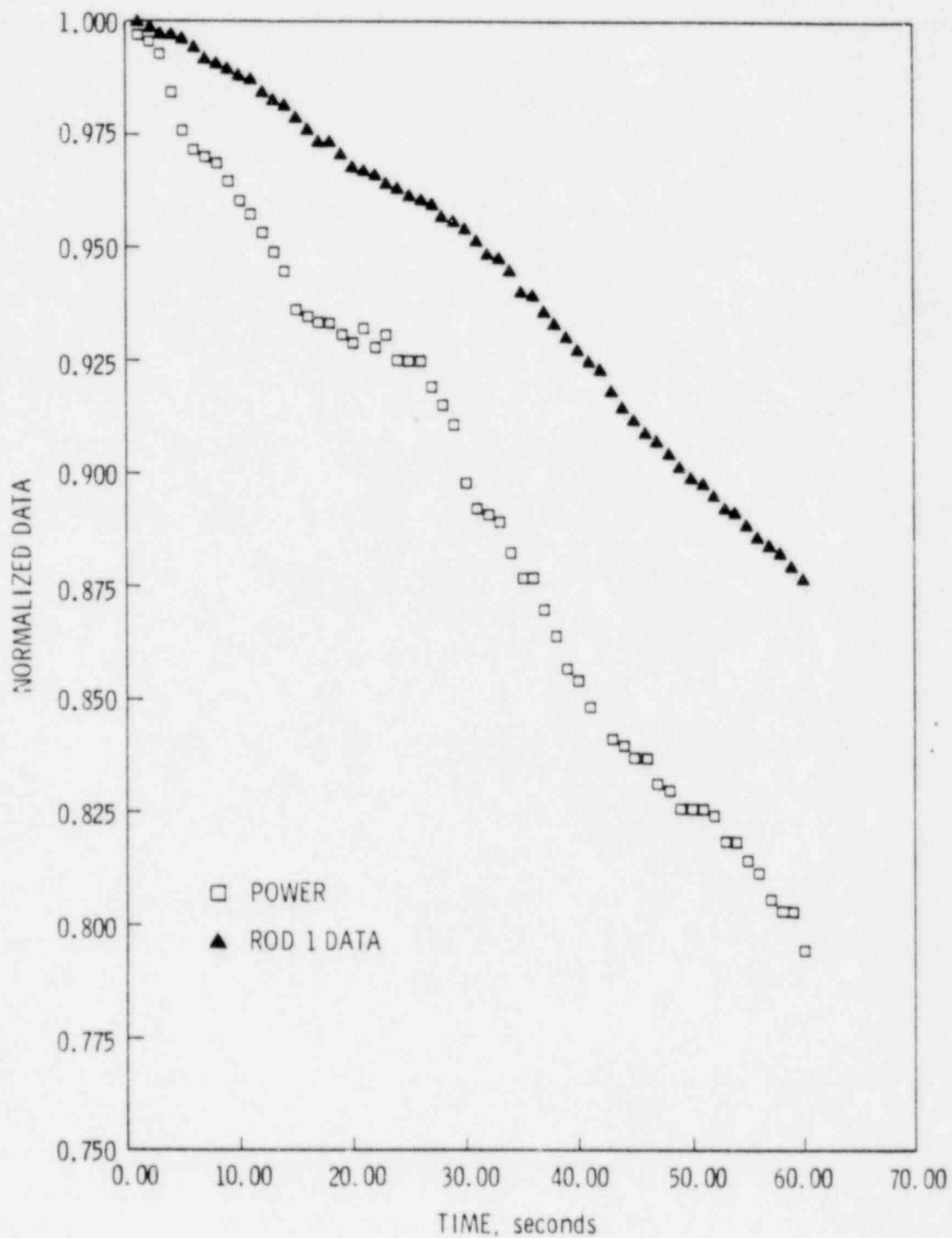


FIGURE 8. Normalized Power and Temperature Data from Rod 1, IFA-432 at 14,000 MWd/MTM Rod-Averaged Burnup

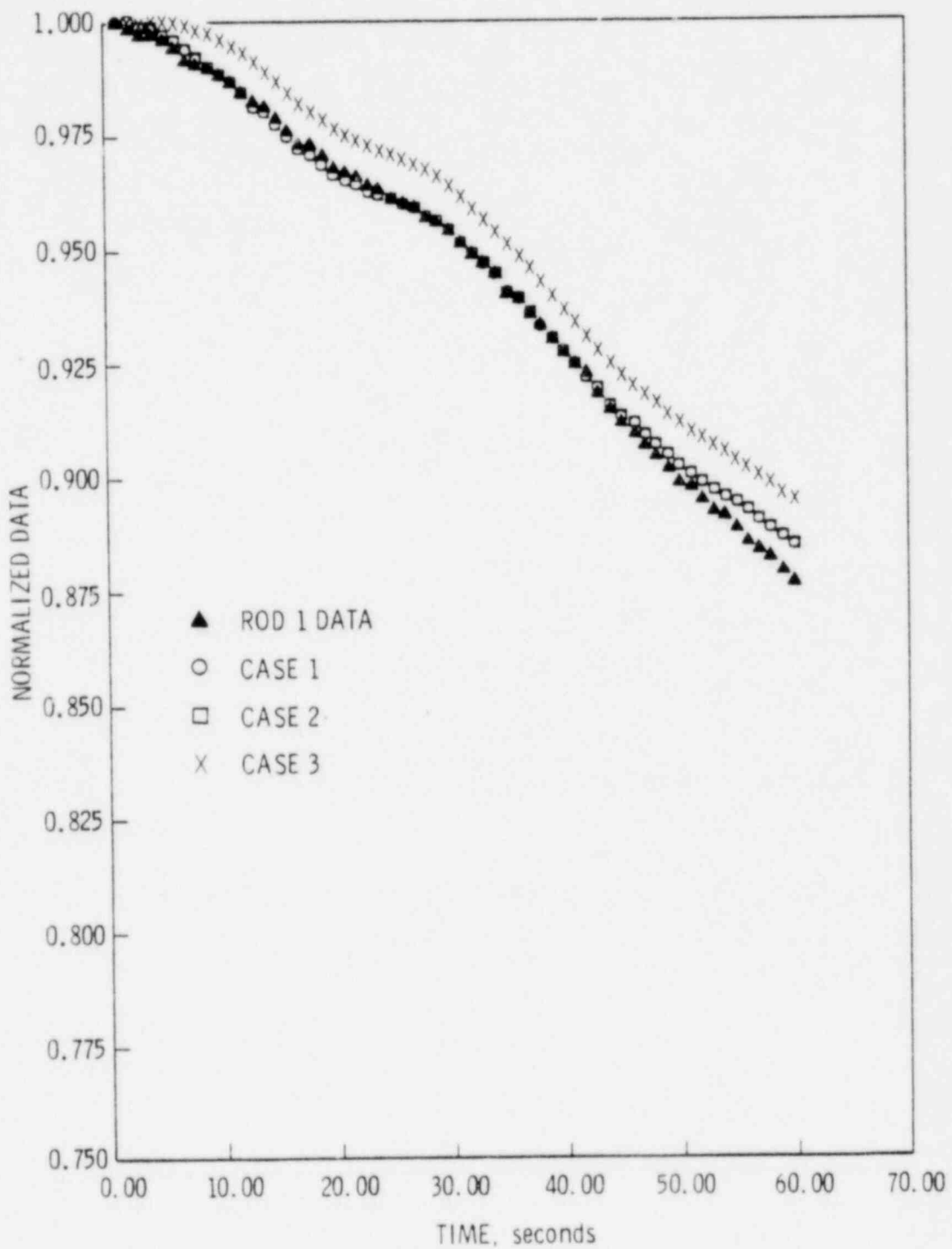


FIGURE 9. Data and Calculated Normalized Temperatures vs. Time for the First 3 Cases in Figure 7

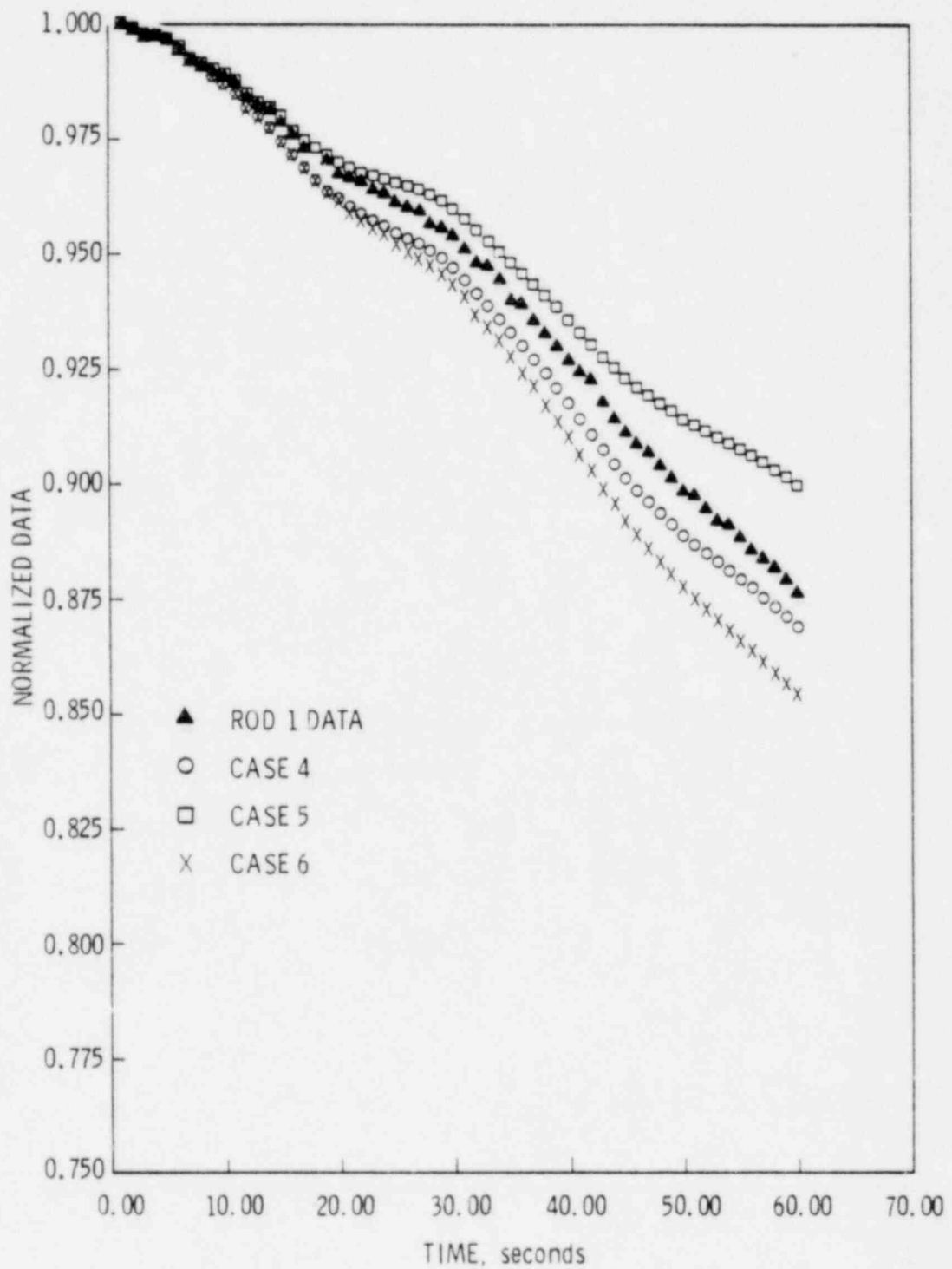


FIGURE 10. Data and Calculated Normalized Temperatures for the Last Three Cases in Figure 7

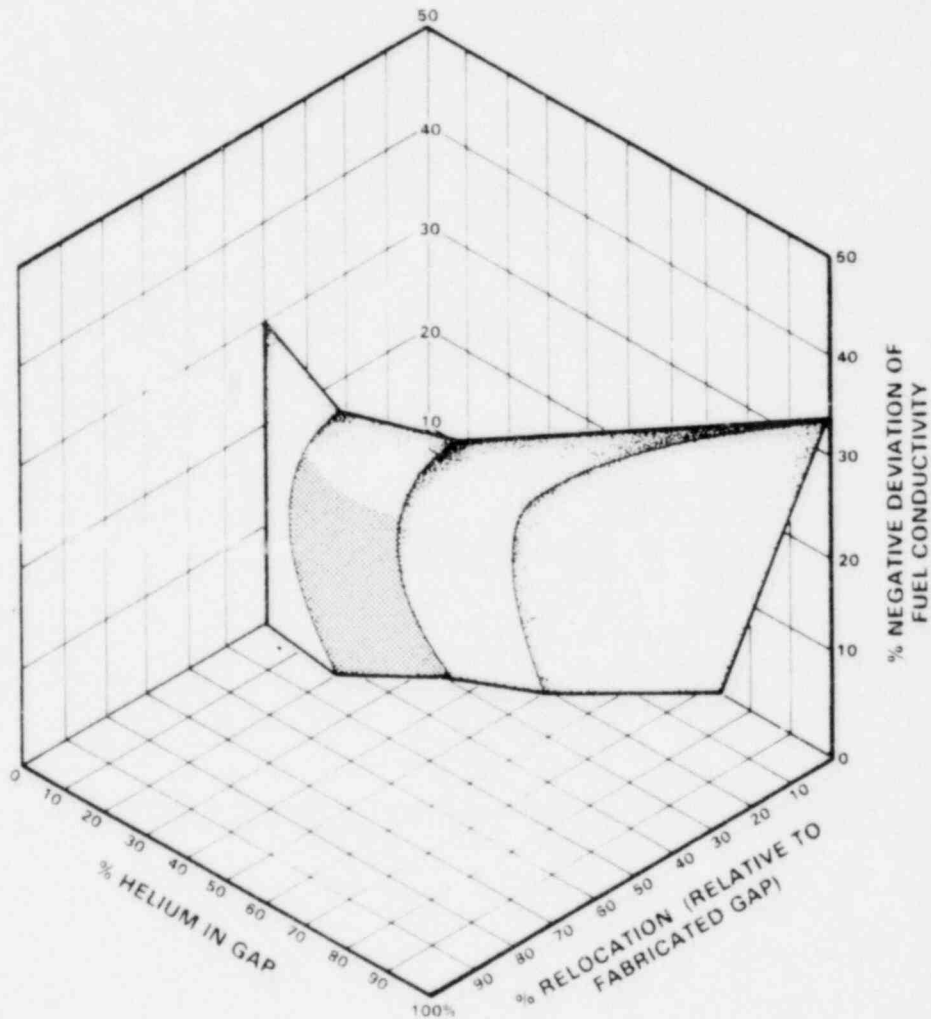


FIGURE 11. The Shaded Area Represents the Narrowed Range of Possibilities for Rod 1 at 14,000 MWd/MTM Burnup, Based on R-P and Transient Data Analysis

## DATA ANALYSIS FOR IFA-432 RODS

The Halden six-rod assembly, IFA-432, was designed by PNL under the US NRC program "Experimental Verification of Steady-State Fuel Codes." Several parameters varied from rod to rod; they include fuel type, fuel density, gap size, and fill gas composition. In this section, we will first briefly describe the assembly and the rods; then we will follow through the thermal histories of several rods for which the ideas developed in the previous Section can profitably be applied.

### DESCRIPTION OF ASSEMBLY

Since a recent report<sup>(4)</sup> includes details of the design and operation of IFA-432, we will only briefly review them. Figure 12 shows a schematic of the assembly, and notes the instrumentation used. Tungsten-rhenium fuel centerline thermocouples were installed in both ends of each fuel rod.<sup>(a)</sup> The thermocouple tips at the upper and lower ends were coplanar; three vanadium self-powered neutron detectors (SPNDs) were centered at each plane of the thermocouple junctions. The SPNDs were used to estimate the spatial distribution of the thermal neutron flux. In addition, a cobalt SPND is centered axially and radially in the assembly; it responds virtually instantaneously to rapid thermal neutron flux changes.

The various rods are described in Table 2. Rod 1 is filled with helium and has a standard U.S. BWR gap-to-pellet ratio, pellet diameter, and gas-volume to fuel-volume ratio.

Rod 2 has a larger gap and simulates instantaneous densification. Rod 3 has a very small gap to minimize gap resistance, and thus acts as an internal power standard.

Rod 4 was Xenon filled, and was designed to check the validity of previous reports on Xe-filled rods. In addition, the upper and lower ends of the fuel column were held concentric and eccentric, respectively, to check the effect of eccentricity on fuel temperatures.

<sup>(a)</sup> The exception is Rod 2 which had an ultrasonic thermometer in the top end.

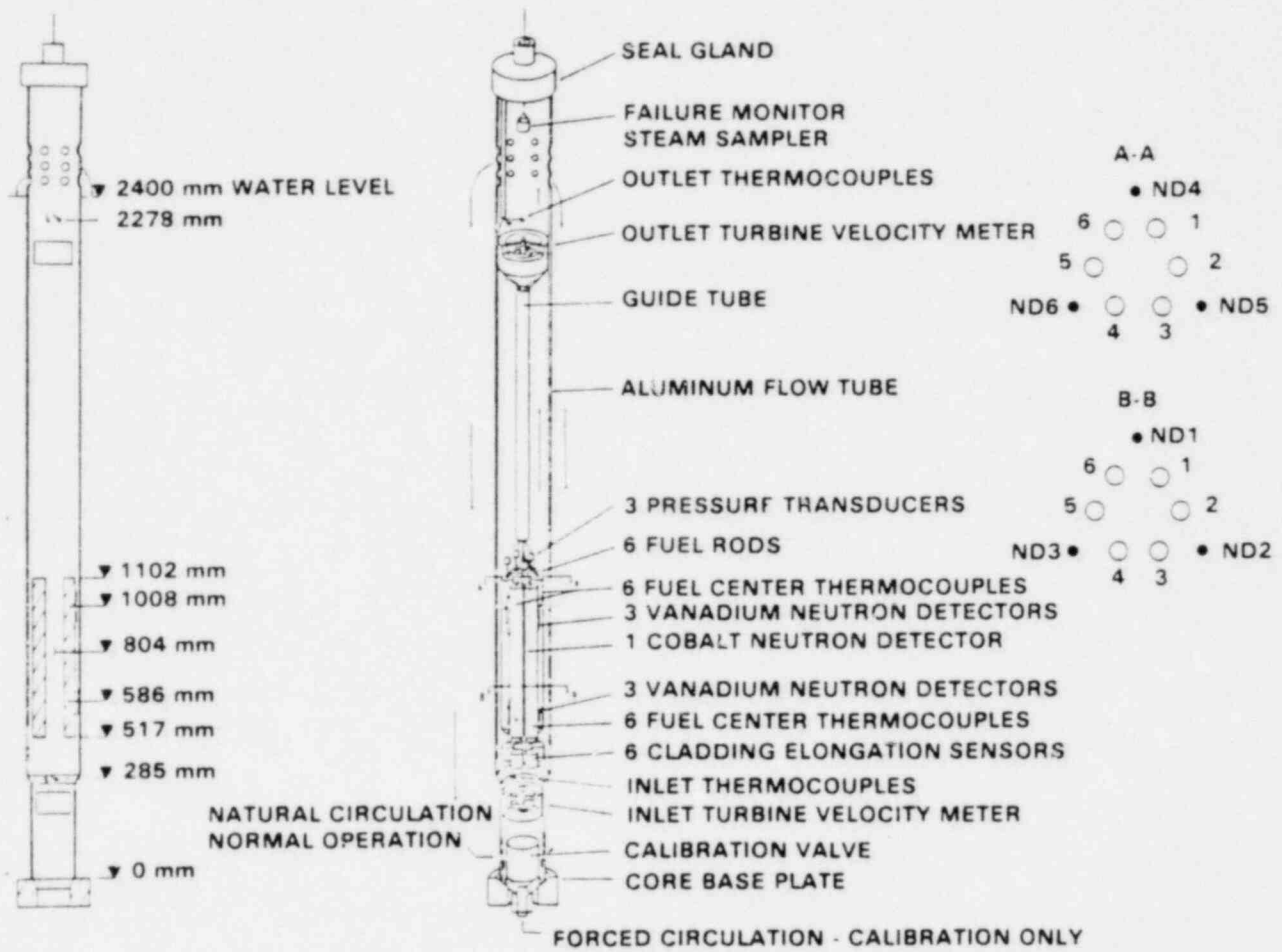


FIGURE 12. Schematic of Instrumented Fuel Assembly---IFA-432

TABLE 2. Description of IFA-432 Rods

Rod Number	Density of UO <sub>2</sub> , % TD (a)	Diametral Gap, m x 10 <sup>-4</sup>	Fill Gas (all at 1 atm, 293 K)
1	95	2.3	He
2	95	3.8	He
3	95	0.76	He
4	95	2.3	Xe
5	92 stable	2.3	He
6	92 unstable	2.3	He

(a) Theoretical density (TD) of UO<sub>2</sub> is taken to be 10960.Kg/m<sup>3</sup>

Rods 5 and 6 were He-filled, 230 μm gap rods. Both these rods had 92% TD fuel pellets, rod 5 was intentionally made very stable with respect to in-reactor densification. Rod 6 was deliberately made susceptible to densification. All the other rods had 95% TD stable fuel.

All the rods contained UO<sub>2</sub> fuel pellets enriched to 9.9%. The fuel length of all rods was 0.58 m. The rods were all clad in Zircaloy tubing with nominal dimensions 0.01279 X 0.01090 m (OD X ID).

Peak local power in the assembly was about  $5.0 \times 10^4$  W/m. The goal peak burnup was 20,000 MWd/MTM. However, the survival of instrumentation has been good enough to warrant pushing the peak burnup to 30,000 MWd/MTM or more. The peak/average power ratio at beginning of life was about 1.13. The upper thermocouple plane lay in the peak of the axial power distribution; the power at the lower thermocouple plane was about 30% less.

We shall examine beginning-of-life data for both thermocouples from all 6 rods in the next subsection, and then examine the life histories of rods 1, 2, 3, and 6. The reasons for excluding rods 4 and 5 are as follows: in rod 4, the thermocouples failed after a very short period of operation (probably due to the high temperatures this rod experienced) and rod 5 appeared to develop very abnormal fuel properties early in life (as will be discussed), therefore, its life history may not convey much useful information.

Various investigations were performed within the IFA-432 irradiation. These investigations, and the rods involved in each, follow:

- effect of gap size on fuel temperature (1,2,3)
- speed and effect of densification (1,5,6)
- effect of fill gas and eccentricity on gap conductance (1,3,4)
- effect of fuel relocation (1,2)
- performance of standard BWR fuel design to high burnup (1).

#### BEGINNING-OF-LIFE DATA

The first few reactor startups for IFA-432 were interspersed with rapid decreases in power from 100% to 80% of full power. Thus, the extent to which rod-to-rod differences in the steady-state data are confirmed by the transient data is observable. Figure 13 shows the beginning-of-life (BOL) resistance vs. power curves for the lower end thermocouples of the helium-filled rods. We see the resistances lining up in absolute value as would be expected for rods 1, 2, and 3. Rod 1 has a nominal diametral gap; its resistance is intermediate between small-gap rod 3 and large-gap rod 2. Rods 5 and 6 have greater resistance than rod 1, as might be expected, since the density and the ex-reactor measured conductivity for those fuel types was less than that for rod 1.<sup>(5)</sup> But the magnitude of the difference is somewhat larger than would be predicted on the basis of ex-reactor measurements. Furthermore, the behavior of the resistances for rods 5 and 6 is somewhat unexpected. The curves are increasing, which is characteristic of a closed-gap rod. Yet these rods had the same fabricated gaps as rod 1, which is inferred to have an open gap at comparable power. Figure 14 compares the upper thermocouple data for rods 1, 5, and 6. The differences observed in the lower thermocouples are even more pronounced in the upper thermocouples. This behavior can only be accounted for by postulating significant degradation of the fuel thermal conductivity, coupled with gap closure.

Figure 15 shows the resistances for the upper and lower ends of rod 4, the Xenon-filled rod. Both ends evidence domination of the gap resistance, as might be expected. Recall that the pellets in the lower end were forced to be eccentric while those in the upper end were held concentric. The

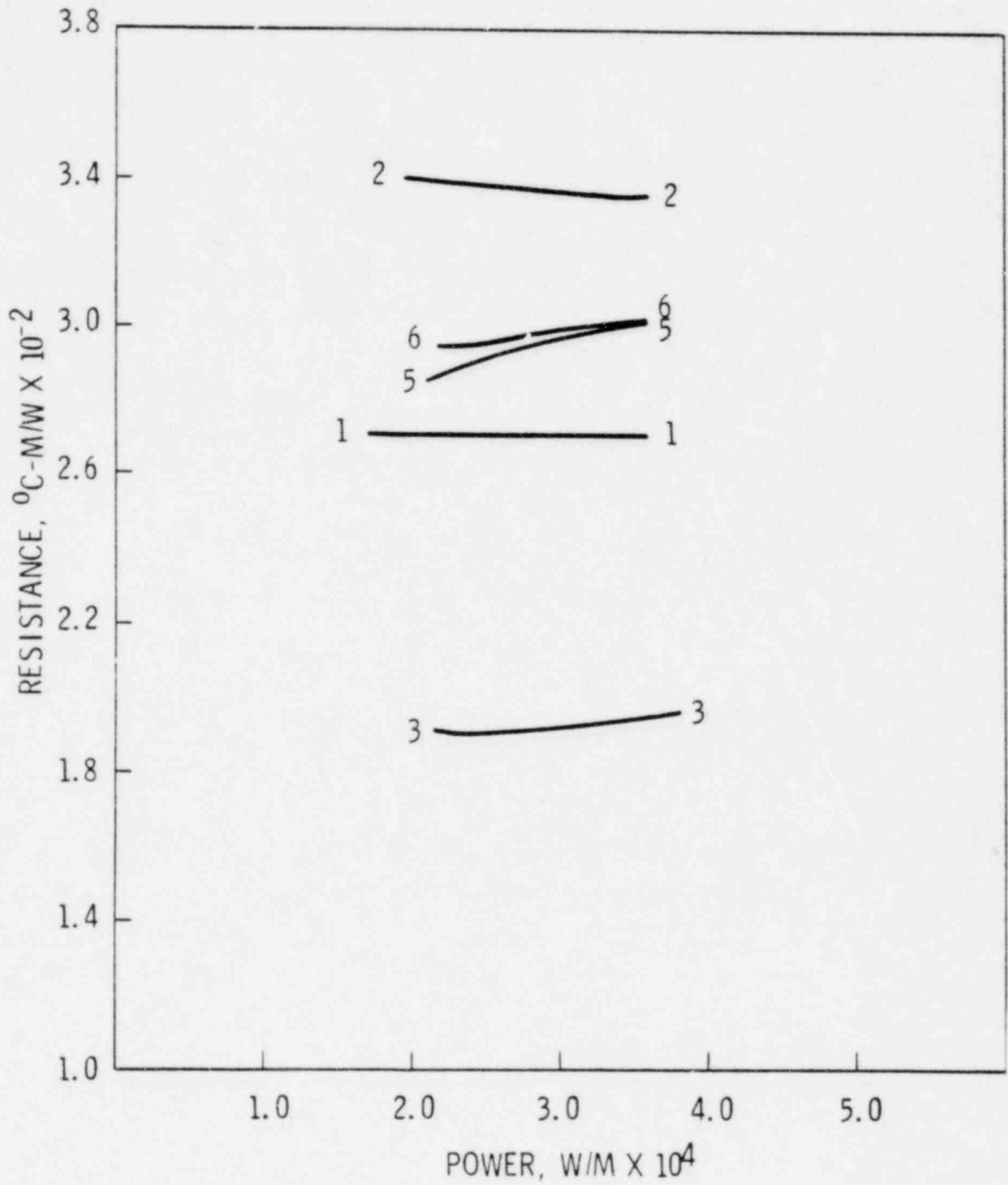


FIGURE 13. Beginning of Life R-P Data Trends for the Helium-Filled Rods in IFA-432 (Lower Thermocouples)

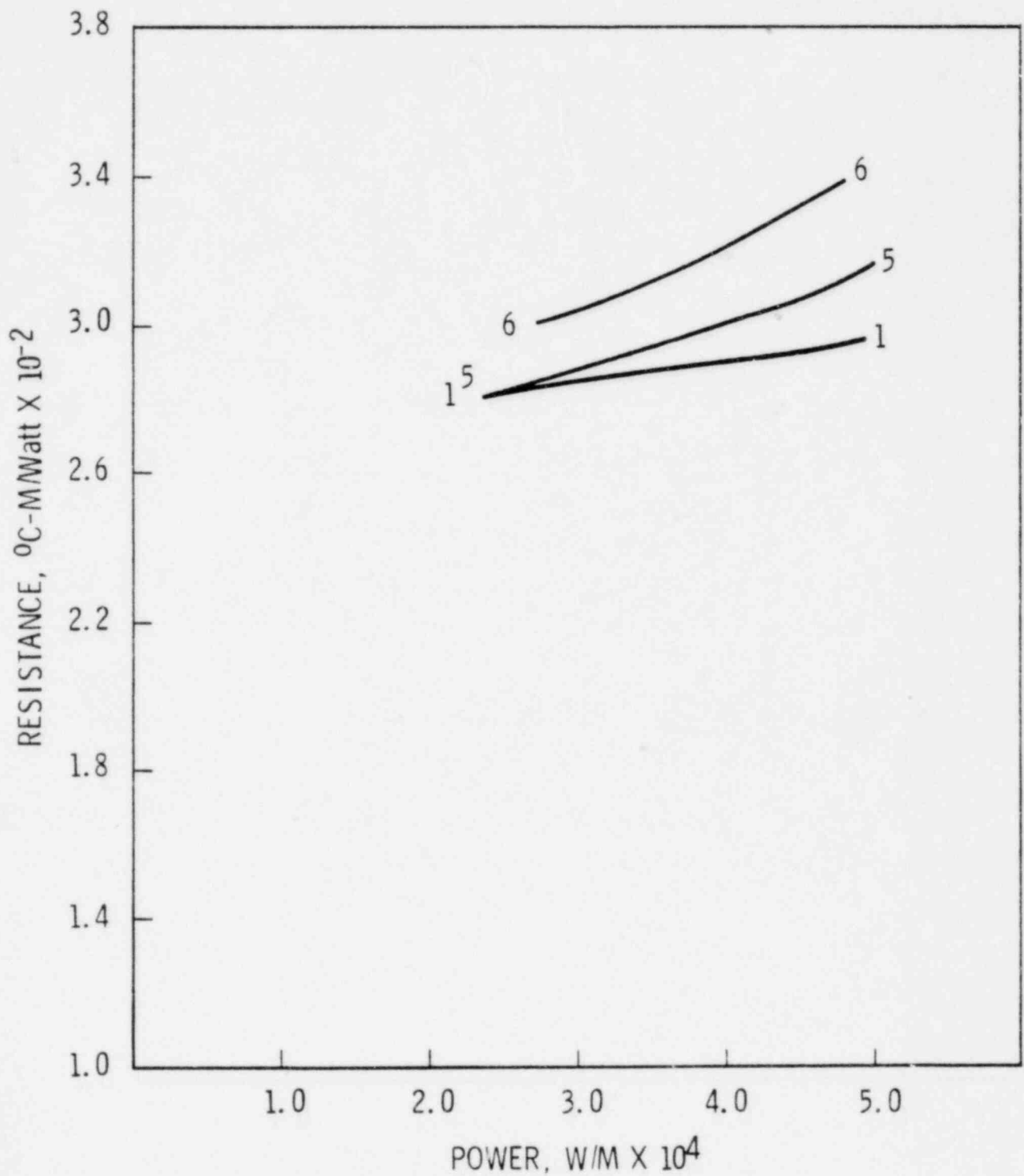


FIGURE 14. Beginning of Life R-P Data Trends for the Upper Thermocouples of Rods 1, 5 and 6

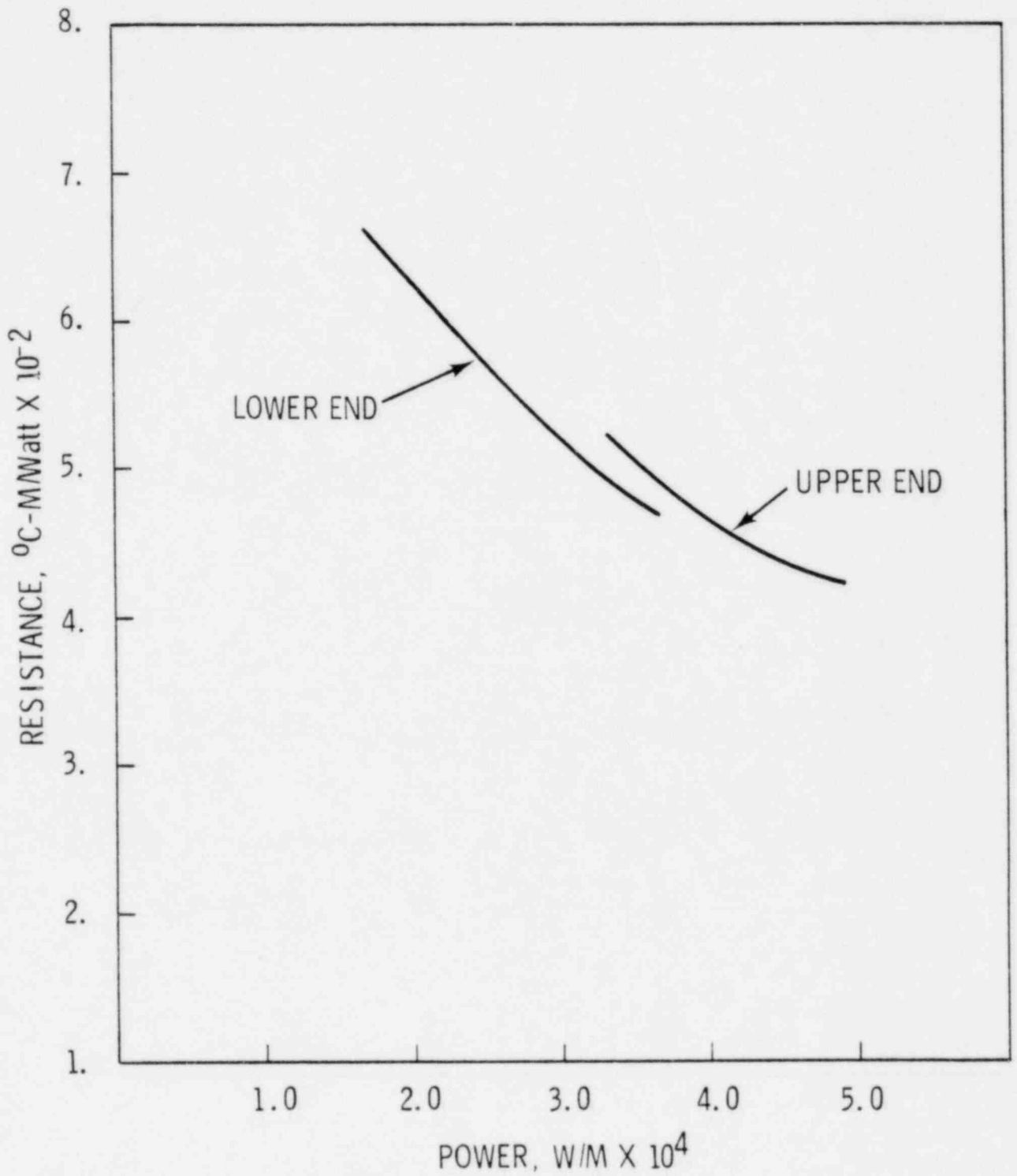


FIGURE 15. Beginning-of-Life R-P Data Trends for the Upper and Lower Thermocouples in Rod 4 (Xenon-Filled Rod)

slight displacement of the resistance curves (the lower end having the lower resistance) is probably due to the effect of eccentricity. However, the effect is slight, indicating a relatively small gap prevailing at both ends. (a)

Now let us consider what sort of transient data we might expect from a linear power decrease, based on these rod-to-rod comparisons, and whether the actual transient data qualitatively fulfills our expectations. (b)

Figure 16 shows calculated responses for rods 1, 3, and 4 to hypothetical power decrease. The initial and boundary conditions for these calculations were taken from Figures 13 and 15, and the calculations were performed the same way as described in the previous section (appendix B includes details). Note that the different gap conditions yield different normalized temperature slopes. The slope of the gap-dominated rod, 4, is much less than that of the power; that of the fuel-dominated rod, 3, is greater than that of the power, and the slope of the balanced rod, 1, is about equal to that of the power.

By transferring these ideas to the data in Figures 13-15, we may predict the thermocouple responses as listed in Table 3. Figure 17 gives normalized power and temperature data for the first three rods. Our qualitative expectations are confirmed: rods 1 and 2 have slopes visually similar to the power slope; whereas the slope for rod 3 is definitely greater.

As Figure 18 indicates, slopes at both ends of gap-dominated rod 4 definitely are less than that of the power. Furthermore, the slope of the eccentric lower end is greater than that of the upper end. We might expect this, since the lower end should experience less fractional change in gap resistance as a function of power than the concentric upper end.

---

(a) Reference 6 shows that thermal expansion and cladding deformation may be enhanced with the rod 4 design, resulting in a hot gap at power approximately equal to that of rod 3, the small-gap rod.

(b) Unexplained anomalies in the transient data for the first few runs makes quantitative comparison questionable.

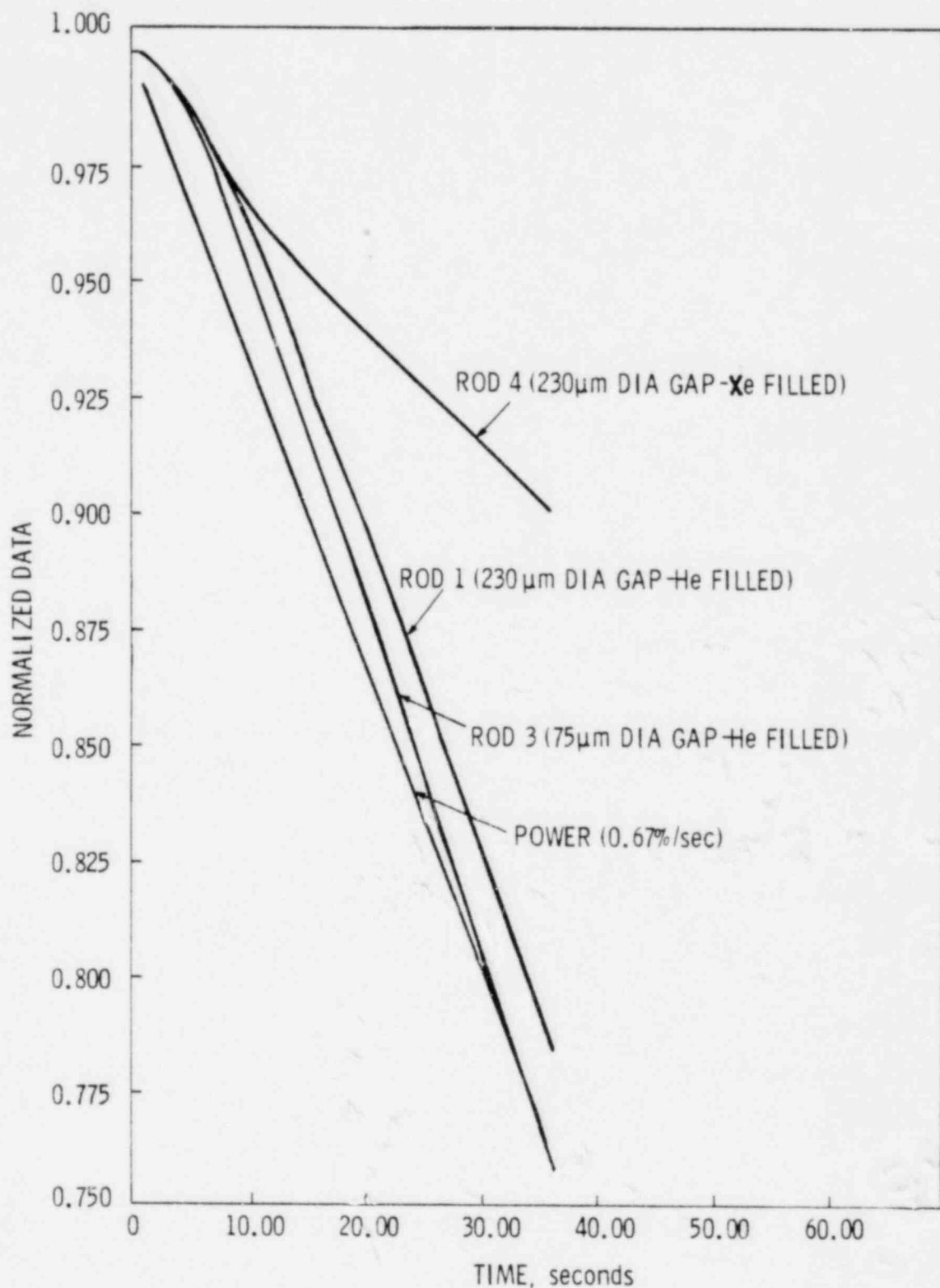


FIGURE 16. Calculated Response of Rods 1, 3, and 4 to a Hypothetical Linear Power Decrease of 0.67%/sec from  $\sim 3.0 \times 10^4$  W/m

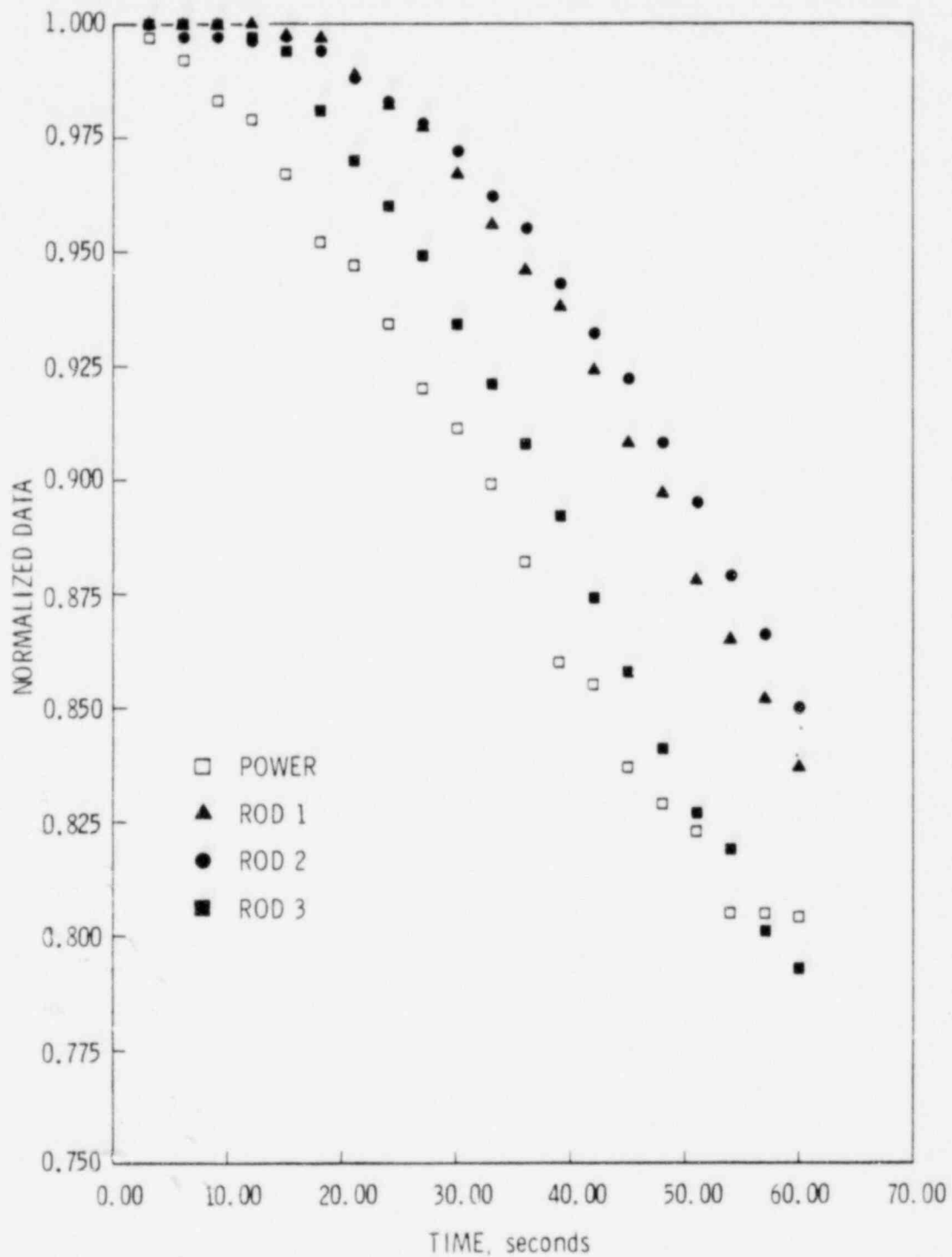


FIGURE 17. Response of Rods 1, 2, and 3 to a Beginning-of-Life Linear Power Decrease (Run 31, Lower Thermocouples)

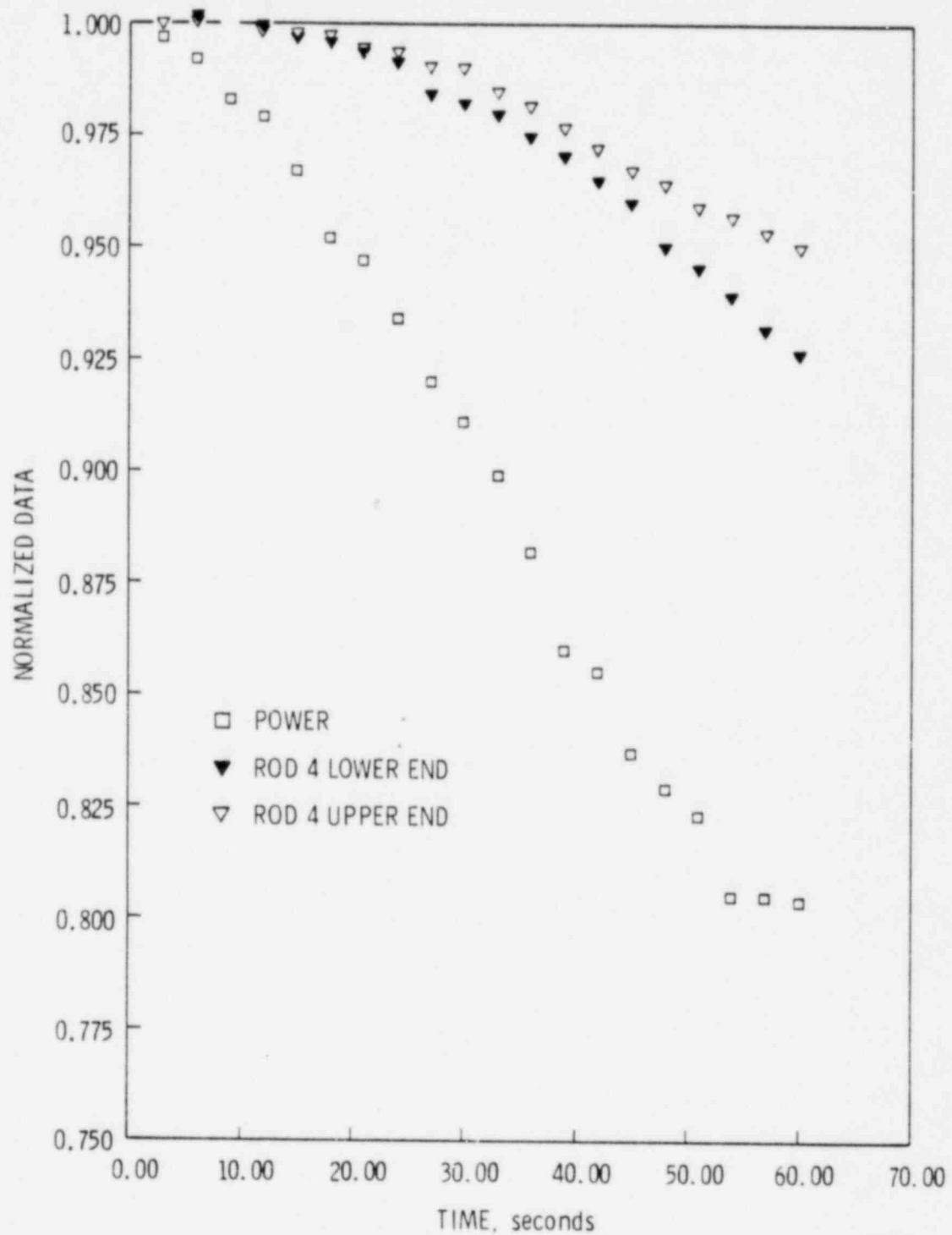


FIGURE 18. Response of Upper and Lower Ends of Rod 4 to Beginning-of-Life Power Decrease (Run 31)

TABLE 3. Expected Thermocouple Response to Linear Power Decrease

Rod No.	R-P Characteristics	Qualitative Fuel Type	Predicted Normalized Temperature Slope
1	Flat, both thermocouples	Balanced	Equal to power slope
2	Flat	Balanced	Equal to power slope
3	Slight upward trend	Fuel Dominated	Greater than power slope
4	Sharp downward trend (both thermocouples)	Gap Dominated	Much less than power slope
5	Upward trend (both ends)	Fuel Dominated	Greater than power slope
6	Upward trend (both ends)	Fuel Dominated	Greater than power slope

Figures 19 and 20 indicate that temperature slopes at both ends of rods 5 and 6 are greater than the power slopes. We might expect this due to the R-P curves for these rods. The upper end (higher power end) of rod 6 shows the least effect. Enhanced densification at this site may be counteracting the fuel domination evident elsewhere.

In summary, the resistance plots again evidence absolute values and slopes which are characteristic of the particular gap conditions. Furthermore, these characteristics are at least qualitatively confirmed by thermocouple response to linear power decreases.

#### LIFE HISTORIES OF THE RODS

Throughout the life of IFA-432, a total of 27 rapid power decreases have been performed, generally in sets of 3 and spaced 3-6 months apart. Of these, at least seven had linear portions sufficient for use in corroborating resistance vs. power data. Table 4 gives dates and rod-average burn-ups representative of these linear power drops, together with the least-squares fit slope of the linear portion of the normalized power vs. time curve. The precision of that slope estimate is also shown.

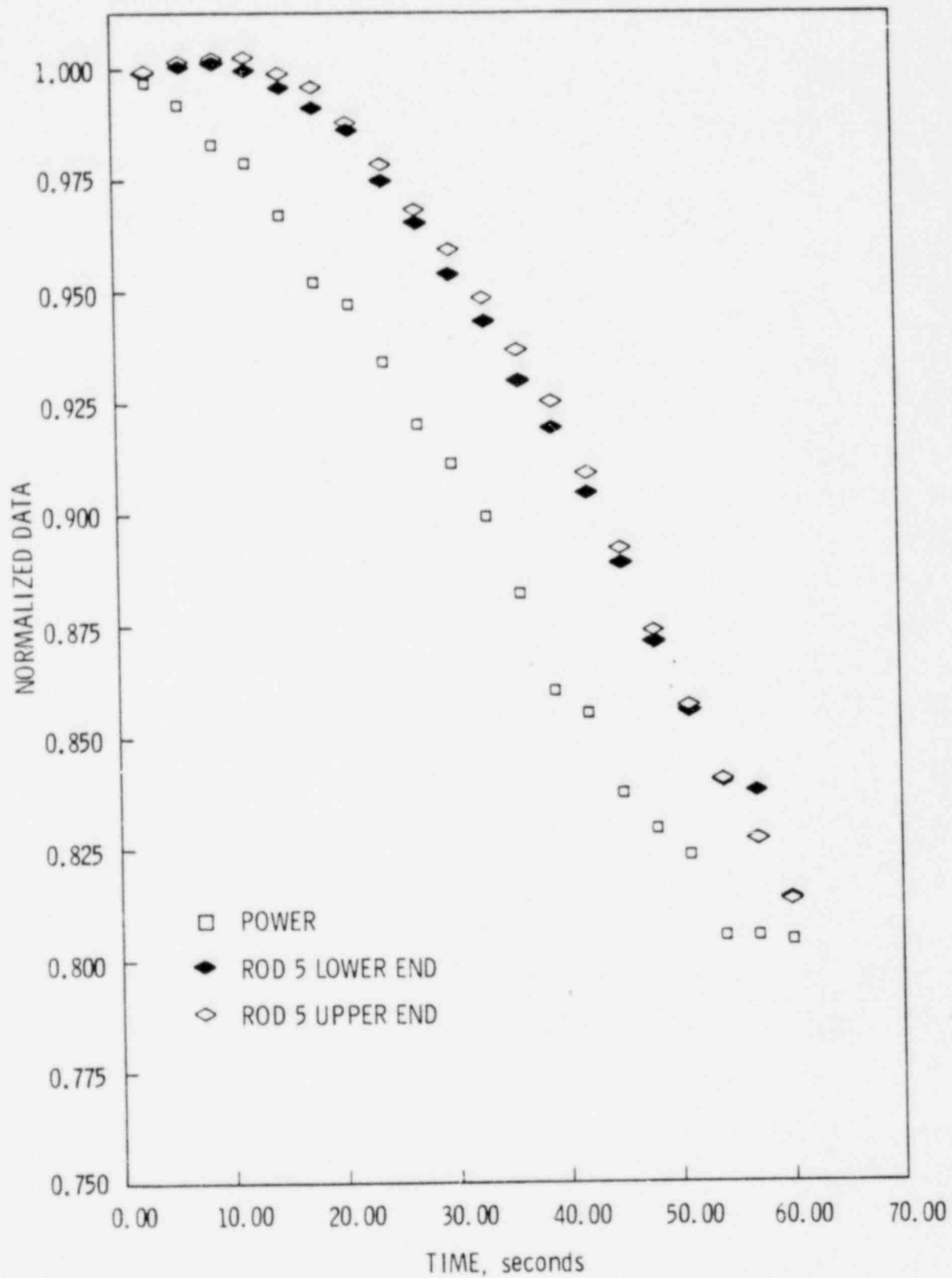


FIGURE 19. Run 31 Response of Rod 5

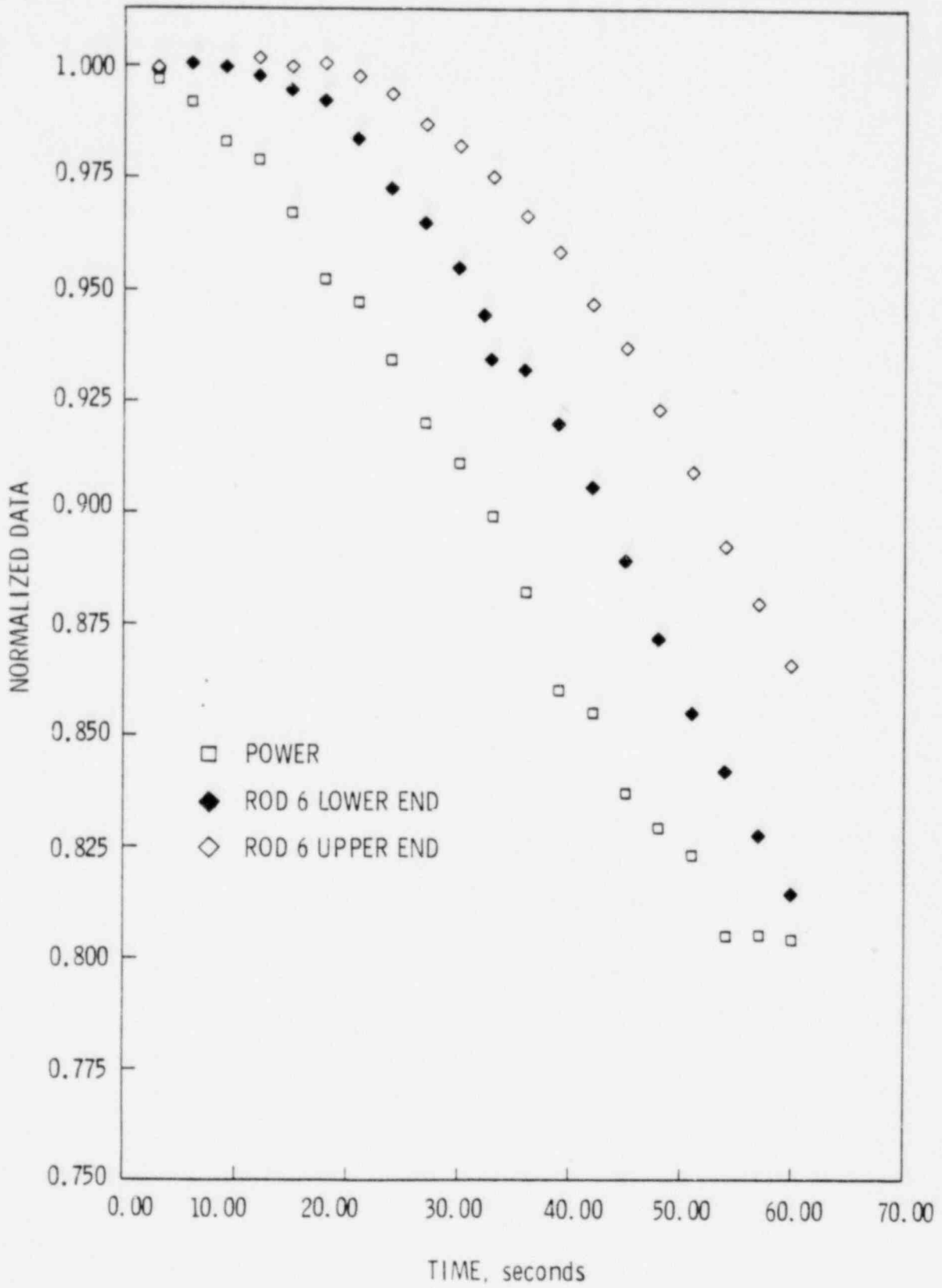


FIGURE 20. Run 31 Response of Rod 6

TABLE 4. Power Drop Dates and Identity

Date	Run Number	Rod 1 Average Burnup		Normalized Power vs. Time Slope, %/sec ( $\pm 2\sigma$ )
		Gj/kg U	MWD/MTM	
12/19/75	31	0	0	0.4607 $\pm$ 0.039
1/19/76	43	121	1400	0.6914 $\pm$ 0.063
8/12/76	62	450	5300	0.5229 $\pm$ 0.073
1/18/77	68	690	8000	0.4054 $\pm$ 0.030
5/4/77	84	920	10,600	0.6789 $\pm$ 0.038
8/23/77	92	1100	13,000	0.4827 $\pm$ 0.027
1/5/78	100	1200	14,000	0.4934 $\pm$ 0.026

Rod 1

The lower thermocouple of rod 1 survived throughout the indicated burnups; therefore, companion R-P plots could be prepared using steady-state data for one month centered about each of the indicated dates. Figure 21 brings together these seven resistance plots. We see that the resistance is progressively rising and attaining a negative slope with respect to power. It is easiest to explain this trend as the result of fission gas release to the gap, which would certainly raise the resistance, and would also tend to make the rod progressively "gap dominated."

Based on our previous examples, we would expect the normalized temperature/power slope ratio to progressively decrease from near unity to some much lower value during the life of this rod. Table 5 summarizes the data for the temperature/power slope ratio from the seven linear power drops; it certainly confirms our qualitative expectation. To find out if this trend constitutes *quantitative* confirmation of the R-P trend, we shall have to develop from the plots a scenario of possible changes in fuel and gap conditions and see if that scenario results in calculated temperature/power slope ratios which match the transient data.

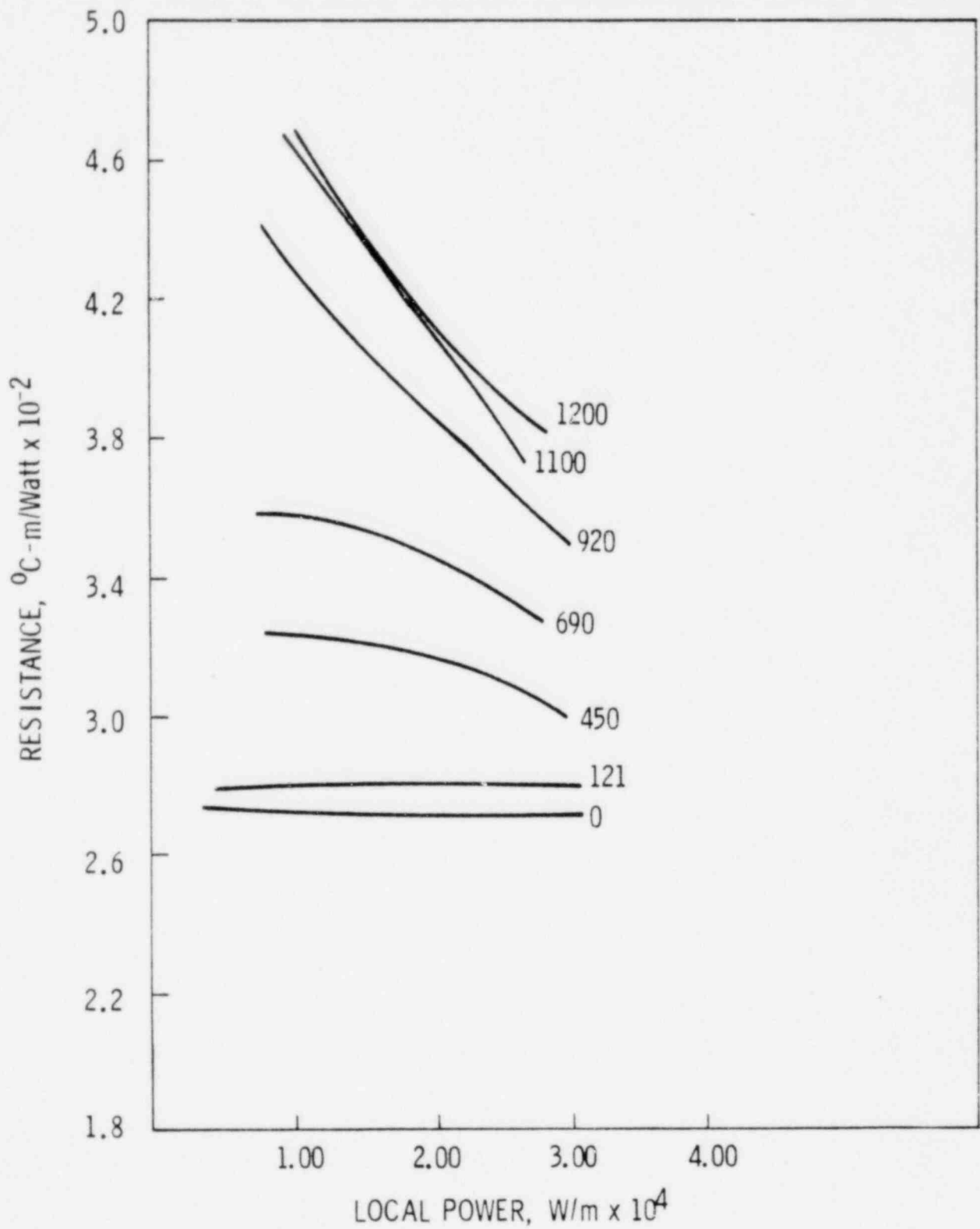


FIGURE 21. Resistance-Power Data Trends for Rod 1 (Lower Thermocouple). The numbers represent burnup in  $\text{Gj}/\text{kgU}$

TABLE 5. Data for Temperature/Power  
Slope Ratios

<u>Run Number</u>	<u>Slope Ratio</u>
31	1.05
43	0.87
62	0.72
68	0.68
84	0.53
92	0.54
100	0.58

In order to develop such a scenario, we shall have to repeat (for each of the seven representative burnups) the procedure carried out in the data analysis example, page 14. There, we narrowed down the range by assuming different conditions (all of which "hit" a reasonable target data point). We then compared the measured R-P curve to those calculated by GAPCON-3 using the assumed conditions. The refinement to which we carry this procedure is limited by time and money and the scatter of the data. At least 3 trial GAPCON runs are necessary to produce one target run for a chosen fixed value, of say 30% He. To attempt 10 variations of conditions at each representative burnup would mean making a minimum of  $3 \times 10 \times 7 = 210$  GAPCON runs (plus a similar number of transient calculator, plot routine, and regression code runs) to trace the life of just this one rod! But there must be some variation of conditions at each burnup. Using prior experience, we have picked three conditions for each burnup that, in general, bracket the R-P data. These choices are summarized in Table 6, together with the calculated temperature/power slope ratios they produce. Figures 22 to 28 show the calculated R-P plots superimposed on the data trends.

The combinations giving the best match to the transient data are underlined in the table; they match the R-P curves fairly well. Conversely, the combinations which do not match the transient also do not match the R-P data.

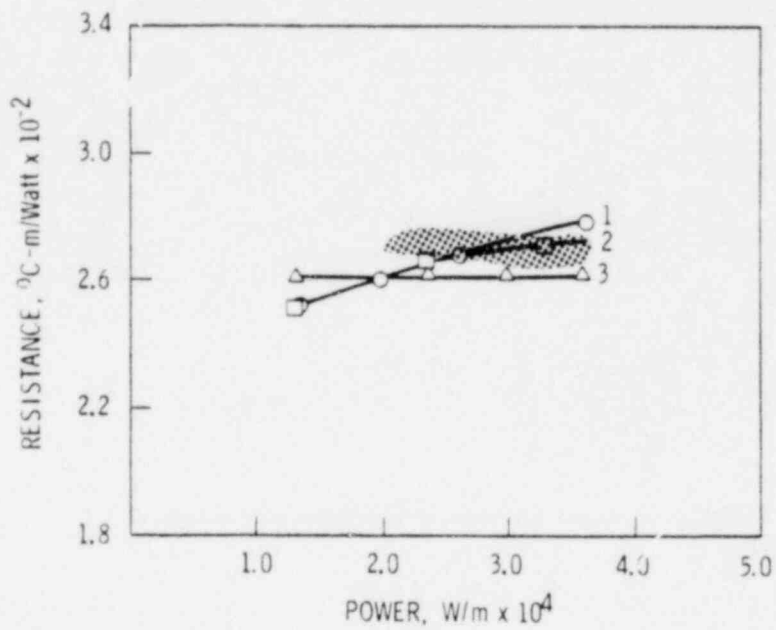


FIGURE 22. Calculated R-P Curves for Rod 1 at 0 GJ/kgU Burnup. The numbers refer to "choices" in Table 7 (Run 31). The shading represents data scatter.

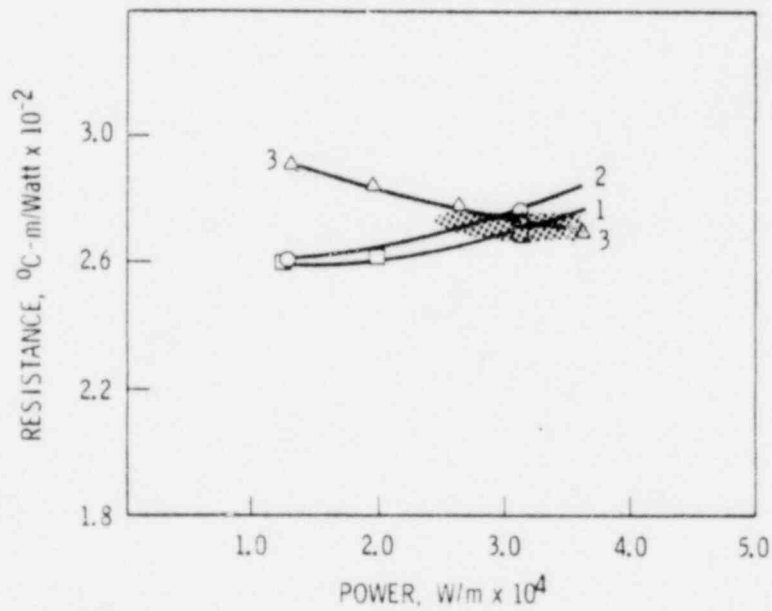


FIGURE 23. Data and Calculated R-P Response for Rod 1 at 121 GJ/kgU (Run 43)

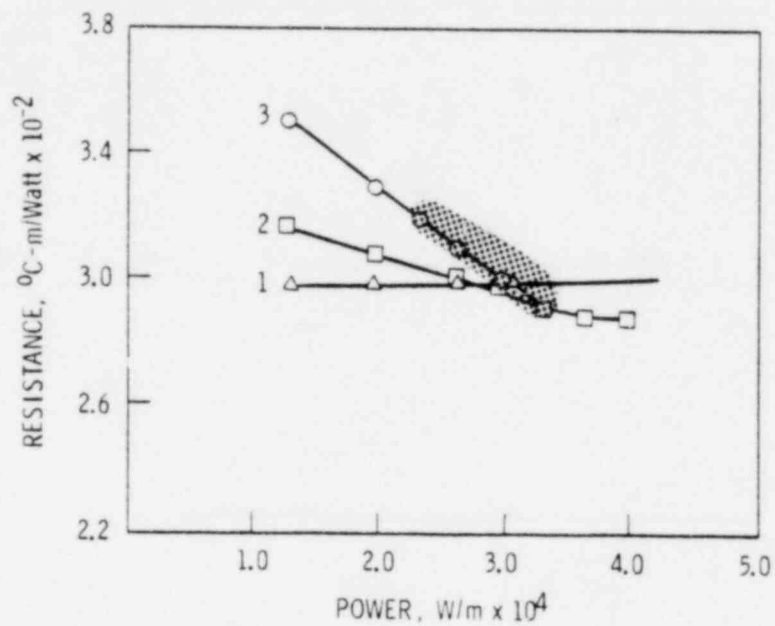


FIGURE 24. Data and Calculated R-P Response for Rod 1 at 450 GJ/kgU Burnup (Run 62)

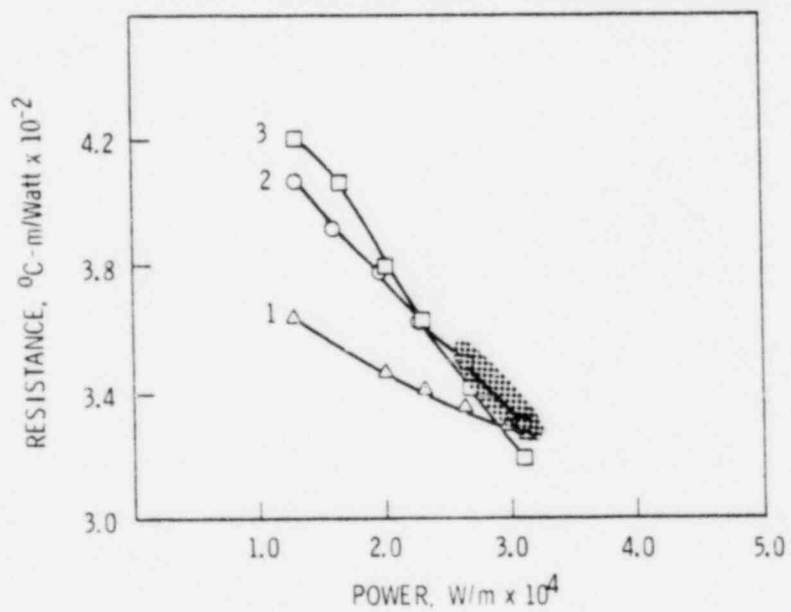


FIGURE 25. Data and Calculated R-P Response for Rod 1 at 690 GJ/kgU (Run 68)

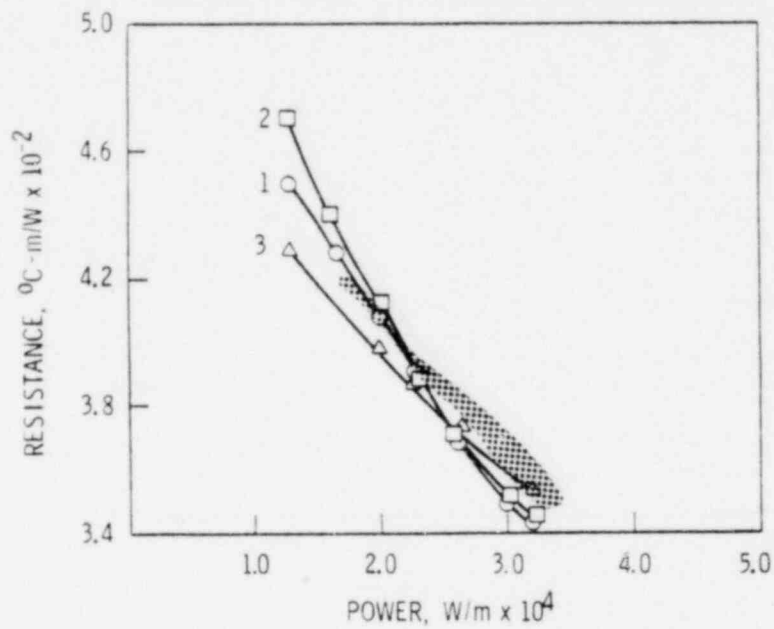


FIGURE 26. Data and Calculated R-P Responses for Rod 1 at 920 GJ/kgU Burnup (Run 84)

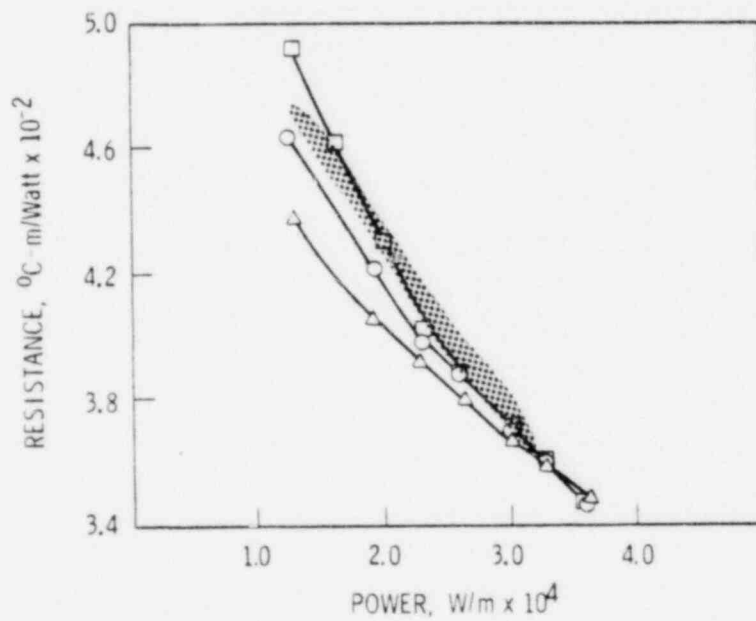


FIGURE 27. Data and Calculated R-P Response for Rod 1 at 1100 GJ/kgU Burnup (Run 92)

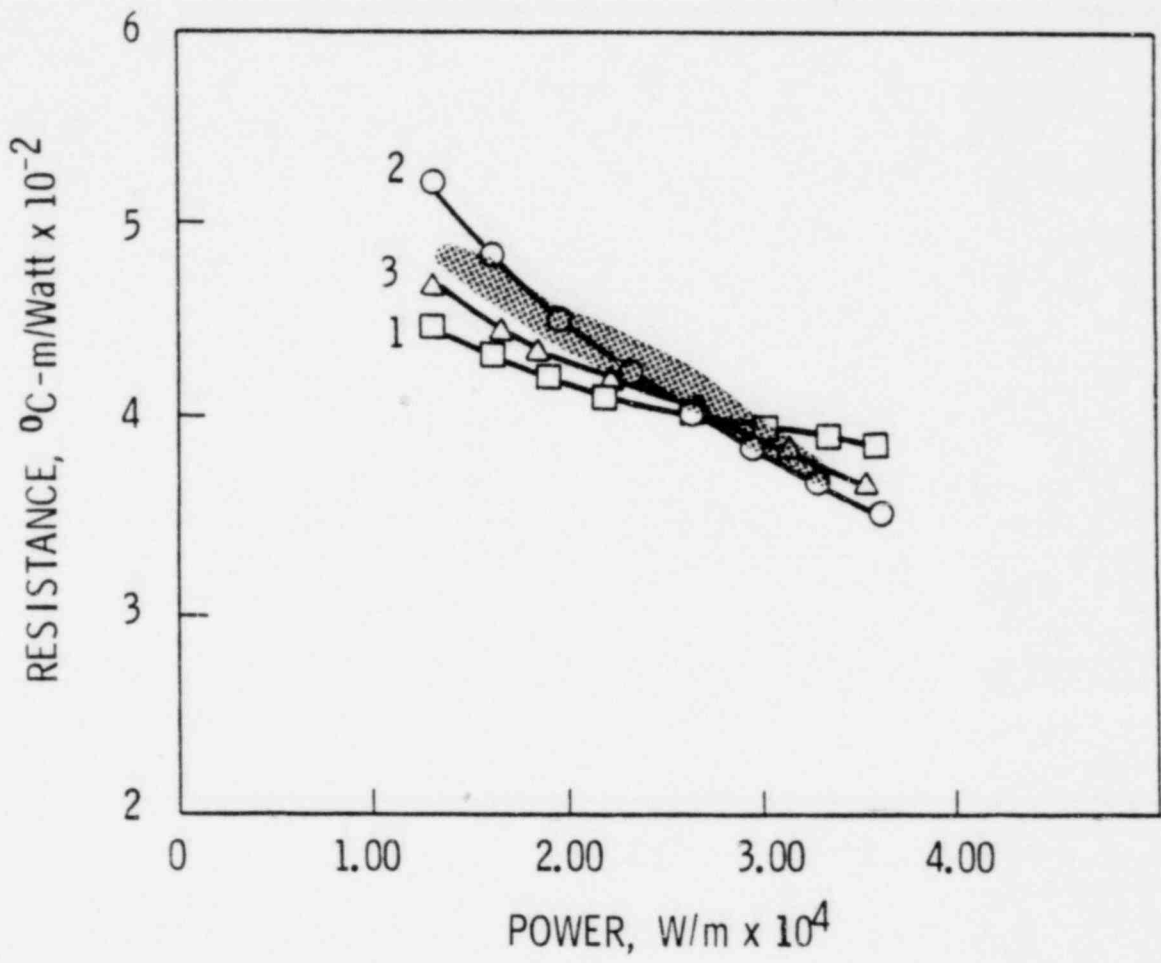


FIGURE 28. Calculated R-P Responses for Rod 1 at 1200 Gj/kgU Burnup (Run 100)

TABLE 6. Data and Calculations for Temperature/Power Slope Ratio from Linear Power Decreases for Rod 1, Lower Thermocouple

Run Number	Measured Slope Ratio( $\pm 2\sigma$ )	Calculated Slope Ratios for Various Combinations of Major Variables <sup>(a)</sup>					
		Choice	Ratio	Choice	Ratio	Choice	Ratio
31	1.05 $\pm$ 0.09	<u>100,31,0</u>	1.01	100,60,-20	1.00	80,50,0	0.96
43	0.87 $\pm$ 0.08	90,40,0	0.89	<u>80,51,0</u>	0.86	60,55,0	0.76
62	0.72 $\pm$ 0.10	80,50,0	0.86	50,50,0	0.77	<u>40,54,0</u>	0.71
68	0.68 $\pm$ 0.05	60,36,0	0.83	<u>30,50,0</u>	0.66	25,53,0	0.63
84	0.53 $\pm$ 0.03	<u>27,45,0</u>	0.54	20,48,0	0.50	40,37,0	0.59
92	0.54 $\pm$ 0.03	<u>20,45,0</u>	0.54	40,35,0	0.73	30,40,0	0.65
100	0.58 $\pm$ 0.03	50,20,0	0.62	<u>20,40,0</u>	0.55	35,33,0	0.59

(a) The entries under each choice represent % helium, fuel relocation (as a percent of initial fabricated gap), and percent deviation from the Lyons UO<sub>2</sub> thermal conductivity equation. Underlined entries represent the most probable choices in the light of the present data.

The combinations chosen do not in general include variation in fuel thermal conductivity. In the light of the previous section's more detailed comparison, there is a chance that the thermal conductivity has degenerated, but the data are not definite enough to state the extent of degradation closer than +0, -15%.

Figure 29 charts the probable life history of rod 1, based on these data.

#### Rod 2

To date, the lower thermocouple of Rod 2 has survived, permitting an analysis similar to the one just presented for rod 1. The same seven power decreases and representative burnups used in Table 4 apply.

The Rod 2 R-P data trends at these seven representative burnups are displayed in Figure 30, which is similar to Figure 21 for rod 1. Upon comparing Figures 21 and 30, we see that the initial value of resistance for rod 2 is greater than that for rod 1, as would be expected due to its

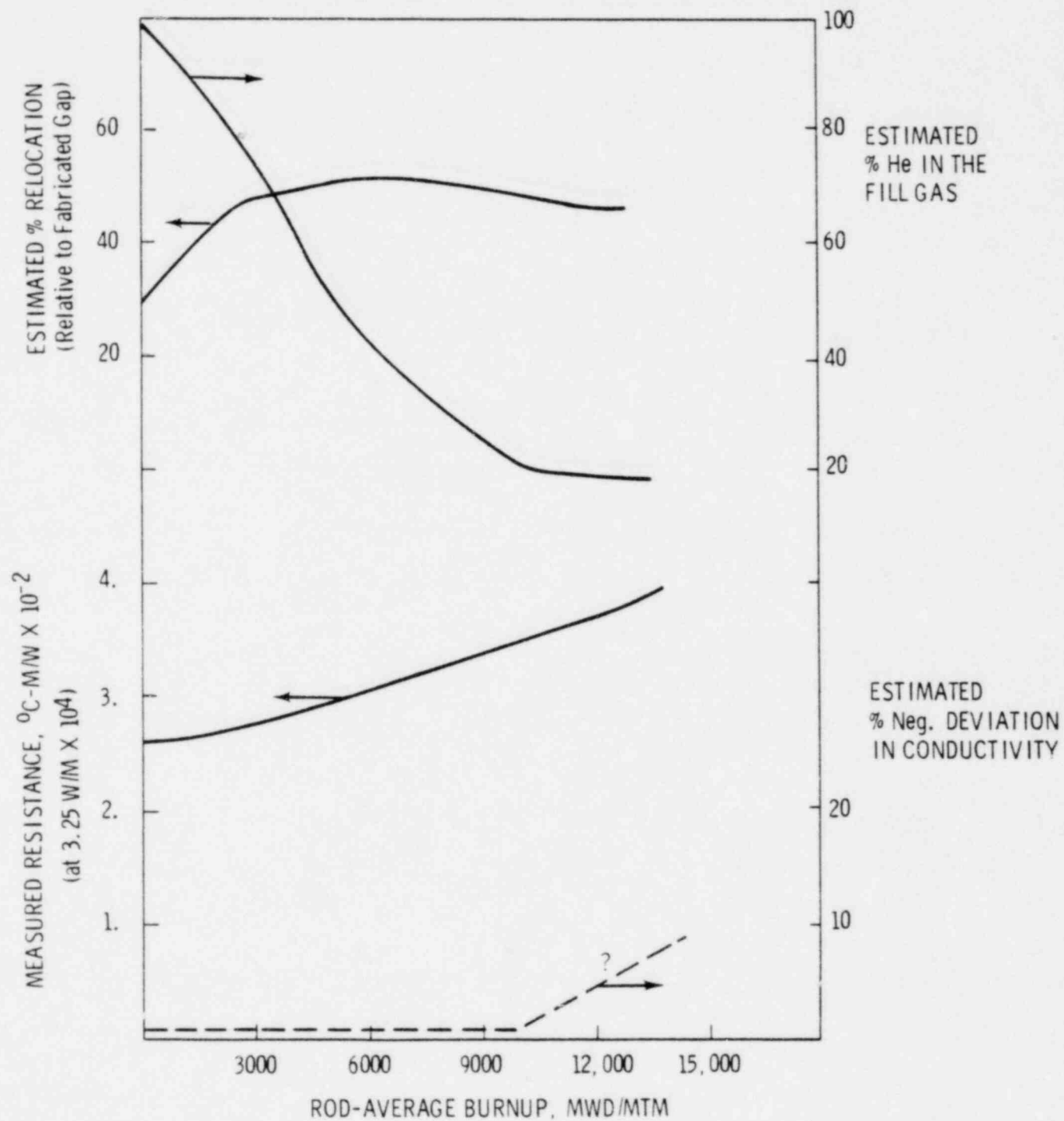


FIGURE 29. Estimated Life History for Rod 1 (Lower Thermocouple)

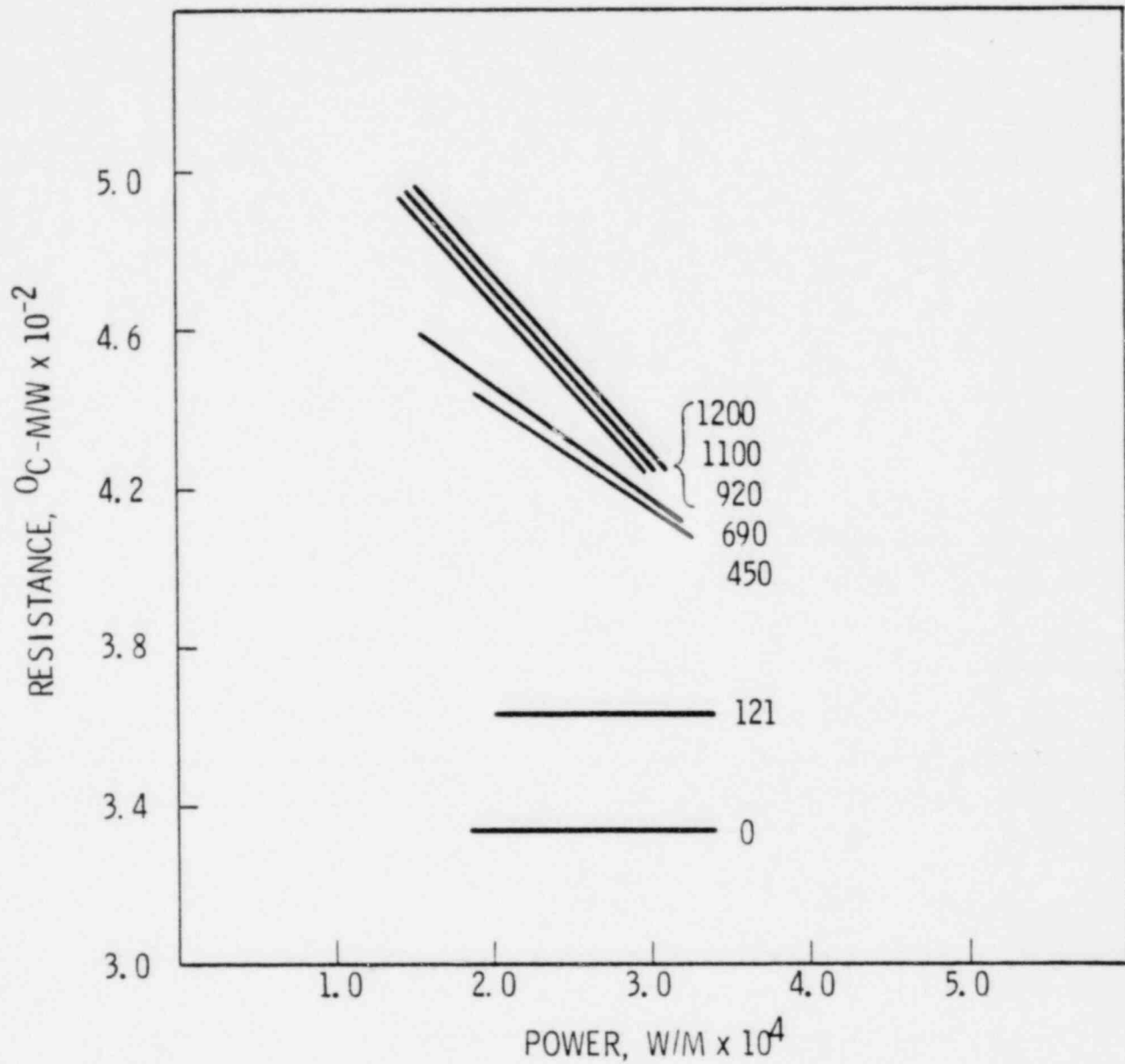


FIGURE 30. Resistance vs. Power Data Trends for Rod 2, IFA-432 (Lower Thermocouple). The numbers refer to burnup in units to Gj/KgU. The numbers refer to "choices" in Table 8

larger gap. (a) The resistance curves for both rods rise and become negatively sloped with increasing burnup; however, the rate of rise with burnup is much faster for rod 2. The curves above 900 GJ/kgU burnup (10,000 MWd/MTM) are all very similar to one another and to the final (1200 GJ/kgU) curve for rod 1.

The above trends in the R-P curves are confirmed by the transient temperature/power slope data. Table 7 assembles these data for Rod 2. By comparing it with similar Table 5 for rod 1, we see the rod 2 slope ratios falling much faster. There are detectable differences, however, in the mechanism leading to the similar resistance curves and slope ratios at the 1200 GJ/kg (Run 100) mark.

The more rapid rise in resistance vs. burnup experienced by rod 2 can be explained on the basis of enhanced fission gas release rate. Enhanced gas release is certainly probable, due to the higher temperatures experienced initially by rod 2. The fact that rod 2 resistances are very similar after 420 GJ/kgU (5,000 MWd/MTM) and identical after 900 GJ/kgU (10,000 MWd/MTM) is probably due to enhanced fuel relocation. Fuel relocation would also be enhanced by higher initial temperatures, since more thermal expansion of the inner fuel would be experienced. In any case, fission gas release, as we shall see, appears to have been inhibited beyond 500 GJ/kgU.

Figures 31-37 show the data scatter for the R-P response of rod 2, together with various calculated responses, at each representative burnup. The numbers identifying each calculated resistance curve refer to choices of input conditions. Table 8 includes these conditions and the resulting calculated temperature/power slope ratio for each choice of input conditions. The transient data are a little more definitive than the R-P plots in most cases. The underlined choices in Table 8 represent the combinations which most nearly match the data slope ratio.

---

(a) Refer also to Figure 13.

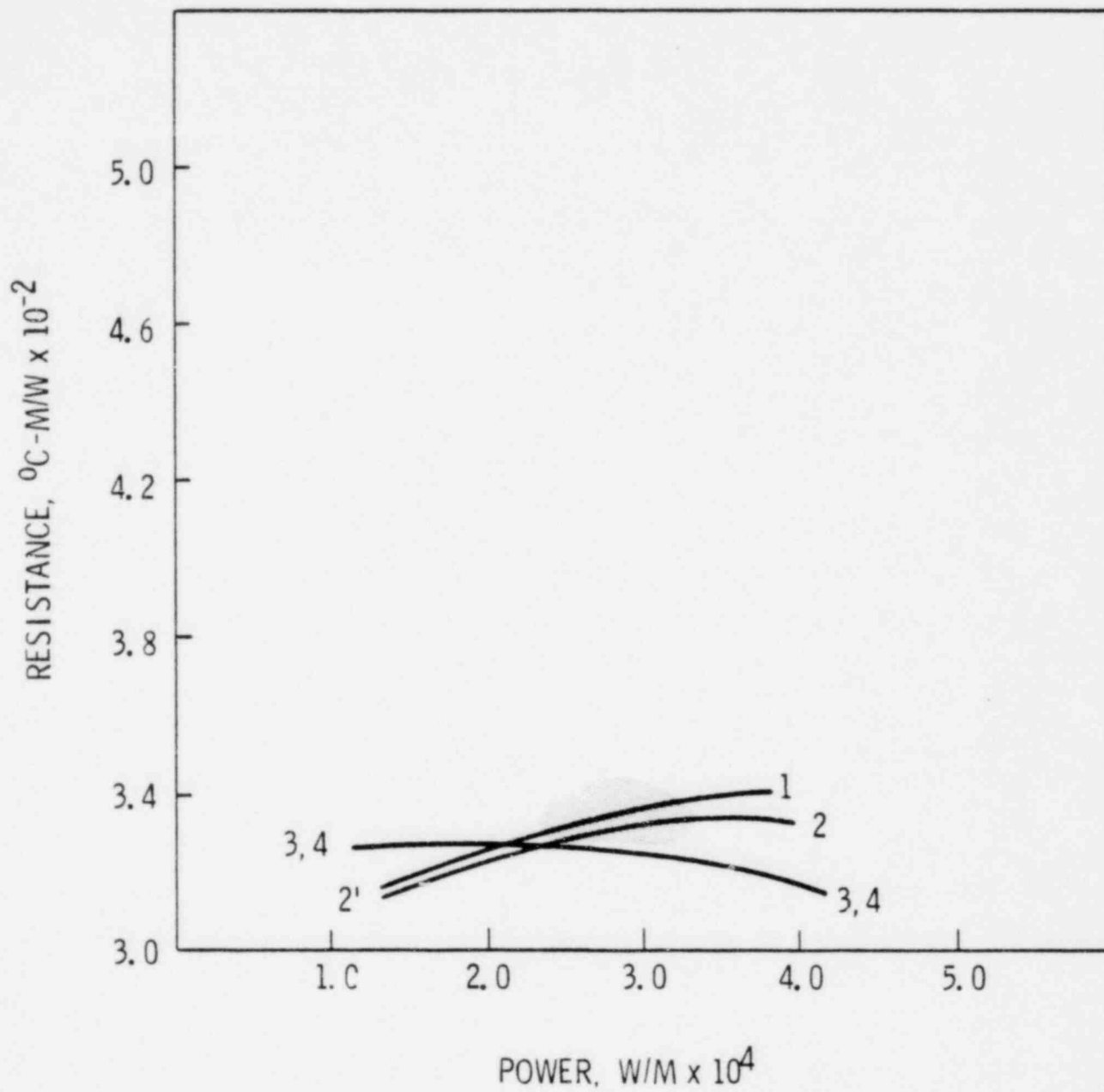


FIGURE 31. R-P Calculated Responses for Rod 2 at 0 GJ/kgU (Run 31).

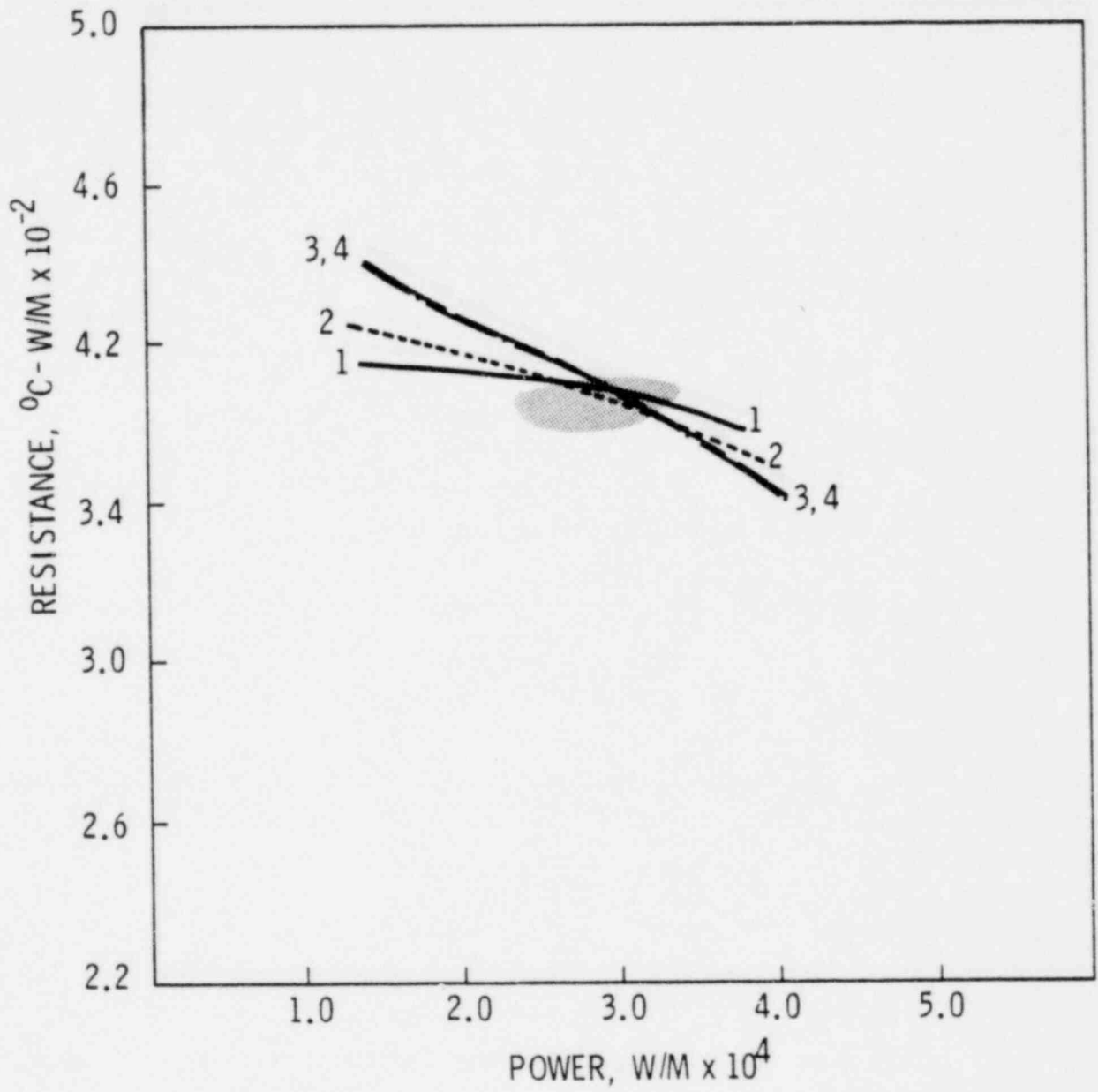


FIGURE 32. Data and Calculated R-P Responses for Rod 2 at 121 Gj/kgU (Run 43)

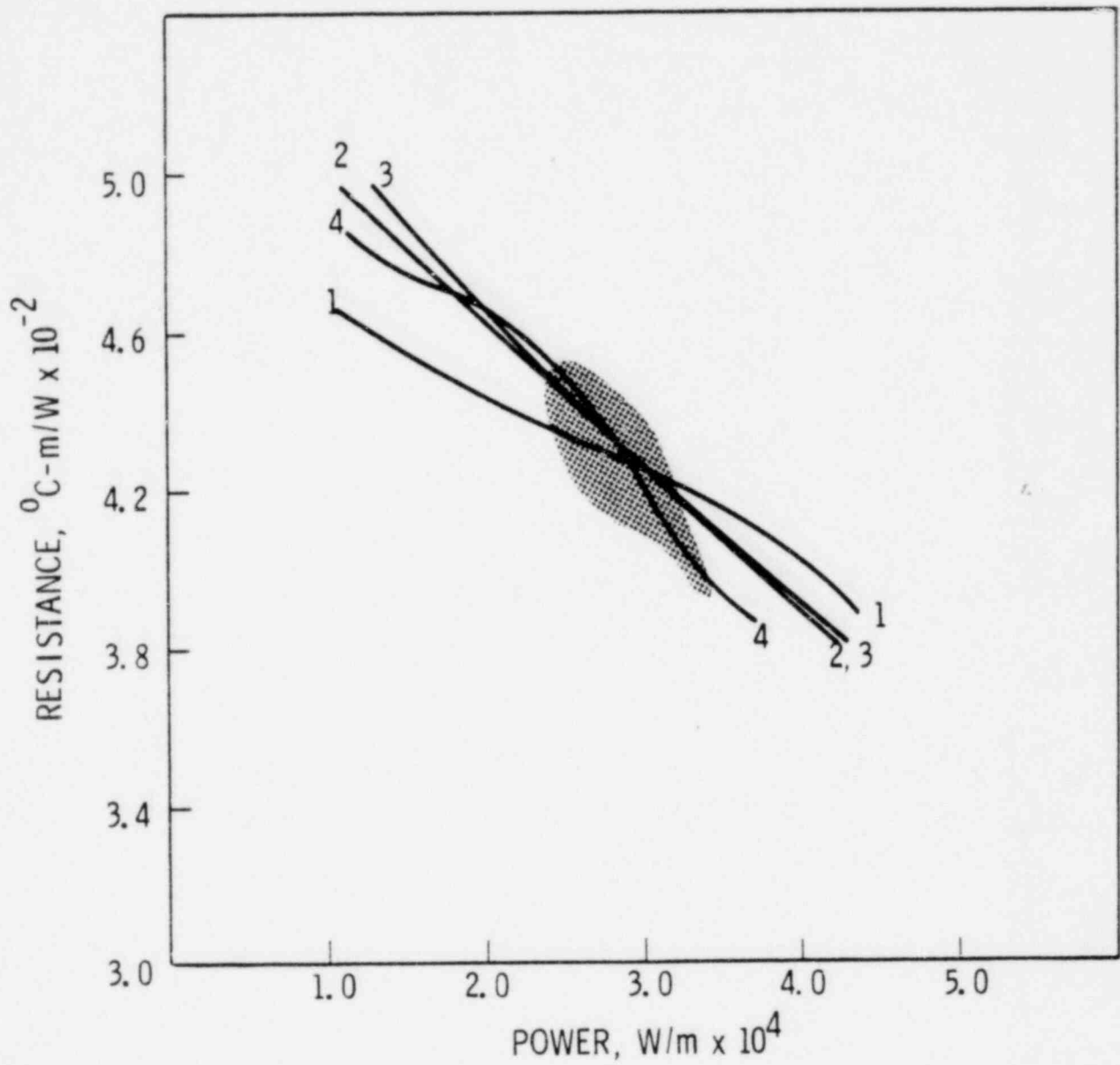


FIGURE 33. Data and Calculated R-P Responses for Rod 2 at 450 Gj/kgU (Run 62)

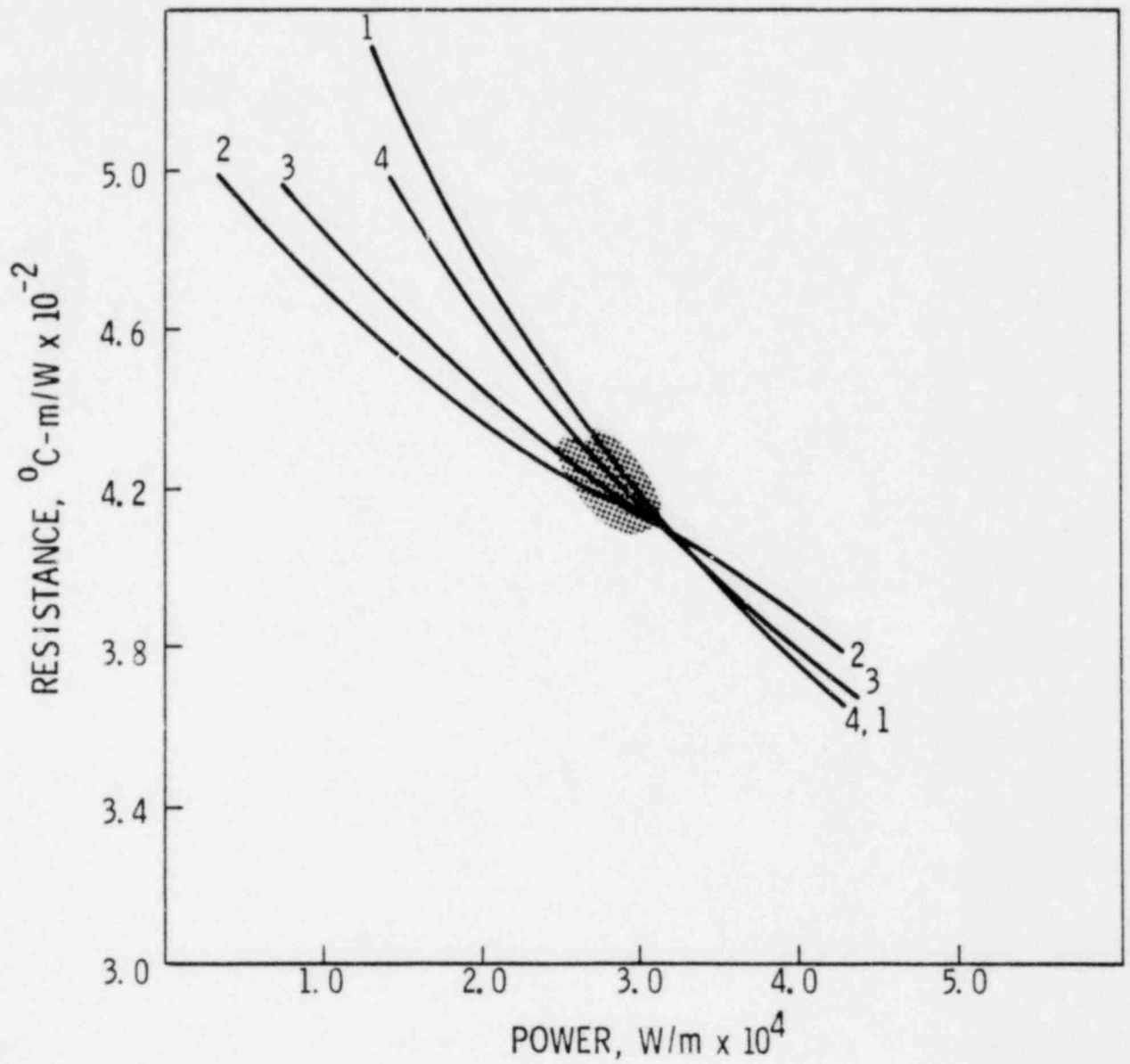


FIGURE 34. Data and Calculated R-P Responses for Rod 2 at 690 GJ/kgU Burnup (Run 68)

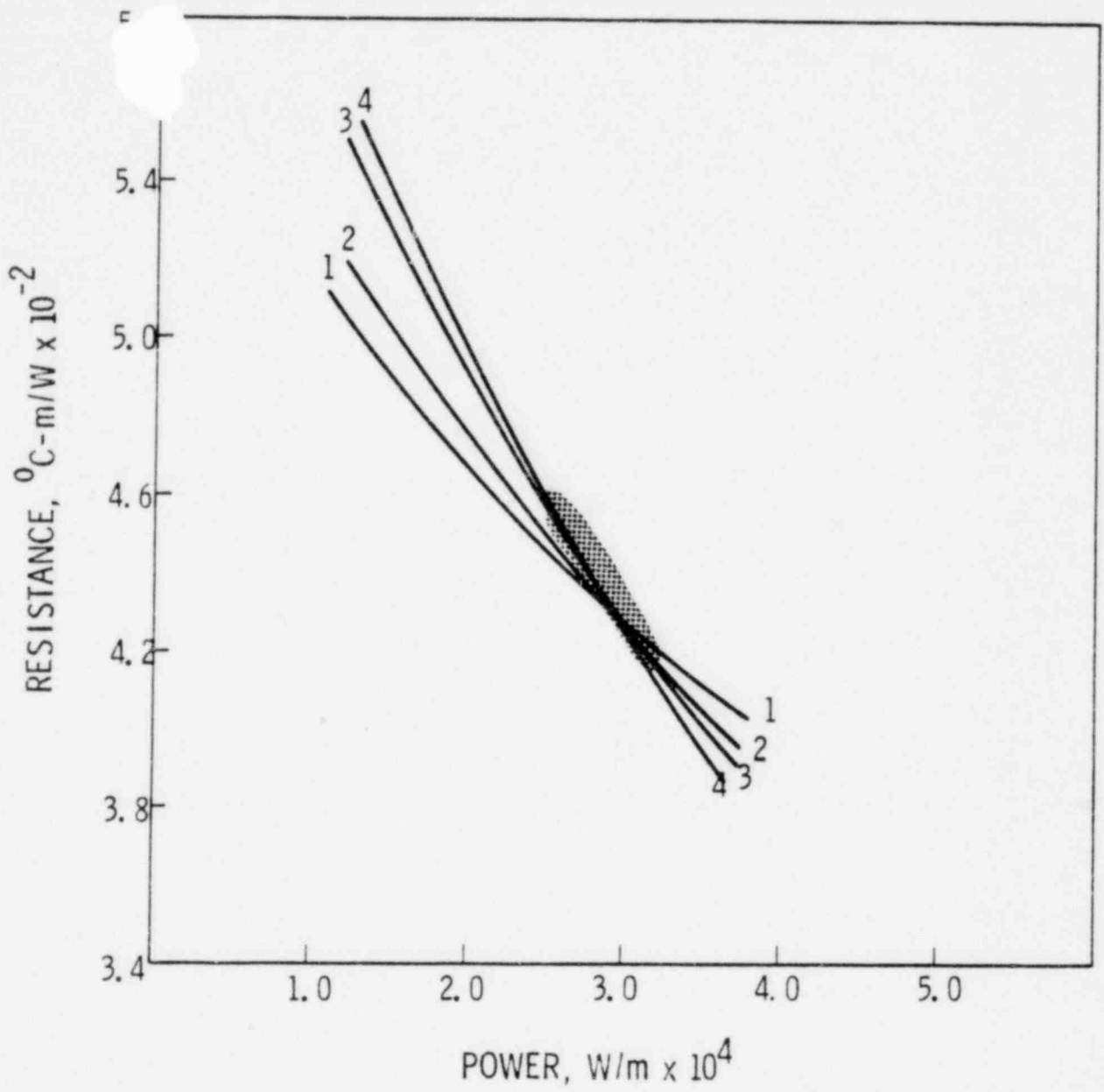


FIGURE 35. Data and Calculated R-P Responses for Rod 2 at 920 Gj/kgU (Run 84)

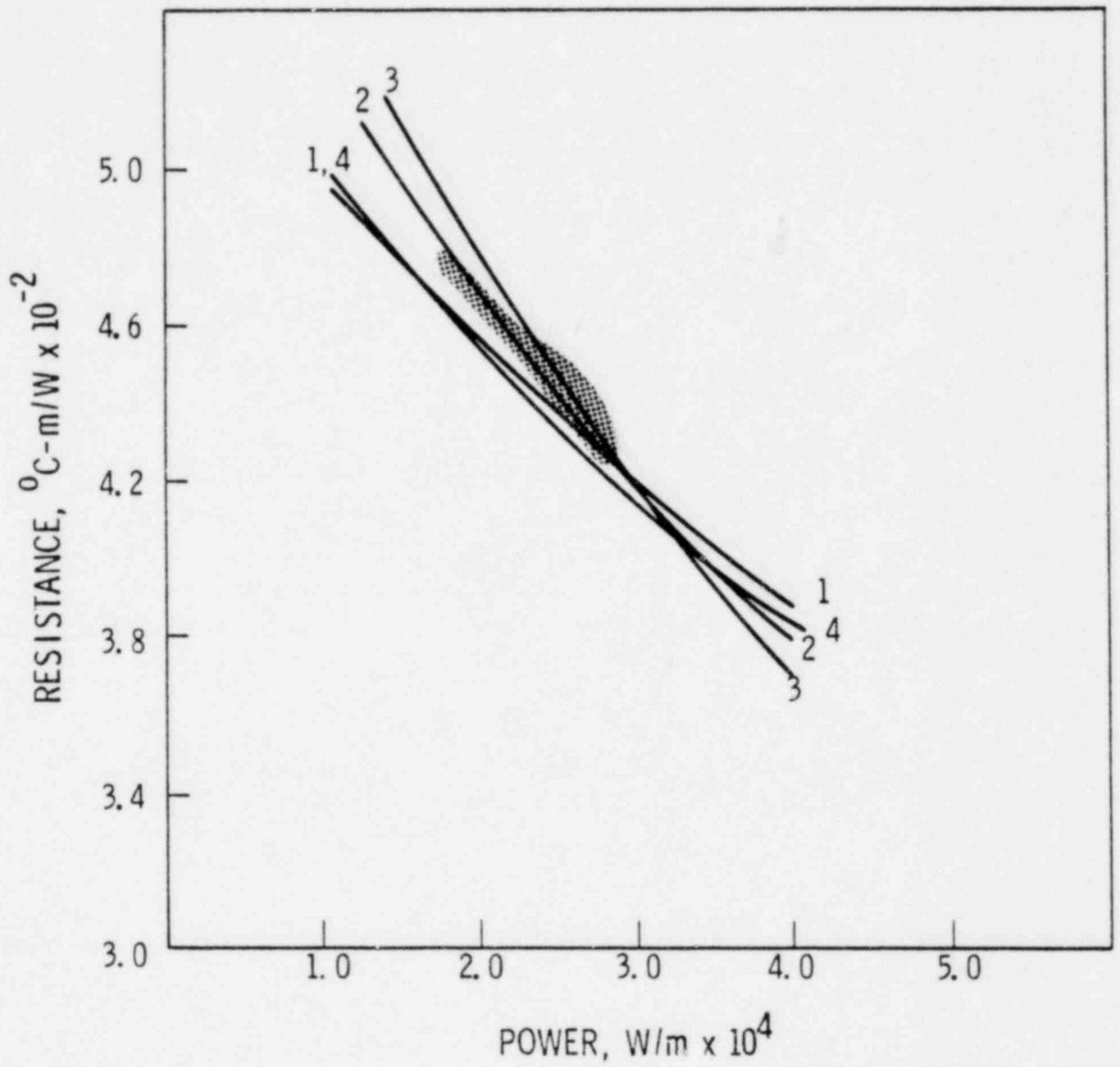


FIGURE 36. Data and Calculated R-P Responses for Rod 2 at 1100 Gj/kgU (Run 92)

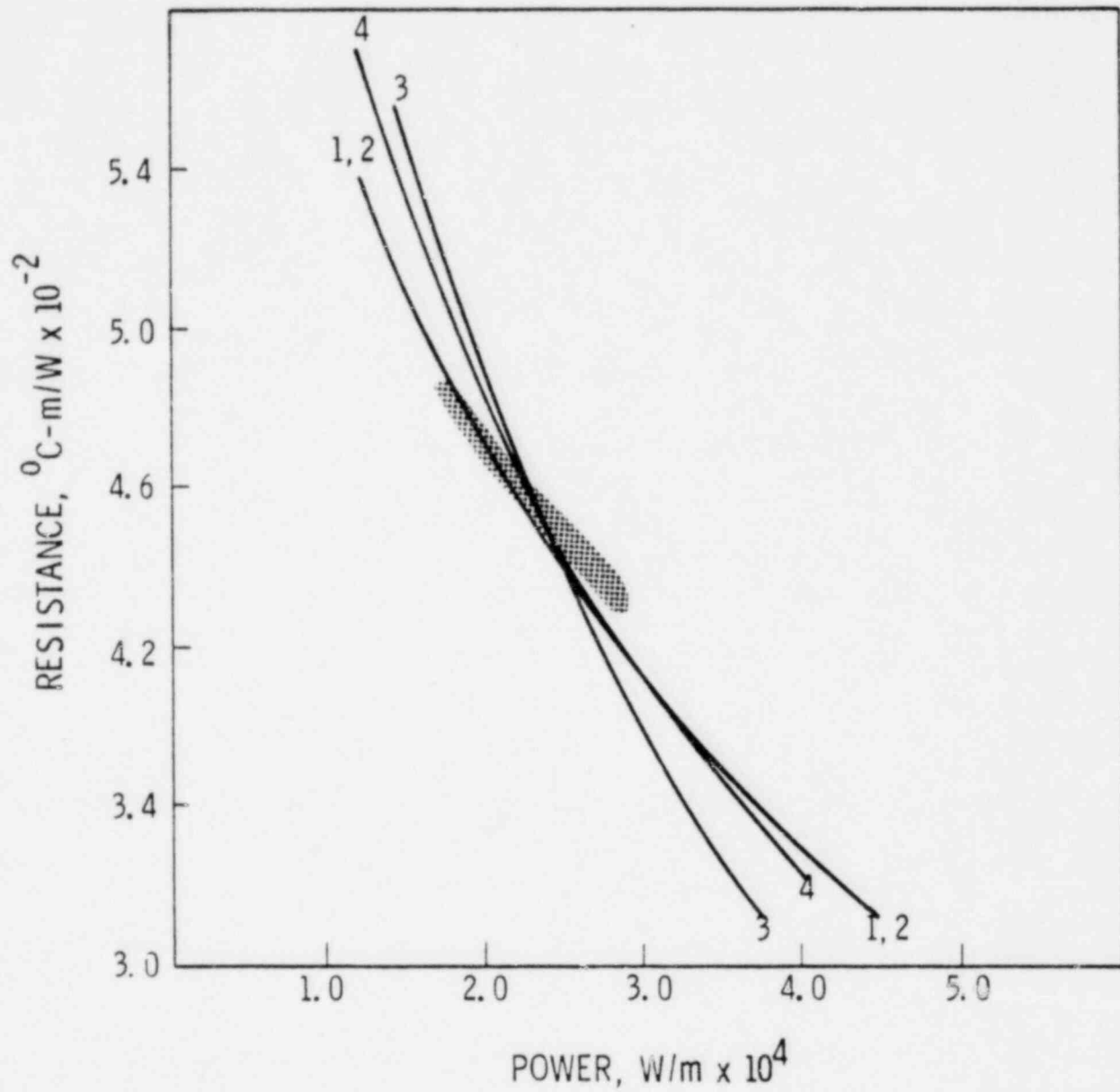


FIGURE 37. Data and Calculated R-P Responses for Rod 2 at 1200 Gj/kgU (Run 100)

TABLE 7. Rod 2 Data for Temperature/  
Power Slope Ratios

<u>Run Number</u>	<u>Slope Ratios</u>
31	1.05
43	0.83
62	0.56
68	0.68
84	0.49
92	0.61
100	0.62

Rod 2 appears to "saturate" at  $70 \pm 5\%$  fission gas in the gap and  $55 \pm 5\%$  fuel relocation. Figure 38 is the graph of information in Table 8 and includes the measured ( $3.25 \text{ W/m} \times 10^4$ ) resistance as a function of burnup, and the estimated development of gas release and fuel relocation (assuming there is no conductivity degradation).

Neither the steady-state nor transient data were definitive enough to limit the possible fuel conductivity degradation closer than -20%. This shortcoming is typical of data from large-gap rods. We shall see in the next section that a small gap rod is more definitive with respect to fuel conductivity.

#### Rod 3

The small-gap rod, 3, had a life history somewhat different than rods 1 and 2. The small gap resulted in high conductance and relatively low center-line temperatures at power. Both the upper and lower thermocouples have survived to date. The resistance (at  $3.25 \text{ W/m} \times 10^4$  versus burnup for the lower thermocouple position in Figure 39. The change in resistance over the full burnup range is rather small. Therefore, we will only examine data from the rod's BOL and the 14,000 MWd/MTM (1200 GJ/kgU) mark. These burnups correspond to transient runs 31 and 100, respectively.

TABLE 8. Measured and Calculated Temperature/Power Slope Ratios for Rod 2

Run Number	Measured Slope Ratio ( $\pm 2\sigma$ )	Choice 1		Choice 2		Choice 3		Choice 4	
		Slope Ratio	Conditions						
31	1.05 $\pm$ 0.08	1.01	100,32,0	1.01	100,52,-20	0.94	80,53,0	0.95	80,65,-20
43	0.83 $\pm$ 0.08	0.89	80,40,0	0.86	70,48,0	0.83	60,53,0	0.82	60,62,-20
62	0.56 $\pm$ 0.08	0.705	70,29,0	0.65	50,44,0	0.65	50,52,-20	0.57	30,55,0
68	0.68 $\pm$ 0.05	0.67	30,56,0	0.762	60,2,0	0.74	50,25,-20	0.70	40,51,0
84	0.49 $\pm$ 0.03	0.57	50,44,0	0.57	40,50,0	0.54	30,54,0	0.52	25,56,0
92	0.61 $\pm$ 0.03	0.751	50,46,0	0.703	40,51,0	0.60	30,56,0	0.751	50,54,-20
100	0.62 $\pm$ 0.03	0.59	30,56,0	0.59	30,61,-20	0.45	10,64,0	0.55	20,60,0

(a) The entries under each choice represent % helium, fuel relocation (as a percent of initial fabricated gap), and percent deviation from the Lyons  $UO_2$  thermal conductivity equation. Underlined entries represent the most probable choices in the light of the present data.

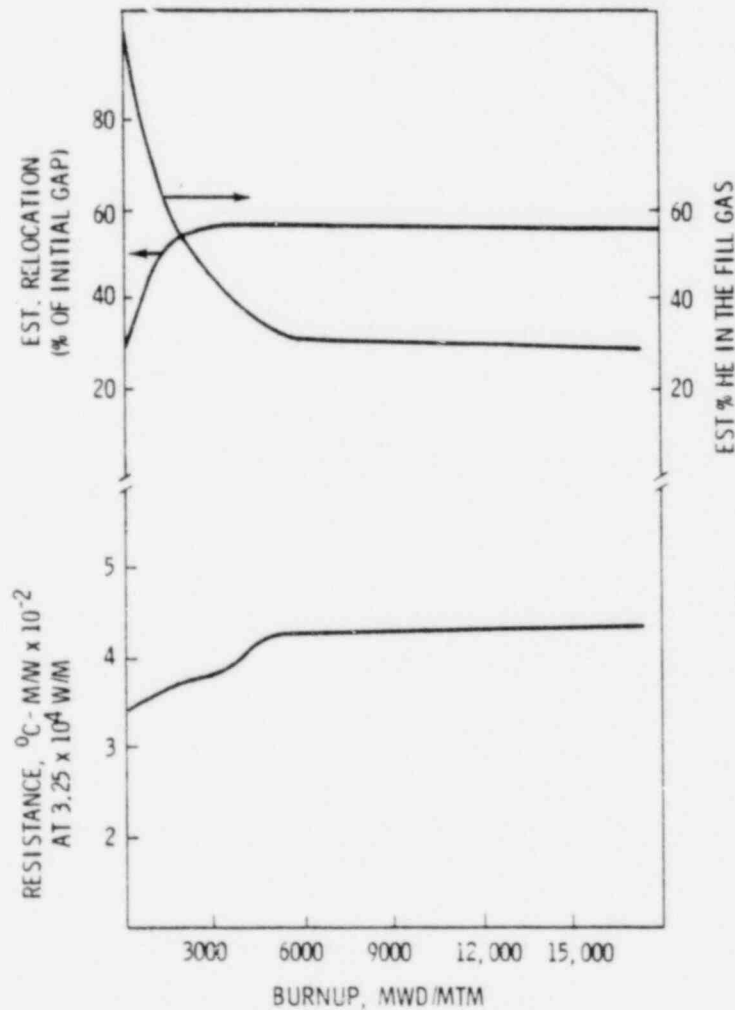


FIGURE 38. Estimated Life History of Rod 2, IFA-432

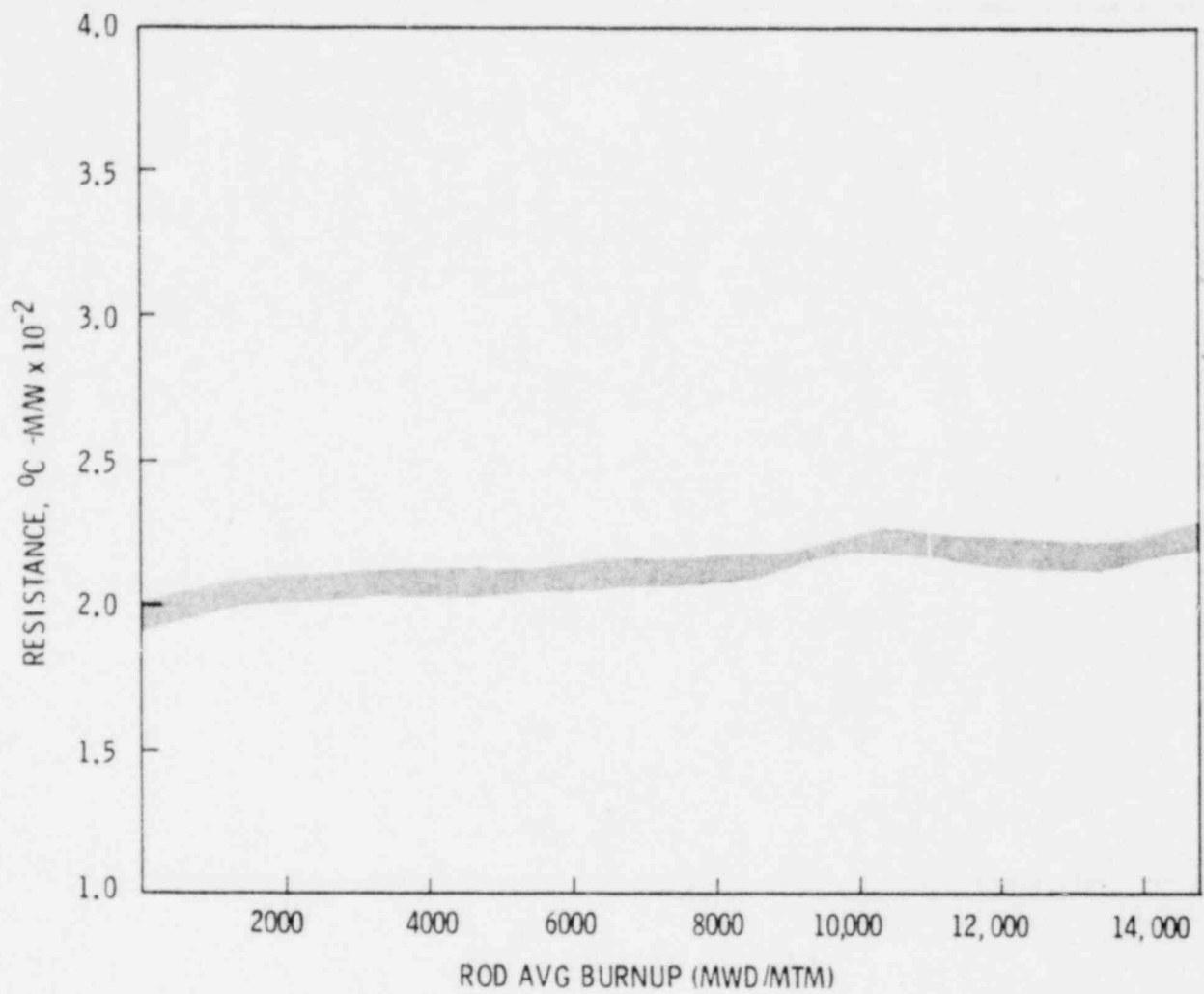


FIGURE 39. Resistance vs. Burnup for Rod 3, IFA-432 (Lower Thermocouple)

The resistance vs. power plots for these two burnups appear in Figure 40. In this case, we show the data scatter from both the upper and lower thermocouples. The increase in resistance with burnup is slight, but still significant relative to the data scatter. Notice also that the curvature of the R-P plot has not changed over the burnup range. This fact will be important as we try to sort out the *cause* of the resistance increase.

There are at least 2 potential causes of the apparent increase in resistance. We will attempt to use our analysis technique to decide which of these is the cause:

- The increase is not real at all, but is due to thermocouple decalibration.
- The increase is due to fission gas release or fuel thermal conductivity degradation, or some combination of the two.

First let us attempt to ascertain the BOL conditions. We will assume 80-100% He in the gap and try to pin down the initial amount of fuel conductivity degradation, if any.<sup>(a)</sup>

Table 9 lists both the various choices for the gas mixture, fuel relocation, and fuel conductivity, and the temperature/power slope ratios which they produce. The calculated R-P response produced by these choices is plotted in Figure 41 for the BOL (run 31) case. It is apparent from Figure 41 that assumed fuel conductivity degradation of 10% or greater leads to calculated R-P response that does not hit any target within the data scatter. In fact, it seems unlikely that there is any degradation of the effective conductivity of this rod at BOL.

Now let us go to the high burnup case. The data and R-P calculated responses are shown in Figure 42, for the various choices listed in Table 9. First note — there are two extreme cases: (1) no fission gas release, plus large conductance degradation (choice 3) and (2) considerable fission gas release and no thermal conductivity degradation (choice 2). Both of these cases lead to R-P response that does not match the data well. On the other

---

(a) For this small-gap, He-filled rod, the choice of relocation is arbitrary, due to the similar high values of conductance attained at power for any relocation choice.

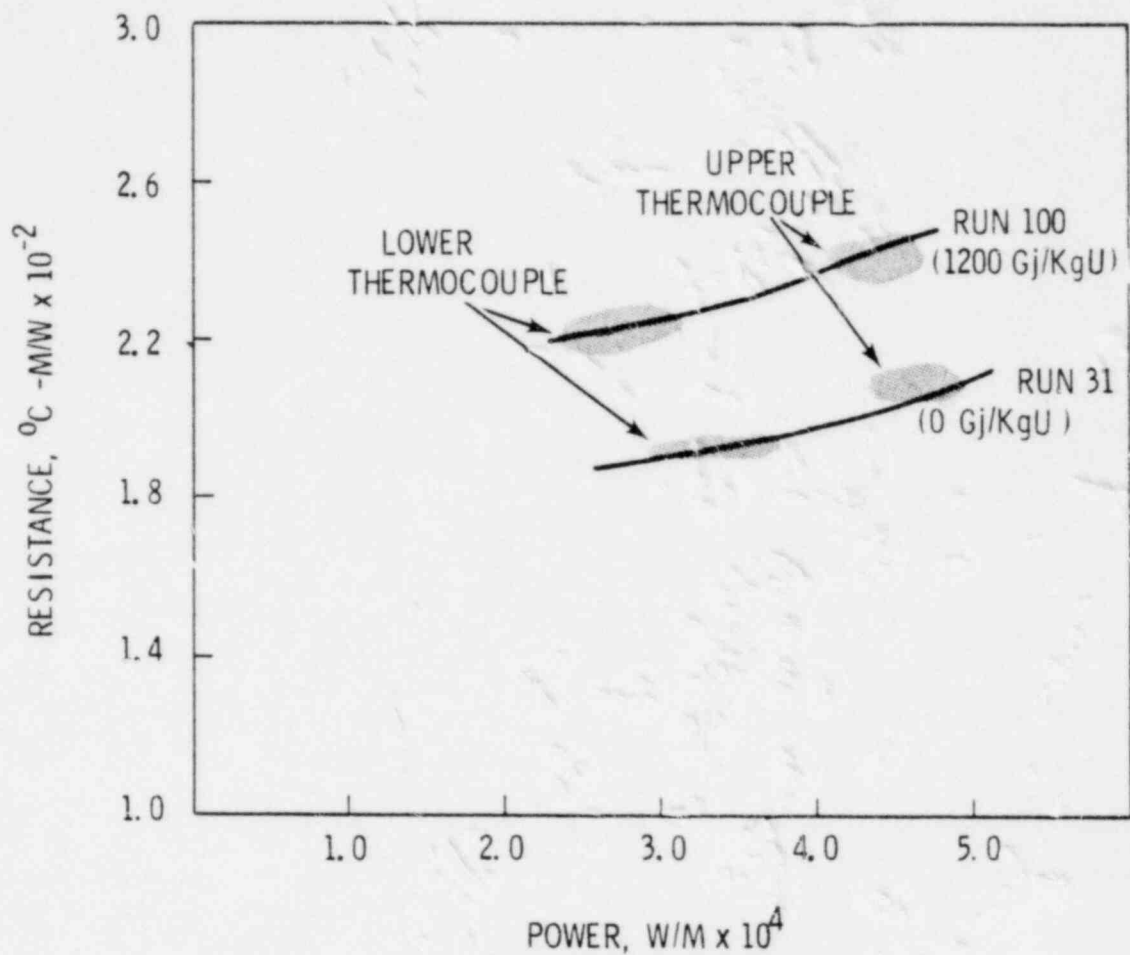


FIGURE 40. Data for Rod 3, IFA-432

TABLE 9. Measured and Calculated Temperature/Power Slope Ratios for Rod 3

Run Number	Measured Slope Ratio	Choice 1		Choice 2		Choice 3		Choice 4	
		Slope Ratio	Conditions	Slope Ratio	Conditions	Slope Ratio	Conditions	Slope Ratio	Conditions
31	1.13±0.10	<u>1.13</u>	<u>100,30,0</u>	1.12	80,80,0	--	100,60,-20	--	100,85,-10
100	0.90±0.05	0.98	60,0,-4	<u>0.96</u>	10,50,0	1.04	100,50,-10	<u>0.94</u>	<u>40,27,0</u>

(a) The entries under each choice represent % helium, fuel relocation (as a percent of initial fabricated gap), and percent deviation from the Lyons UO<sub>2</sub> thermal conductivity equation. Underlined entries represent the most probable choices in the light of the present data.

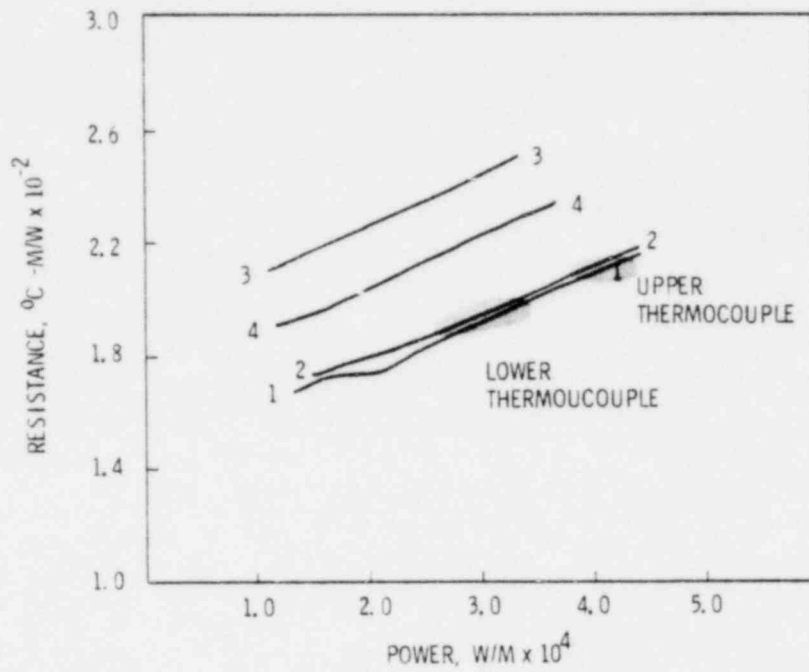


FIGURE 41. Data and Calculated R-P Responses for Rod 3 at 0 GJ/kgU. The numbers refer to choices of conditions listed in Table 10.

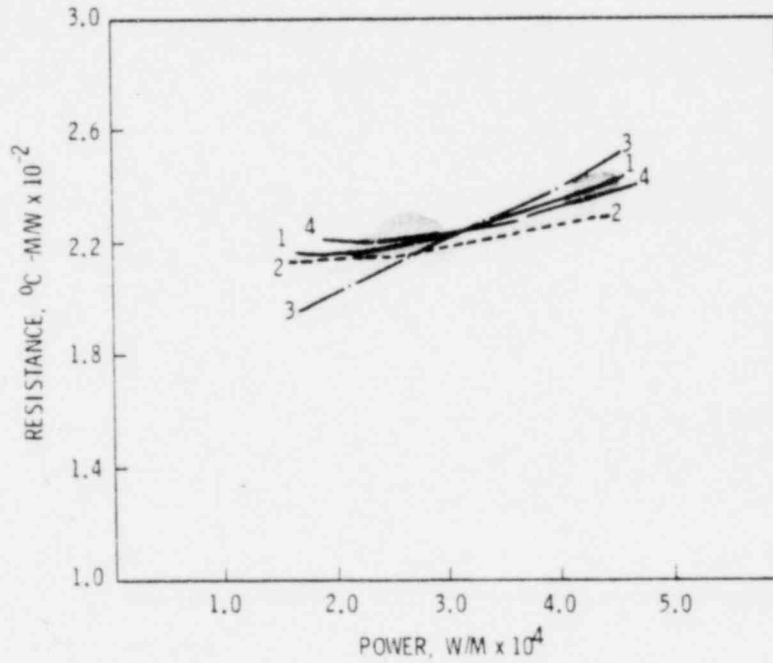


FIGURE 42. Data and Calculated R-P Responses for Rod 3 at 1200 GJ/kgU Burnup

hand, each of the intermediate choices, 1 and 4, match the R-P curvature. Case 4 looks particularly good with respect to temperature/power slope prediction. So in answer to the second question, it appears that fission gas release is the main cause of the resistance increase.

As to the first question (thermocouple decalibration), one can only point to the consistency of match between calculated and measured slope ratios for those combinations of variables which also match the R-P plots. Decalibration could reasonably be expected to affect the steady-state and transient data in different ways, as discussed in Appendix A.

#### Rod 6

The lower thermocouple of rod 6 has survived to date, permitting an analysis of rod 6 history. The R-P data trends for the seven representative burnups are shown in Figure 43. We see that the resistance history is similar to rod 2, in that there is a large increase in resistance early in life, followed by practically no change after 900 GJ/kgU (10,000 MWd/MTM). The measured temperature/power slope ratios obtained from the 7 linear power drops are listed in Table 10. We see a rapid drop in the ratio, which corroborates the rapid rise in gap resistance indicated by the R-P plot, similar to rod 2.

TABLE 10. Measured Temperature/Power Slope Ratios for Rod 6

<u>Run Number</u>	<u>Burnup GJ/kgU</u>	<u>Measured Slope Ratio</u>
31	0	1.16
43	121	0.97
62	450	0.70
68	690	--
84	920	0.51
92	1100	0.55
100	1200	0.60

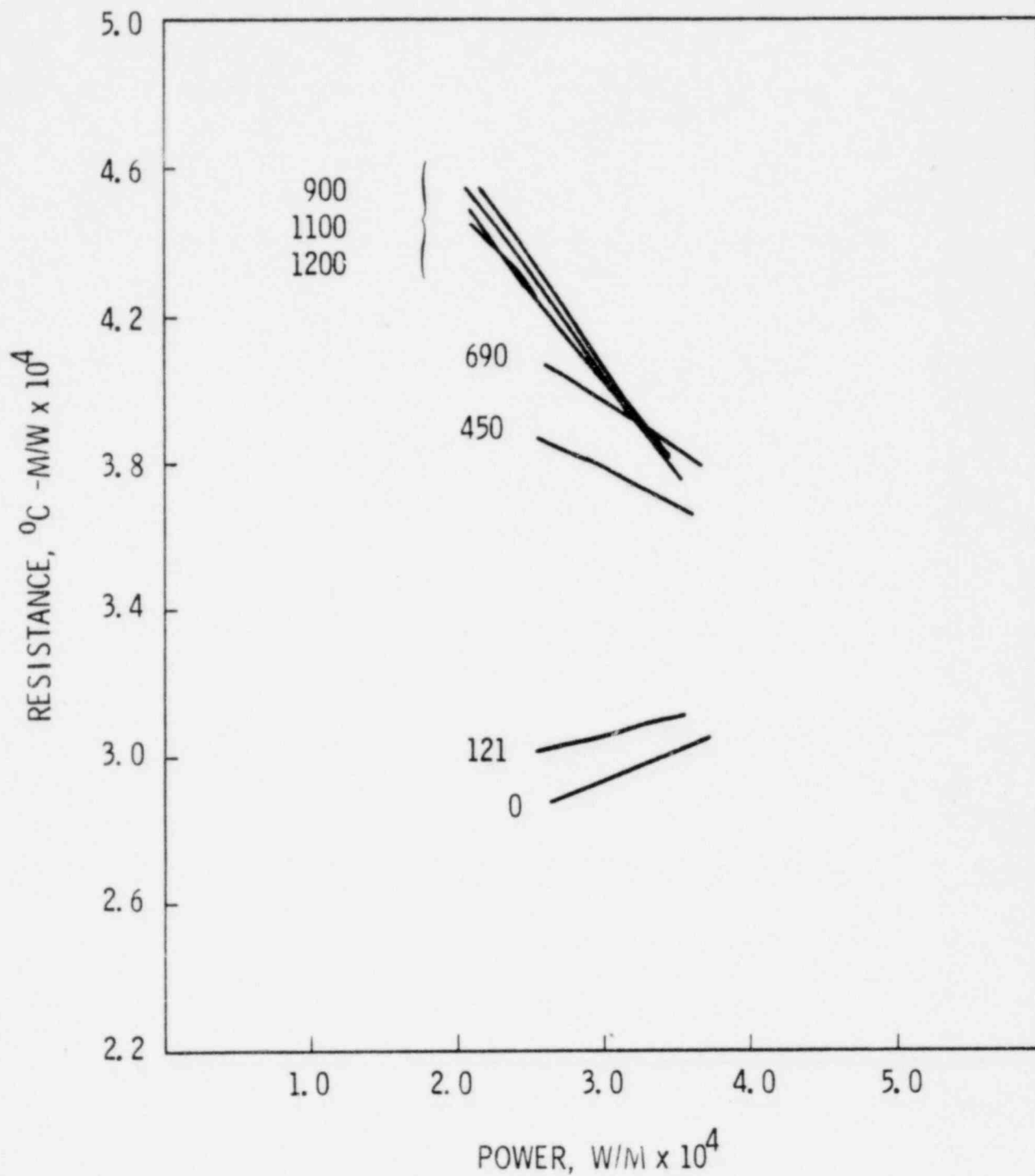


FIGURE 43. R-P Data Trends for Rod 6, IFA-432. The numbers indicate burnup in Gj/kgU

There is a unique feature about this rod, however. Notice that at BOL, the resistance is *rising* as a function of power, and correspondingly, the temperature/power slope ratio is significantly greater than unity. Such behavior is typical of a closed-gap rod. But to have the *magnitude* of the resistance this rod has with helium fill and a closed gap, the conductivity of the fuel would have to be considerably less than that of the 95% theoretical density (TD), stable fuel present in rods 1 and 2. The fuel for rod 6 was 92% TD, and made "unstable" with respect to densification by incomplete sintering, so that in-reactor sintering would occur and its effect could be studied. The ex-reactor measured thermal conductivity for this atypical rod 6 fuel was indeed lower than for the 95% TD stable fuel, as described in reference 5. The two different conductivities are shown vs. temperature in Figure 44. But this difference alone cannot account for the R-P behavior of rod 6; as indicated in Figure 45. We can only conclude that additional degradation of the conductivity took place, perhaps due to randomly oriented cracking from different sintering rates at various points in the fuel.

Let us attempt to be quantitative about the extent of degradation of fuel conductivity at BOL. Consider Table 11, which calculated temperature/power slope ratios for the various runs, and the combinations of variables that were produced. Concentrating on the BOL (Run 31) conditions, we see that a reduction in conductivity (from the Lyon's equation of 95% TD fuel) of 30 to 40% is required to obtain a reasonable match to the data (with helium in the gap). The various choices are plotted in Figure 46, along with the data scatter from both the upper and lower thermocouples. We see that *only* with helium in the gap do we get the proper curvature. All this points to a conductivity degradation of about 35%.

Moving on to conditions for runs 43 and 62 (Figures 47 and 48), we see that the choice of 35% for conductivity degradation is certainly reasonable, although the data are not so definitive. Transient data are lacking for run 68. Various choices for variable combinations are listed in Table 11, and the R-P responses are shown relative to the resistance data in Figure 49. Again, the assumption of 35% conductivity degradation does appear reasonable.

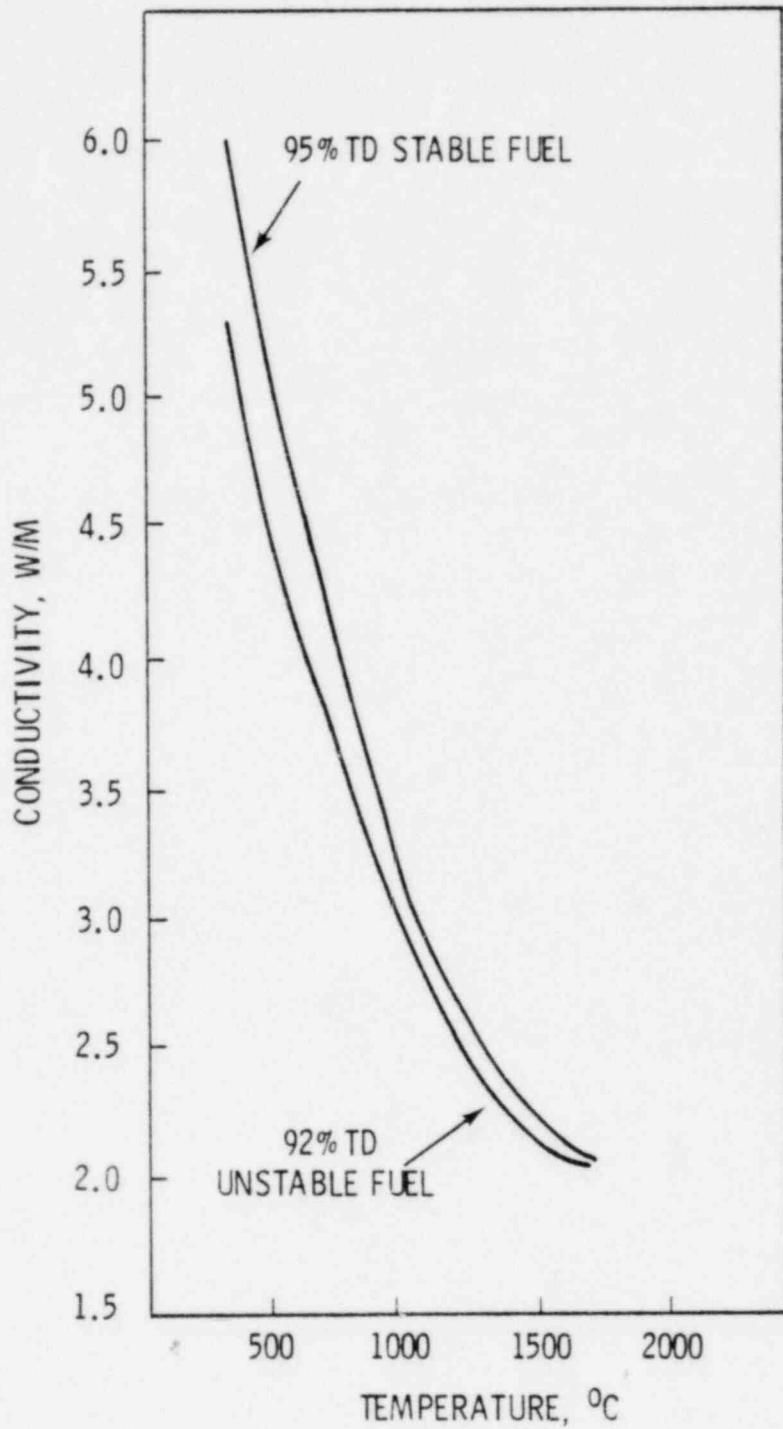


FIGURE 44. Trends of Ex-Reactor Data for Rod 1 and Rod 6 Fuel Conductivity

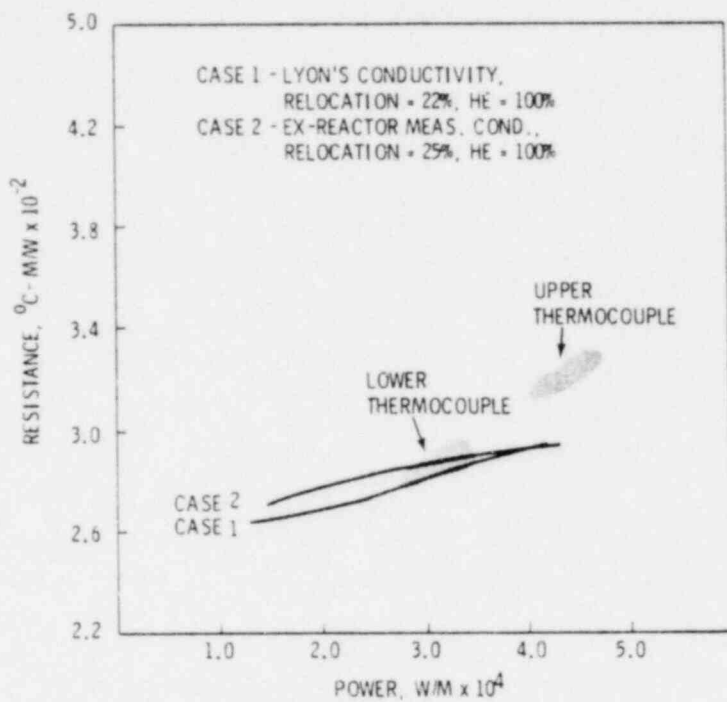


FIGURE 45. Data and Calculated R-P Responses for Rod 6, IFA-432 at 0 GJ/kg Burnup

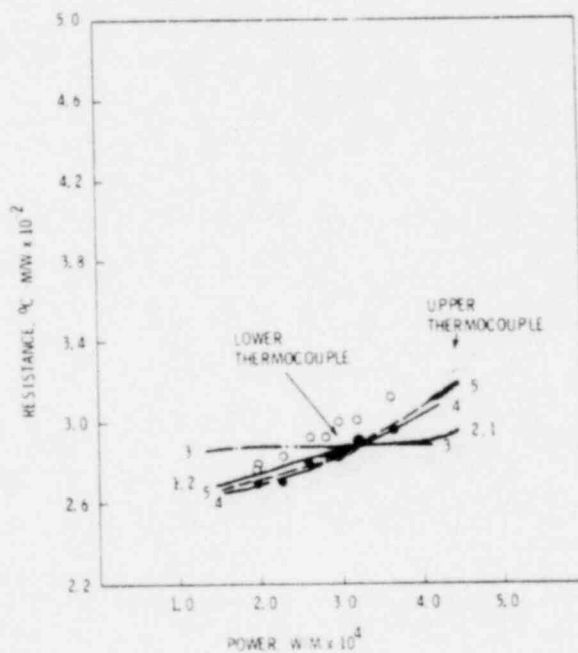


FIGURE 46. Data and Calculated R-P Responses for Rod 6, at 0 GJ/kgU Burnup (Run 31). The numbers indicate choices of conditions listed in Table 12.

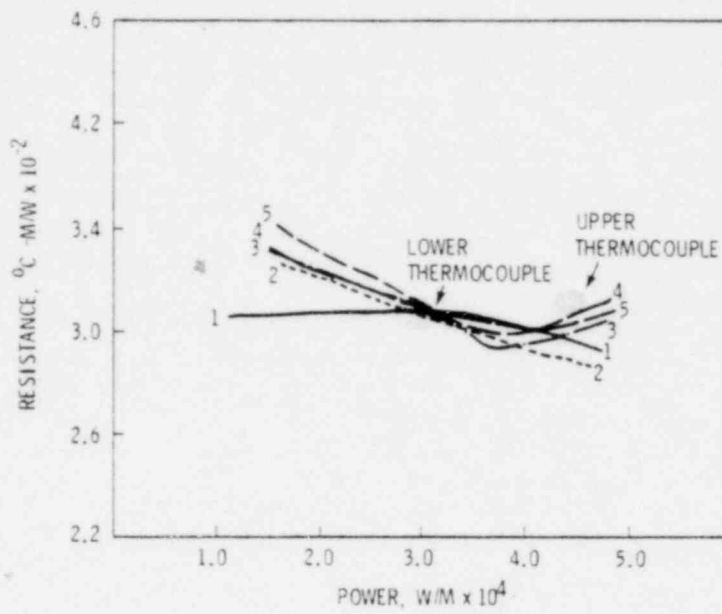


FIGURE 47. Data and Calculated R-P Responses for Rod 6 at 121 GJ/kgU (Run 43)

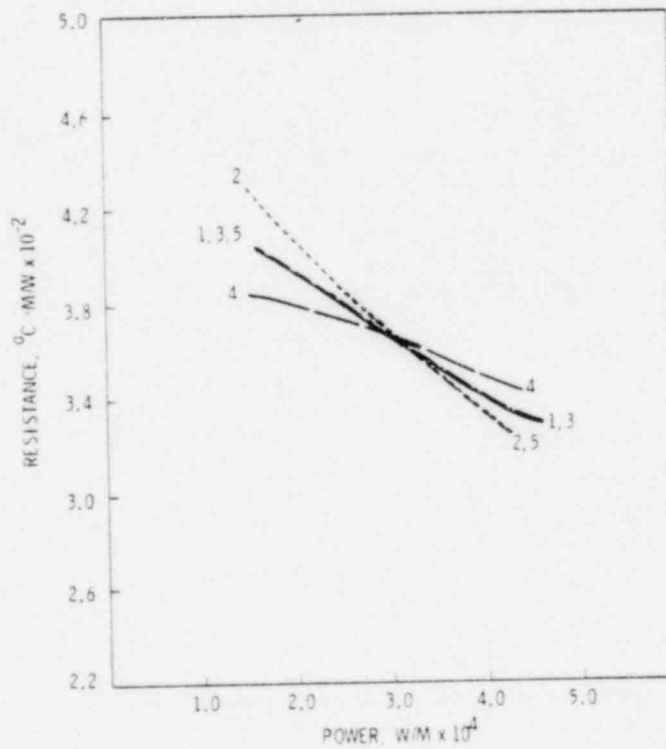


FIGURE 48. Data and Calculated Responses for Rod 6 at 450 GJ/kgU (Run 62)

TABLE 11. Calculated Temperature/Power Slope Ratios for Rod 6, Lower Thermocouple

Run Number	Measured Slope Ratio	Choice 1		Choice 2		Choice 3		Choice 4		Choice 5	
		Slope Ratio	Conditions	Slope Ratio	Conditions	Slope Ratio	Conditions	Slope Ratio	Conditions	Slope Ratio	Conditions
31	1.16	1.01	100,22,0	1.01	100,52,-20	1.08	80,59,-20	<u>1.12</u>	<u>100,90,-40</u>	1.06	100,70,-30
43	0.97	1.24	80,51,-20	1.17	60,44,0	1.16	60,57,-20	1.10	60,60,-20	0.98	<u>60,62,-35</u>
62	0.70	0.67	50,42,-20	0.63	40,45,-20	0.69	50,50,-35	0.73	70,30,-20	0.73	50,31,0
68	(0.58-0.62)	0.78	50,33,-20	0.73	40,28,0	0.66	30,34,0	0.71	40,40,-20	<u>6.61</u>	<u>40,45,-35</u>
84	0.51	0.57	40,36,-20	<u>0.53</u>	<u>30,40,-20</u>	0.58	30,43,-35	0.62	50,20,0	0.54	30,32,0
92	0.55	0.77	50,20,0	<u>0.57</u>	<u>30,45,-35</u>	0.73	40,27,0	0.58	30,40,-20	0.65	30,32,0
100	0.60	0.56	20,37,0	0.56	20,43,-20	0.61	30,40,-20	0.63	35,37,-20	0.62	30,32,0

(a) The entries under each choice represent helium fuel relocation (as a percent of initial fabricated gap), and percent deviation from the Lyons UO<sub>2</sub> thermal conductivity equation. Underlined entries represent the most probable choices in the light of the present data.

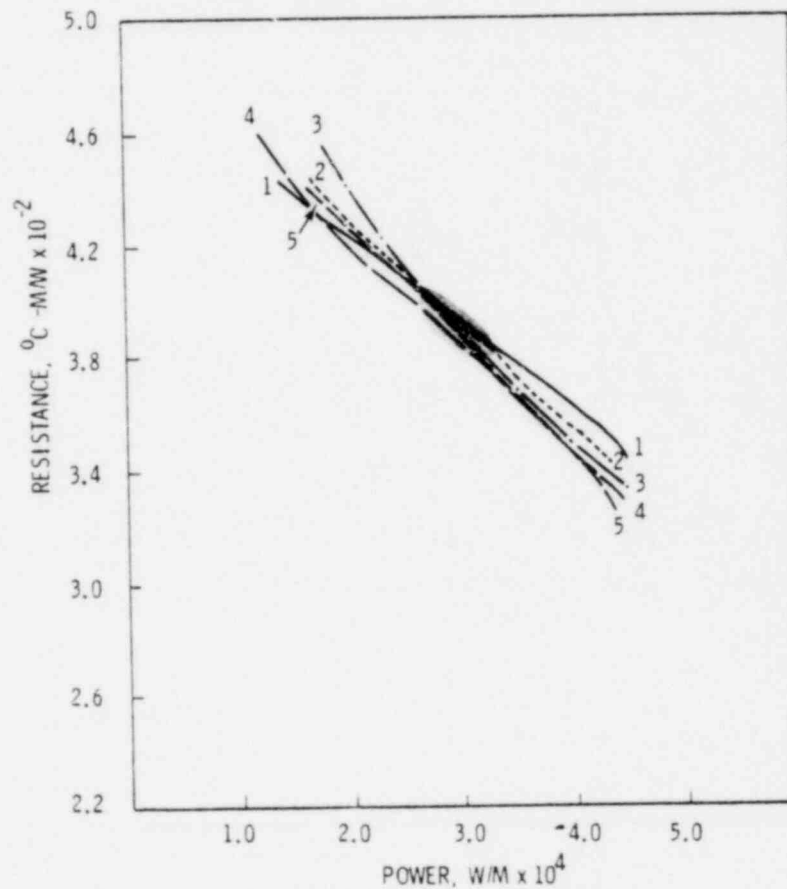


FIGURE 49. Data and Calculated R-P Responses for Rod 6 at 690 GJ/kgU (run 68)

For the higher burnups (Figures 50-52), a conductivity degradation of -20% appears better than -35%. This could be due to the improvement in conductivity with fuel restructuring.

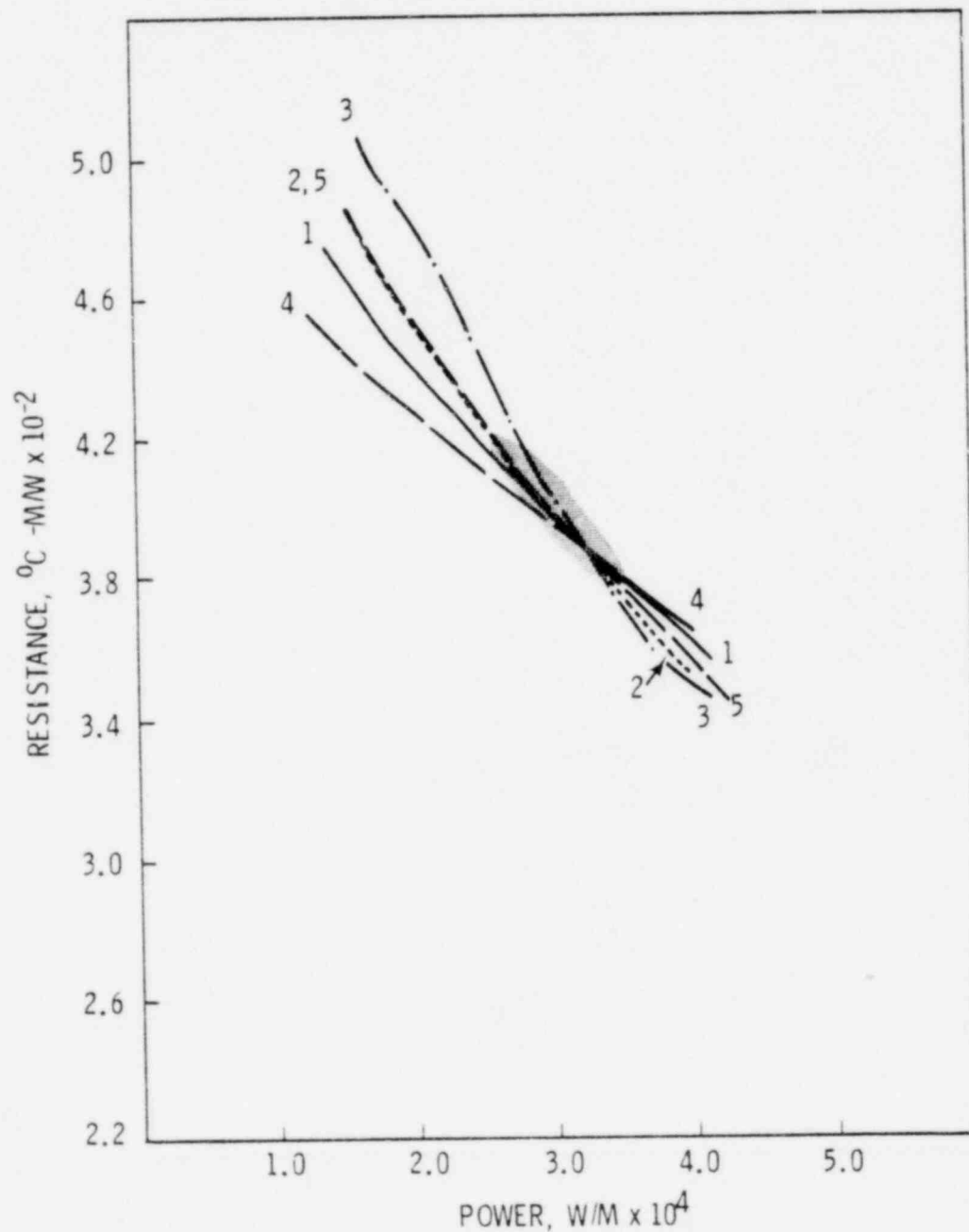


FIGURE 50. Data and Calculated R-P Responses for Rod 6 at 900 GJ/kgU (Run 84)

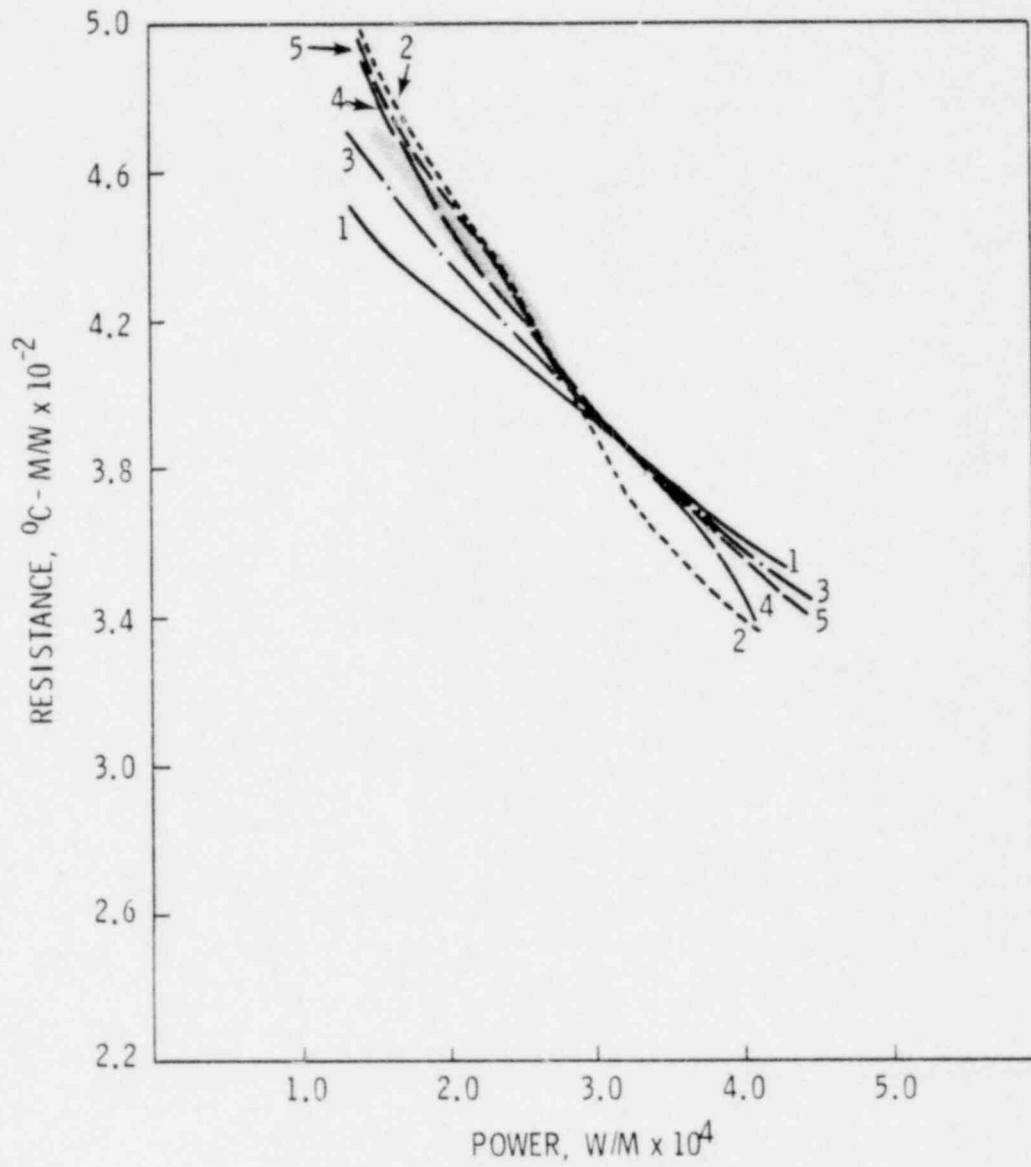


FIGURE 51. Data and Calculated R-P Responses for Rod 6 at 100 GJ/kgU (Run 92)

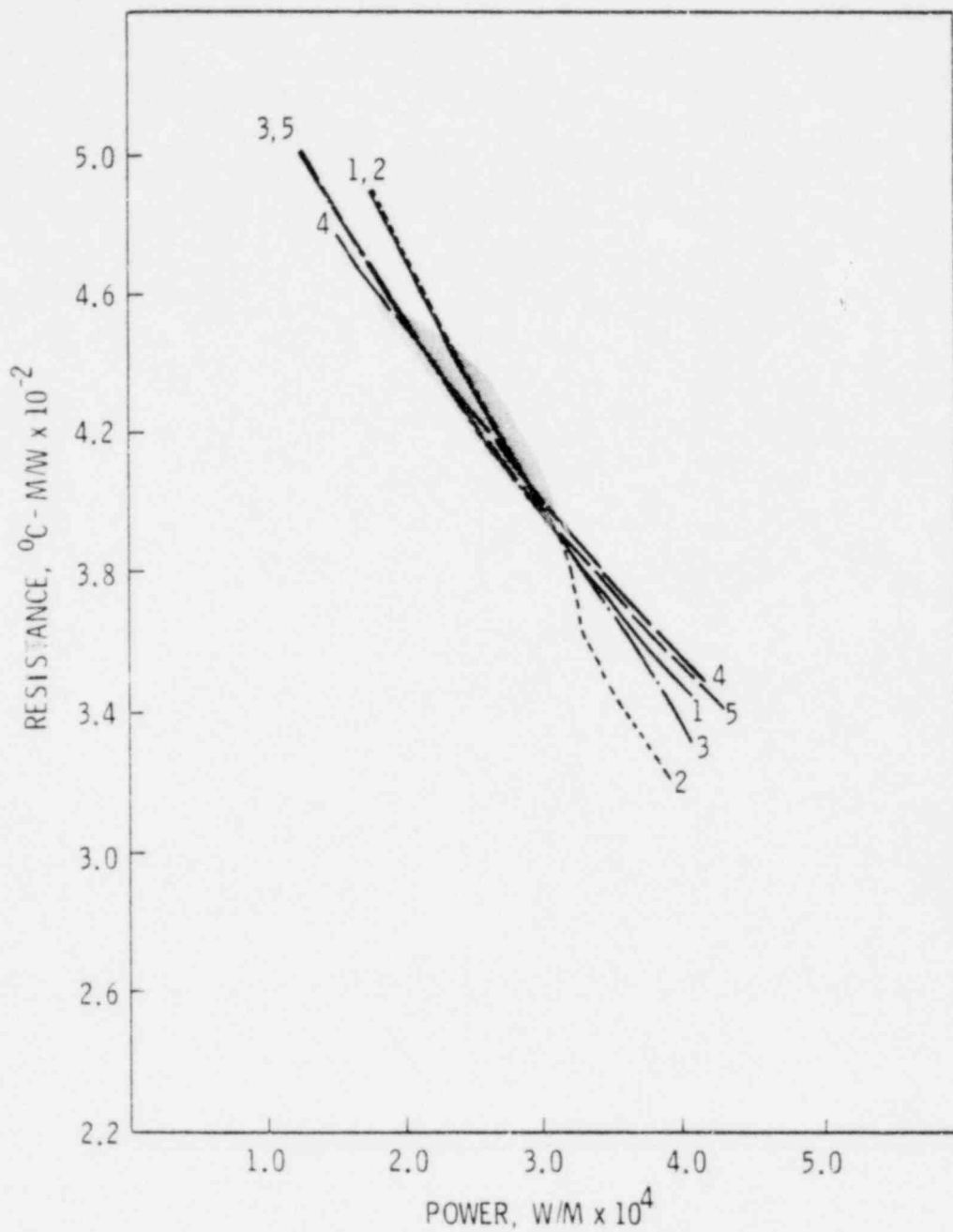


FIGURE 52. Data and Calculated R-P Responses for Rod 6 at 1200 GJ/kgU (Run 100)

Now let us turn to the development of the fission gas release and the fuel relocation/densification. Notice that at beginning-of-life, a relocation of 70-90% had to be assumed to match the data. It is unlikely that this amount of relocation could have reduced to the 50% level appropriate to the later burnups, except by fuel densification. A densification of only 1 to 2% TD would be sufficient to produce this change in effective gap size. The identical fuel in rod 6 of IFA-431, is known to have densified 4-5% in 4300 MWd/MTM rod-average burnup.

The fission gas release rate appears shifted from the rod 2 history, probably due to the time required for densification to bring the temperatures high enough for significant fission gas release. Both fission gas content and fuel relocation seem to "saturate" at values of 60% and 30% respectively (see Figure 53). The reason for this is not clear. Certainly fission gas production is continuing at all burnups. At any rate we again see the time-varying data supporting the steady-state data trends for this rod.

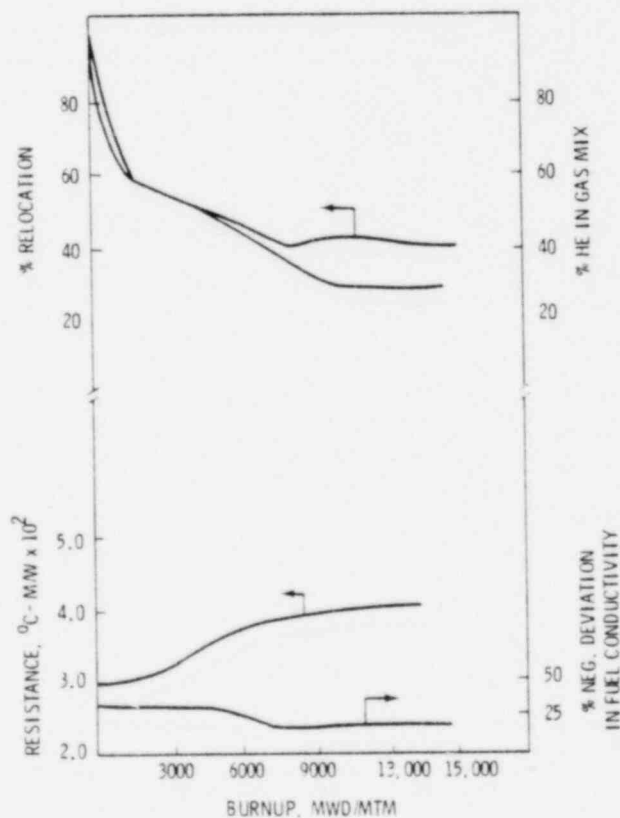


FIGURE 53. Estimated Life History for Rod 6 IFA-432

## APPENDIX A

### ANALYTICAL BASIS FOR THE OBSERVED CORRELATION BETWEEN RESISTANCE PLOTS AND TEMPERATURE/POWER SLOPE RATIOS

In this report, much use has been made of an observed correlation between plots of resistance versus power (R-P) on the one hand and quasi-steady state ratios of normalized temperature and power slopes on the other. In brief, the correlation is this:

1. When R-P increases, the temperature/power slope ratio (during a linear power change) is greater than unity.
2. When R-P decreases, the slope ratio is less than unity.
3. When R-P is constant (flat), the slope ratio is near unity.

This correlation was first observed directly from data, then confirmed by computer calculations of the sort described in Appendix B. Appendix A will show, for simplified cases, why this behavior is to be expected from analytical considerations. This appendix will also include a brief examination of how the correlation may be used to check for temperature or power estimate errors.

A1.0 REVIEW OF SOLUTIONS FOR STEADY STATE AND TRANSIENT TEMPERATURES,  
ASSUMING CONSTANT PROPERTIES AND BOUNDARY CONDITIONS

To explain observed nonlinear behavior in real fuel rods, we will of course have to deal with nonlinear equations of heat transfer. But let us first solve for the temperature response to linear power decrease assuming a linear rod (with constant thermal properties and conductance). The solution techniques, the approximations, and the general nature of the solutions will be useful later. The power history we will consider will in all cases be that sketched in Figure A-1. The power attains a steady state initial level, then drops at 0.5%/sec for 40 seconds to a new level, 80% of the initial.

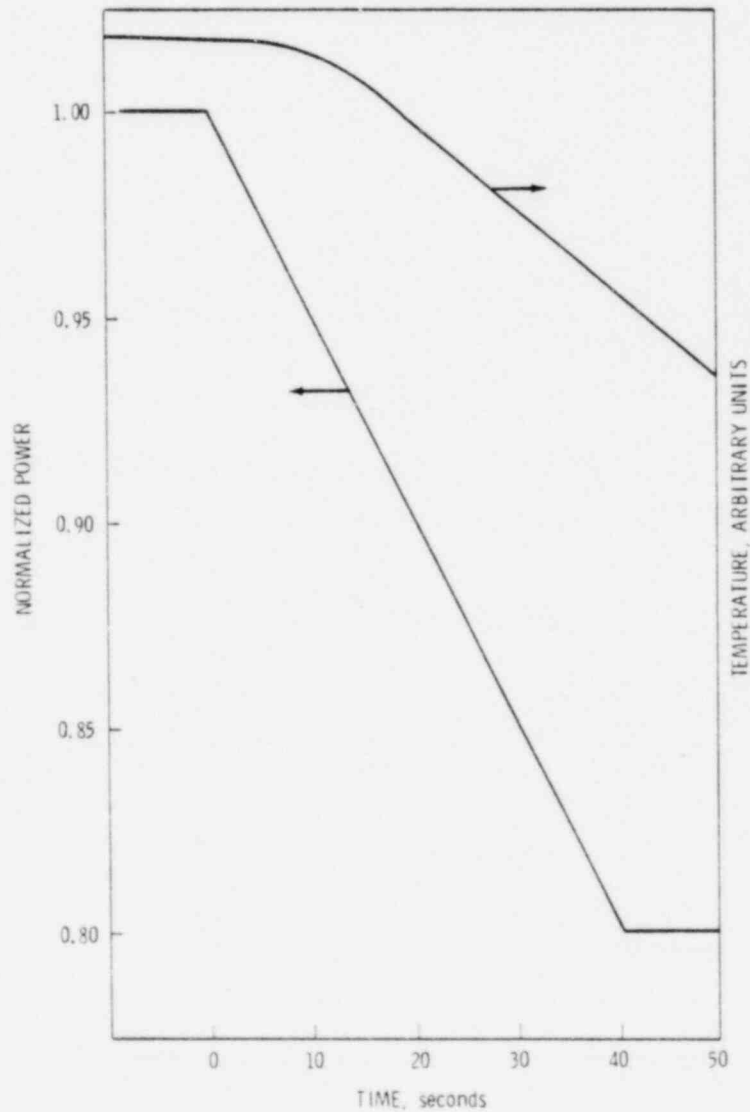


FIGURE A-1. Idealized Linear Power Decrease

Throughout, we will only consider radial heat transfer in a solid pellet with a spatially constant heat source. A radially-dependent heat source might be more realistic, but the inclusion of radial dependence does not effect the quasi steady-state behavior, and greatly complicates the derivations. The same holds for a central void in the fuel. The radial heat transfer equation in this case is:

$$\frac{cd}{K} \frac{\partial T(r,t)}{\partial t} = \frac{\partial^2 T}{\partial r^2} + \frac{1}{r} \frac{\partial T}{\partial r} + \frac{Q(t)}{K} \quad (\text{A1.1})$$

where

- c = heat capacity (joule/kg-°C)
- d = density (kg/m<sup>3</sup>)
- K = conductivity (W/M-°C)
- Q(t) = heat source (W/m<sup>3</sup>)
- r,t = radial position and time
- T = temperature (°C).

The boundary conditions we take to be

$$\frac{\partial T}{\partial r} = 0 \text{ at } r = 0 \quad (\text{A1.2})$$

$$\frac{-K\partial T}{\partial r} = H \left[ T(R,t) - T_{\infty} \right] \text{ at } r = R \quad (\text{A1.3})$$

where

- R = pellet radius
- T<sub>∞</sub> = coolant temperature
- H = fuel surface-to-coolant conductance (gap and cladding resistance having been lumped together).

This formulation of the boundary conditions ignores energy storage in the cladding; but that approximation does not affect quasi-steady state behavior, and again greatly simplifies the derivation.

Now we will reduce equation A1.1 to a purely transient equation. Let us represent  $Q(t)$  and  $T(r,t)$  as follows:

$$\begin{aligned} Q(t) &= Q_0 - bt \\ T(r,t) &= T_0(r) + \Delta T(r,t) \end{aligned}$$

We take  $T_0(r)$  to be the steady-state solution of

$$0 = \frac{\partial^2 T_0(r)}{\partial r^2} + \frac{1}{r} \frac{\partial T_0}{\partial r} + \frac{Q_0}{K} \quad (\text{A1.3})$$

such that  $T(r,t) = T_0(r)$  is the initial condition for A1.1. It is well known that

$$T_0(r) = \frac{Q_0}{4K} \left[ R^2 - r^2 \right] + \frac{Q_0 R}{2H} + T_\infty \quad (\text{A1.4})$$

when boundary conditions similar to A1.2 are applied. (See, for example, Reference 7).

Making the substitutions for  $Q$  and  $T$  into equation A1.1 and eliminating the steady-state terms, we have a reduced equation:

$$\frac{1}{\alpha} \frac{\partial \Delta T(r,t)}{\partial t} = \frac{\partial^2 \Delta T}{\partial r^2} + \frac{1}{r} \frac{\partial \Delta T}{\partial r} - \frac{bt}{K} \quad (\text{A1.5})$$

where

$$\alpha = \frac{K}{\rho c} = \text{diffusivity.}$$

The reduced boundary conditions are

$$\frac{\partial \Delta T}{\partial r} = 0 \text{ at } r = 0 \quad (\text{A1.6a})$$

$$-k \frac{\partial T}{\partial r} = H \Delta T(R, t) \text{ at } r=R \quad (\text{A1.6b})$$

The reduced initial condition is  $\Delta T(r, 0) = 0$

Before proceeding to solve equation A1.5, it is useful to normalize  $r$  and  $t$  as

$$y = r/R$$

$$\tau = \alpha t/R^2$$

The normalized equation becomes:

$$\frac{\partial \Delta T(y, \tau)}{\partial \tau} = \frac{\partial^2 \Delta T}{\partial y^2} + \frac{1}{y} \frac{\partial \Delta T}{\partial y} - \frac{b\tau R^4}{\alpha K} \quad (\text{A1.7})$$

Now apply Laplace transformation to each term, in the form

$$F(y, \sigma) = \int_0^{\infty} e^{-\sigma \tau} f(y, \tau) d\tau = L [f(y, \tau)]$$

The transformed equation is

$$\sigma \Delta T(y, \sigma) - \Delta T(y, t = 0) = \frac{d^2 \Delta T^*}{dy^2} + \frac{1}{y} \frac{d\Delta T^*}{dy} - \frac{bR^4}{\alpha K \sigma^2} \quad (\text{A1.8})$$

We use the initial condition to eliminate the term  $\Delta T(y, 0)$ . The homogeneous portion of the remaining equation can be written in the form:

$$y^2 \frac{d^2 \Delta T^*}{dy^2} + y \frac{d\Delta T^*}{dy} - y^2 \sigma \Delta T^* = 0$$

which is a modified Bessel's equation of zero order. The solution is well known to be:

$$\Delta T^* = AI_0(qy) + BK_0(qy)$$

where  $q = \sqrt{\sigma}$

and  $I_0$  and  $K_0$  are zero order Bessel functions of first and second kind. (See, for example, Reference 8).

Our inner boundary condition can be used to set  $B = 0$ . A particular solution to (A.1.8) is  $\Delta T^* = -\frac{bR^4}{\sigma^3 \alpha K}$  so that the total solution is

$$\Delta T^* = AI_0(qy) - \frac{bR^4}{\alpha K \sigma^3} \quad (A1.9)$$

Let us summarize the solution steps to this point, since they will be referenced and not explicitly carried out in later sections. To solve for the temperature response we took the following approach:

1. *Noted* the appropriate heat transfer equation and physical boundary conditions and initial conditions.
2. *Reduced* the equation and its conditions by the elimination of steady-state terms.
3. *Normalized* the independent variables to clean up the algebra.
4. *Transformed* the equation and its conditions to the LaPlace range, to change it to an ordinary differential equation.
5. *Solved* in the LaPlace range utilizing the inner boundary and initial conditions. The outer boundary condition will be used to specify the one unknown coefficient in the solution.

It remains to apply the outer boundary condition and transform the solution back to real space and time variables.

The transformed and normalized outer boundary condition (A1.6b) is

$$-\frac{K}{R} \frac{\partial \Delta T^*}{\partial y} \Big|_{y=1} = H \Delta T^*(1, \sigma)$$

or

$$-\frac{K}{R} [AqI_1(q)] = H \left[ AI_0(q) - \frac{bR^4}{\alpha K \sigma^3} \right]$$

let  $h = \frac{HR}{K}$ , such that  $-AqI_1 = h \left[ AI_0 - \frac{bR^4}{\alpha K \sigma^3} \right]$ .

Then  $A = \frac{+bR^4}{\alpha \sigma^3 K} \left[ \frac{h}{qI_1 + hI_0} \right]$

and  $\Delta T^*(y, \sigma) = \frac{bR^4}{\sigma^3 \alpha K} \left[ \frac{hI_0(qy)}{qI_1(q) + hI_0(q)} - 1 \right]$  (A1.10)

Now recall that we are seeking the time derivative of the centerline temperature. Let us call it  $D(t)$ . The transform of that derivative is, in normalized time,

$$D^*(\sigma) = L \left[ \frac{d\Delta T(0, \tau)}{d\tau} \right] = \sigma \Delta T^*(0, \sigma)$$

Thus,  $D^*(\sigma) = \frac{bR^4}{\sigma^2 K \alpha} \left[ \frac{h}{qI_1 + hI_0} - 1 \right]$ . (A1.11)

The inverse transform,  $D^*(\sigma)$  can be evaluated as

$$D(\tau) = \frac{1}{2\pi i} \int_{a-i\infty}^{a+i\infty} D^*(\sigma) e^{\sigma\tau} d\sigma = \sum_{K=1}^n \text{res} \left[ D^* e^{\sigma\tau} \right]_K$$

where the sum is over all residues at all poles of  $D^*(\sigma)$ . The residues are given by

$$\text{res} [D^* e^{\sigma\tau}] = \frac{1}{(m-1)!} \lim_{\sigma \rightarrow \sigma_k} \left( \frac{d^{m-1}}{d\sigma^{m-1}} \left[ (\sigma - \sigma_k)^m D^* e^{\sigma\tau} \right] \right)$$

where  $\sigma_k$  is the  $k^{\text{th}}$  pole of  $D^*(\sigma)$  and  $m$  is the multiplicity. (See, for example, Reference 9). The conditions for the above technique to apply are that

1.  $|D^*(\sigma)| \rightarrow 0$  as  $|\sigma| \rightarrow \infty$
2. The poles of  $D^*(\sigma)$  should be located to the left of some line  $\text{Re}(\sigma) = a$  in the complex plane.
3.  $D^*(\sigma)$  should be single-valued and analytic everywhere within a contour enclosing all its singularities (except, of course, at the poles).

It is not immediately obvious that  $D^*(\sigma)$  meets all these conditions, but we shall now show that to be the case. We will make use of the series expansions of  $I_0(q)$  and  $I_1(q)$ , given by

$$I_0(q) = \sum_{n=0}^{\infty} q^{2n} / 2^{2n} (n!)^2$$

$$I_1(q) = \sum_{n=0}^{\infty} q^{2n+1} / 2^{2n+1} n!(n+1)!$$

Then  $D^*(\sigma)$  can be written as

$$D^*(\sigma) = hB \left[ h \sum_{n=0}^{\infty} \frac{\sigma^2 q^{2n}}{2^{2n} (n!)^2} + \frac{q \sum_{n=0}^{\infty} \sigma^2 q^{2n}}{2^{2n+1} n!(n+1)!} \right]^{-1} - \frac{B}{\sigma^2}$$

where  $B = bR^4/\alpha K$ .

Realizing  $q = \sqrt{\sigma}$ ,

$$D^*(\sigma) = hB \left[ h \sum_{n=0}^{\infty} \frac{\sigma^{n+2}}{2^{2n} (n!)^2} + \sum_{n=0}^{\infty} \frac{\sigma^{n+3}}{2^{2n+1} n! (n+1)!} \right]^{-1} - \frac{B}{\sigma^2}$$

The above can be written as

$$D^*(\sigma) = Bh \left[ \sum_{n=2}^{\infty} A_n \sigma^n \right]^{-1} - \frac{B}{\sigma^2}$$

where the  $A_n$  are real, positive numbers.

Now for  $\sigma = \alpha + i\beta$ , the sum can be expanded and rearranged such that

$$D^*(\sigma) = Bh \left[ \sum_{\ell=1}^{\infty} C_{\ell} + i \sum_{\ell=1}^{\infty} D_{\ell} \right]^{-1} - \frac{B}{\sigma^2}$$

where the  $C_{\ell}$  and  $D_{\ell}$  are real.

As  $|\sigma| \rightarrow \infty$ ,  $(\sum C_{\ell})$  or  $(\sum D_{\ell})$  or both go to  $\infty$  such that  $|D^*| \rightarrow 0$ , and the first condition is satisfied.

The location of the poles (condition 2) will be examined next. In addition to the poles at  $\sigma = 0$ ,  $D^*(\sigma)$  will have poles whenever  $qI_1(q) + hI_0(q) = 0$ . This condition will be satisfied at certain points along the negative real axis, and only at those points. To confirm this, first note that  $I_0(i\alpha_n) = J_0(\alpha_n)$  and  $i\alpha_n I_1(i\alpha_n) = \alpha_n J_1(\alpha_n)$ , as can be verified by reference to the series expansions for  $I_0$ ,  $I_1$ ,  $J_0$ , and  $J_1$ . Then the equation  $qI_1(q) + hI_0(q) = 0$  can be written (for  $q = i\alpha_n$ ), as  $hJ_0(\alpha_n) + \alpha_n J_1(\alpha_n) = 0$ . The roots of this equation are real, positive, nonzero numbers. Thus  $D^*(\sigma)$  has poles along the negative real axis at  $q^2 = \sigma = -\alpha_n^2$ , where  $\alpha_n$  are the roots of the above equation. On the other hand  $D^*(\sigma)$  has no poles off the negative real axis. From the series expansion,

$$F(\sigma) = qI_1(q) + hI_0(q)$$

$$= \sigma \sum_{n=0}^{\infty} B_n \sigma^n + h \sum_{n=0}^{\infty} A_n \sigma^n$$

where

$$A_n = \left[ 2^{2n} (n!)^2 \right]^{-1}$$

$$B_n = \left[ 2^{2n+1} n! (n+1)! \right]^{-1}$$

Now let  $\sigma = \alpha + i\beta$ . Applying the binomial expansion formula, we have

$$F(\sigma) = \sum_{n=0}^{\infty} \sum_{m=0}^n B_{nm} \alpha^{m+1} (i\beta)^{n-m} + \sum_{n=0}^{\infty} \sum_{m=0}^n B_{nm} \alpha^m (i\beta)^{n+m+1}$$

$$+ h \sum_{n=0}^{\infty} \sum_{m=0}^n A_{nm} \alpha^m (i\beta)^{n-m}$$

$$= \underbrace{h I_0(\sqrt{\alpha}) + \sqrt{\alpha} I_1(\sqrt{\alpha})}_{\text{Term 1}} + \left. \begin{aligned} & \sum_{n=1}^{\infty} \sum_{m=0}^{n-1} \alpha^{m+1} (i\beta)^{n-m} B_{nm} \\ & + \sum_{n=0}^{\infty} \sum_{m=0}^n \alpha^m (i\beta)^{n-m+1} B_{nm} \\ & + \sum_{n=1}^{\infty} \sum_{m=0}^{n-1} \alpha^m (i\beta)^{n-m} A_{nm} \end{aligned} \right\} \text{Term 2}$$

where

$$A_{nm} = \left[ (n-m)! m! 2^{2n} n! \right]^{-1}$$

$$B_{nm} = \left[ (n-m)! m! 2^{2n+1} (n+1)! \right]^{-1}$$

Now for  $\alpha \neq -\alpha_n^2$ , term 1  $\neq 0$ , and  $|F(\sigma)| \neq 0$ , since term 2 is either zero ( $\beta = 0$ ) or contains both real and imaginary parts ( $\beta \neq 0$ ). For  $\alpha = -\alpha_n^2$ ,  $|F(\sigma)| \neq 0$  if  $\beta \neq 0$ , for the same reason. So  $|F(\sigma)|$  only = 0 for  $\sigma = -\alpha_n$ .

So condition 2 is satisfied, the line  $\text{Re}(\sigma) = \alpha$  can be taken for any real  $a > 0$ .

Condition 3 is satisfied, as can be seen from the series expansion form of  $D^*$  (A1.11a). Since the general polynomial is everywhere analytic, single valued, and nonzero (except at its roots), so is its inverse, and so is  $D^*$ .

Having shown that the conditions are satisfied, we can now apply residue theory to find  $D(\tau)$ :

$$D(\tau) = \lim_{\sigma \rightarrow 0} \frac{d}{d\sigma} \left[ \sigma^2 D^*(\sigma) e^{\sigma\tau} \right] + \sum_{n=1}^{\infty} \lim_{\sigma \rightarrow -\alpha_n} \left[ D^*(\sigma) e^{\sigma\tau} \right]$$

The residues at  $\sigma \rightarrow 0$  will yield the quasi-steady-state solution, since  $\sigma \rightarrow 0$  implies  $\tau \rightarrow \infty$ . Since we are only concerned with the quasi-steady-state behavior, we will ignore the other residues (which yield transient terms) and find

$$\begin{aligned} D(\tau \rightarrow \infty) = D_{\infty}(\tau) &= \lim_{\sigma \rightarrow 0} \frac{d}{d\sigma} \left( \sigma^2 D^* e^{\sigma\tau} \right) \\ &= \lim_{\sigma \rightarrow 0} \left[ \tau D^* \sigma^2 e^{\sigma\tau} \right] + \lim_{\sigma \rightarrow 0} \left[ e^{\sigma\tau} \frac{d}{d\sigma} (\sigma^2 D^*) \right] \end{aligned}$$

Applying this relationship, we have

$$\begin{aligned} D_{\infty}(\tau) &= \frac{bR^4}{K\alpha} \left[ \lim_{\sigma \rightarrow 0} \frac{h\tau e^{\sigma\tau}}{qI_1 + hI_0} + \lim_{\sigma \rightarrow 0} \frac{e^{\sigma\tau}}{d\sigma} \left[ \frac{h}{qI_1 + hI_0} \right] - \lim_{\sigma \rightarrow 0} \tau e^{\sigma\tau} \right] \\ &= B \left[ \frac{h\tau}{h} - \tau + \lim_{q \rightarrow 0} \frac{-h}{2q} \left[ \frac{(qI_0 + hI_1) e^{\sigma\tau}}{(qI_1 + hI_0)^2} \right] \right] \\ &= B \left[ \lim_{q \rightarrow 0} \frac{-h}{2q} \left[ \frac{qI_0}{h^2} + \frac{hI_1}{h^2} \right] \right] \end{aligned}$$

$$= -B \left[ \frac{1}{2h} + \frac{1}{4} \right] = \frac{-bR^4}{\alpha K} \left[ \frac{K}{2RH} + \frac{1}{4} \right]$$

In real time,

$$D_{\infty}(t) = \frac{-bR^2}{K} \left[ \frac{K}{2H} + \frac{1}{4} \right] = -b \left[ \frac{R}{2H} + \frac{R^2}{4K} \right]$$

Now recall Equation A1.3, which implies that the original steady-state center-line temperature is  $T_o(0) = \frac{Q_o R^2}{4K} + \frac{Q_o R}{2H} + T_{\infty}$ , or  $T_o - T_{\infty} = Q_o \left[ \frac{R^2}{4K} + \frac{R}{2H} \right]$ . If we define relative temperature  $T_r$ , as  $T - T_{\infty}$ , and normalized relative temperature as  $T_N = T_r / T_{r_o} = (T_o(0) + \Delta T(0,t) - T_{\infty}) / (T_o(0) - T_{\infty})$  then we have a very simpler result for  $D_{N_{\infty}}$ , the quasi-steady-state normalized temperature slope:

$$D_{N_{\infty}} = \frac{1}{T_o - T_{\infty}} \frac{d\Delta T(0,t \rightarrow \infty)}{dt} = \frac{-b \left[ \frac{R^2}{4K} + \frac{R}{2H} \right]}{Q_o \left[ \frac{R^2}{4K} + \frac{R}{2H} \right]} = \frac{-b}{Q_o} = -b_N \quad (A1.12)$$

What we have called  $b_N$  is the power slope normalized to the initial value of power. Thus, the slopes of normalized relative temperature and normalized power should be *equal* in quasi-steady state, under the assumption of constant properties and boundary conditions.

Furthermore, the temperature/power slope ratio is inversely proportional to initial resistance:

$$\frac{D_{N_{\infty}}}{b_N} = \frac{D_{\infty}}{\frac{b}{Q_o}} = \left[ \frac{Q_o}{T_o(0) - T_{\infty}} \right] \frac{D_{\infty}}{b} = \text{Resistance}^{-1} \times \text{Constant}$$

Thus, the temperature/power slope ratio should be as sensitive to system nonlinearities as the resistance itself. We explore this sensitivity in the next two sections.

But first, note that the above results and conclusions hold equally well for the case of fixed surface temperature, rather than fixed conductance. In that case, the outer boundary condition is  $T(R,t) = T_s$  (constant) and the steady-state initial temperature distribution  $T_0(r)$  is given by

$$T_0(r) = T_s + \frac{Q_0}{4K} [R^2 - r^2] \quad (\text{A1.13})$$

The normalized and transformed transient equation is identical to A1.8, and the general solution (A1.9) is the same in form. However, the term "A" is now found from the new boundary condition, which is

$$\Delta T^*(1, \sigma) = 0$$

or

$$A I_0(q) - \frac{bR^4}{\alpha K \sigma^3} = 0$$

from which

$$A = \frac{bR^4}{\sigma^3 \alpha K I_0(q)} \text{ and } \Delta T^*(y, \sigma) = \frac{bR^4}{\alpha K \sigma^3} \left[ \frac{I_0(qy)}{I_0(q)} - 1 \right] \quad (\text{A1.14})$$

Again, since we seek only the derivative of the centerline temperature, we need only find

$$D^*(\sigma) = L \left[ \frac{d\Delta T(\sigma, \tau)}{d\tau} \right] = \sigma \Delta T^*(\sigma, 0) = \frac{B}{\sigma^2} \left[ \frac{1}{I_0(q)} - 1 \right]$$

And again, since we are only interested in the quasi-steady-state value  $D_\infty = \frac{\partial \Delta T}{\partial \tau}(0, \tau \rightarrow \infty)$ , we need only find the residues of  $D^*(\sigma)$  at  $\sigma = 0$ . Again applying the relation for double roots,

$$\text{Residue at } \sigma = 0 = \lim_{\sigma \rightarrow 0} \frac{d}{d\sigma} \left[ \sigma^2 D^*(\sigma) e^{\sigma \tau} \right]$$

we have

$$\begin{aligned} D_\infty(\tau) &= B \lim_{q \rightarrow 0} \left[ \frac{\tau e^{\sigma \tau}}{I_0(q)} - \frac{I_1 e^{\sigma \tau}}{2q(I_0)^2} \right] - B\tau \\ &= B \left[ \tau - \frac{1}{4} - \tau \right] = \frac{-B}{4} = \frac{-bR^4}{4\alpha K} \end{aligned}$$

In real time,

$$D_\infty(t) = \frac{-bR^2}{4K} \tag{A1.15}$$

Again, from the steady-state solution (A1.13) we have relative temperatures given by

$$T_{r_0} = T_0(0) - T_s = \frac{Q_0 R^2}{4K}$$

such that the derivative of the normalized relative temperature, in quasi-steady-state,  $D_{N_\infty}$ , is given by

$$D_{N_\infty} = \frac{\frac{-bR^2}{4K}}{\frac{Q_0 R^2}{4K}} = \frac{-b}{Q_0} = -b_N$$

That is, the slope of normalized relative temperature and normalized power are again equal.

A2.0 TEMPERATURE/POWER SLOPE BEHAVIOR FOR FIXED CONDUCTANCE  
AND TEMPERATURE DEPENDENT CONDUCTIVITY

Consider a rod with a closed gap and high gap conductance, such that the change in fuel surface temperature over the power range of interest (80-100% of full power) is negligible compared to the corresponding change in fuel resistance. Such a situation applies, for example, to Rod 3 of IFA-432, at zero burnup. This problem has an exact solution in steady-state, and an approximate solution in transient cases. The same power history as in A1.0 will of course be used. The equation for heat transfer is

$$cd \frac{\partial T}{\partial t} = \frac{1}{r} \frac{\partial}{\partial r} \left[ K(t)r \frac{\partial T}{\partial r} \right] + Q(t) \quad (A2.1)$$

with the same notation and boundary conditions as before. We neglect variations in heat capacity,  $C$ , since they are of second order for  $UO_2$ . (See Figure A.2 for confirmation of this assertion.) We also neglect energy storage in the cladding, since the (nonlinear) change in that energy storage rate during the mild power decrease under consideration does not affect the quasi-steady-state behavior significantly.

The boundary conditions we will assume to be

$$\frac{\partial T}{\partial r} = 0 \text{ at } r = 0 \quad (A2.2a)$$

and

$$T(r = R) = T_s \text{ (constant)} \quad (A2.2b)$$

We will transform the dependent variable in equation A2.1 to

$$G(T) = \int_{T_s}^T K(T^1) dT^1$$

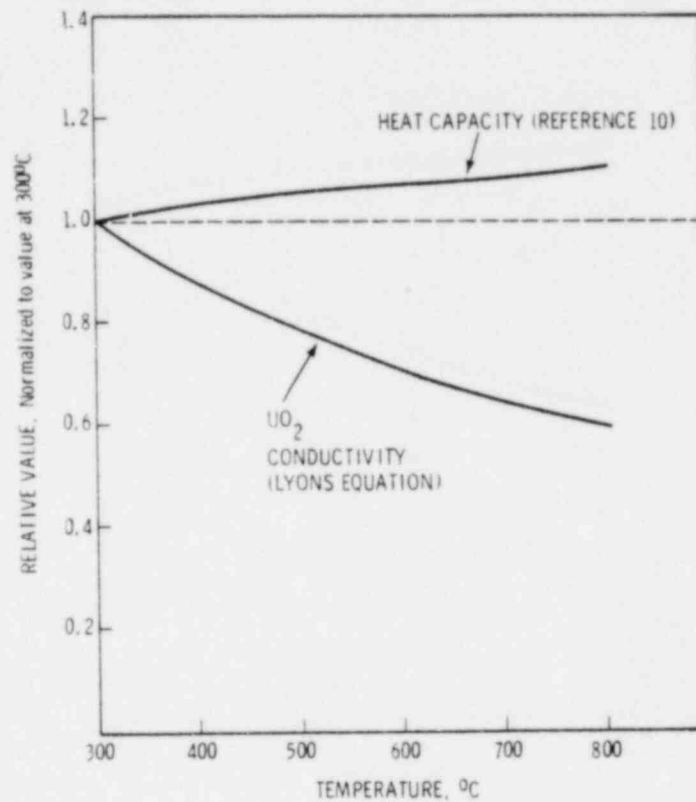


FIGURE A-2. Relative Variation of  $UO_2$  Heat Capacity and Conductivity

This is a well-known Kirchoff transformation, and it has the advantage of rendering equation A2.1 almost linear in  $G$ . For the right hand side, consider

$$\frac{\partial G}{\partial r} = \frac{dG}{dT} \frac{\partial T}{\partial r} = K(t) \frac{\partial T}{\partial r}$$

whereas for the left hand side, consider

$$\frac{\partial T}{\partial G} \frac{\partial G}{\partial t} = \frac{\partial T}{\partial t}$$

Then equation A2.1 becomes

$$cd \frac{\partial G(r,t)}{\partial t} \left[ \frac{\partial T}{\partial G} \right] = \frac{1}{r} \frac{\partial}{\partial r} \left[ r \frac{\partial G}{\partial r} \right] + Q(t) \quad (A2.3)$$

We will make the assumption  $\frac{\partial T}{\partial G} = \text{constant}$ , which is an approximation, but, at least for the numerical examples we will consider, it is an acceptable one. With this approximation, A2.3 becomes a linear equation which we can solve. Again, let us represent  $Q(t) = Q_0 = bt$  and  $G(r,t) = G_0(r) + \Delta G(r,t)$ , where  $G_0(r)$  is the solution to

$$0 = \frac{1}{r} \frac{\partial}{\partial r} \left[ r \frac{\partial G_0}{\partial r} \right] + Q_0$$

or

$$G_0 = \frac{Q_0(R^2 - r^2)}{4}$$

Then, equation A2.3 reduces to

$$cd \frac{\partial \Delta G}{\partial t} \left[ \frac{\partial T}{\partial G} \right] = \frac{\partial^2 \Delta G}{\partial r^2} + \frac{1}{r} \frac{\partial \Delta G}{\partial r} - bt \quad (A2.4)$$

with boundary conditions

$$\frac{\partial \Delta G}{\partial r} = 0 \text{ at } r = 0$$

$$\Delta G(R,t) = 0$$

This equation is identical in form to A1.5, for a fixed surface temperature as the outer boundary condition. Therefore, it can be normalized, transformed, and solved by a method similar to the one just developed. The solution for the quasi-steady-state time derivative of  $\Delta G(0, t \rightarrow \infty)$ , by analogy with (A1.15), is

$$\frac{\partial \Delta G_{\infty}}{\partial t} = \frac{-bR^4}{4}$$

But  $G_0(0) = \frac{Q_0 R^2}{4}$ . So if we define  $G_N = G(0,t)/G_0(0)$ , then

$$\frac{\partial G_{N_{\infty}}}{\partial t} = \frac{1}{G_0(0)} \frac{\partial G_{\infty}}{\partial t} = \frac{-bR^2/4}{Q_0 R^2/4} = \frac{-b}{Q_0} = -b_N$$

Now consider the meaning of this result. We conclude that  $G$ , the area under the  $K$  vs.  $T$  curve, changes at a relative rate equal to that of the power. But since  $K$  vs.  $T$  is not constant, this precludes the possibility that the relative change in *temperature* is equal to that of the power. In fact,  $K$  decreases with increasing temperature. During a power decrease, temperatures decrease and  $K$  *increases*. In order to compensate and hold the relative area variation equal to that of the power, the temperature variation must be *greater* than that of the power. That is, we conclude that

$$\left| \frac{\partial T_{N_{\infty}}}{\partial t} \right| > b_N, \text{ where } T_N = \frac{T(0,t) - T_s}{T_0(0) - T_s}$$

$$\text{and } \frac{\partial T_{N_{\infty}}}{\partial t} = \frac{1}{T_0(0) - T_s} \frac{\partial T(0,t \rightarrow \infty)}{\partial t}$$

All this is entirely consistent with our original formulation, as will now be shown. Let us write down an expression for  $\frac{\partial T_{N_{\infty}}}{\partial t}$  in terms of  $G$ :

$$\frac{\partial T_{\infty}}{\partial t} = \frac{\partial \Delta G_{\infty}}{\partial t} \left[ \frac{\partial T}{\partial G} \right] = \frac{-bR^2}{4} \left[ \frac{\partial T}{\partial G} \right] \quad (\text{A2.5})$$

and

$$\frac{\partial T_{N\infty}}{\partial t} = \frac{1}{T_o(0) - T_s} \left( \frac{\partial T_{\infty}}{\partial t} \right) = \frac{-bR^2}{4} \left[ \frac{\partial T / \partial G}{T_o - T_s} \right] \quad (\text{A2.5 cont'd})$$

But  $T_o(0) - T_s = \frac{Q_o R^2}{4\bar{K}_o}$ , where  $\bar{K}_o = \frac{1}{T_o(0) - T_s} \int_{T_s}^{T_o} K(T) dT$

Since we are evaluating centerline temperatures, we will evaluate

$$\frac{\partial T}{\partial G} \text{ as } \frac{1}{K(T(r=0, t=?))}$$

Altogether then, we have

$$\frac{T_{N\infty}}{\partial t} = \frac{-bR^2 \left( \frac{\partial T}{\partial G} \right)}{\frac{Q_o R^2}{4\bar{K}_o}} = \frac{-b}{Q_o} \left[ \frac{\bar{K}_o}{K(T(0, t=?))} \right] = -b_N \left[ \frac{K_o}{K(T(0, ?))} \right]$$

But, note for all time,  $\frac{\bar{K}_o}{K} > 1.0$ , such that  $\left| \frac{\partial T_{N\infty}}{\partial t} \right| > b_N$

Now  $\bar{K}_o$  is known, but since  $K$  changes with time it is not clear at what time it should be evaluated. As might be expected, it turns out the choices  $t = 0$  and  $t \rightarrow \infty$  neatly bracket the true solution, as will be shown below.

#### Numerical Example

Consider a fuel rod with fuel diameter,  $R$ , of 0.00534 m and fixed fuel surface temperature of 246°C, operating at  $3.00 \times 10^4$  W/m. The initial heat generation,  $Q_o$ , is  $3.35 \times 10^8$  W/m<sup>3</sup>. We will assume conductivity  $K(T)$  to be of the Lyons form, i.e.

$$K(T) = \frac{3824}{402.4+T} + 6.125 \times 10^{-11} (T+273)^3$$

for T in degrees C and K in W/m-°C

The power will be assumed to fall linearly from 0 to 40 seconds at 0.5%/sec and remain constant (at 80% full power) thereafter. The initial and final steady-state temperatures are found from:

$$\text{Initial: } \int_{246}^{T_0} K(T)dT = \frac{Q_0 R^2}{4} = 2388 \text{ W/m} = G_0(0)$$

$$\text{Final } \int_{246}^{T_f(0)} K(T)dT = \frac{Q_0 R^2(0.8)}{4} = 1,910 \text{ W/m} = G_f(0)$$

from which

$$T_0(0) = 802^\circ\text{C}, \bar{K}_0 = 4.29, K(T_0(0)) = 3.25$$

$$T_f(0) = 664^\circ\text{C}, K(T_f(0)) = 3.63$$

The situation is sketched in Figure A.3. The rod temperature moves in G(0) vs. T space from G<sub>0</sub> to G<sub>f</sub>. At G<sub>0</sub>, slope of T with respect to G is 1/K<sub>(802)</sub> = 1/3.25; at G<sub>f</sub>, the slope is 1/3.63. The temperature/power slope ratio is given by  $\bar{K}_0/K$ , from the previous derivation, and is estimated as

$$\frac{4.29}{3.63} <\text{slope ratio}> \frac{4.29}{3.25}$$

or

$$1.18 < \text{slope ratio} < 1.32 \quad (\text{A2.7})$$

The average slope during the transient may be estimated as that of the chord plotted between  $G_0$  and  $G_f$ , i.e.

$$\frac{\partial T}{\partial G} \approx \frac{T_0 - T_f}{G_0 - G_f} = \frac{1}{3.47}$$

From which,

$$\frac{\partial T_{N\infty}}{\partial t} = \frac{-bR^2 (\partial T/\partial G)}{4 (T_0(0) - T_s)} = 0.62\%/sec$$

(using A2.6)

So our best estimate of the slope ratio is  $\frac{0.62}{0.50} = 1.24$ . Notice that this is almost exactly halfway between the limits we estimated in A2.7. A more exact numerical solution, as described in Appendix B, resulted in a slope ratio of 1.26.

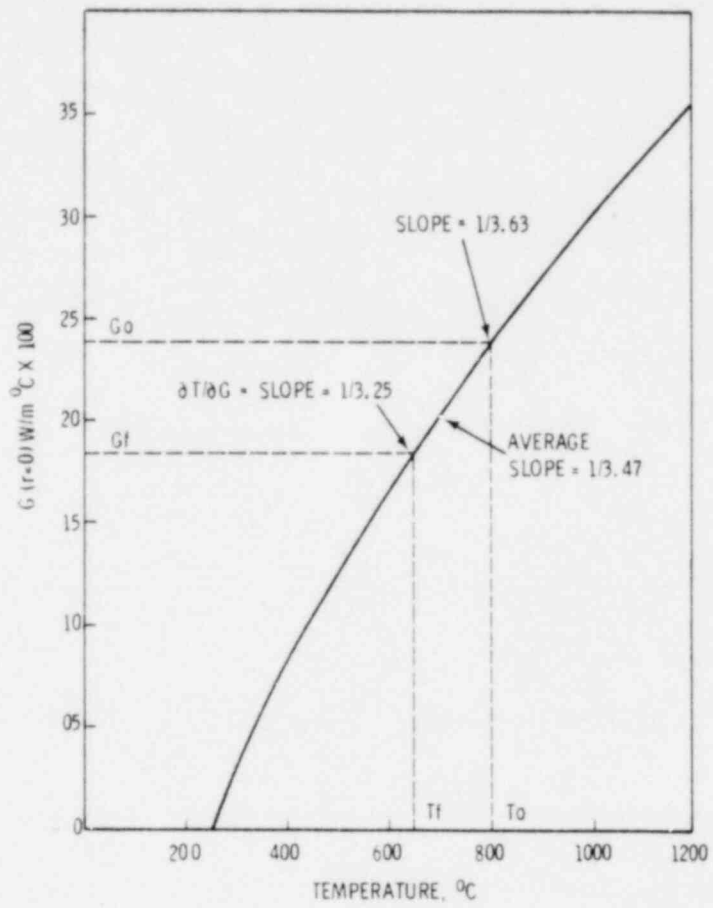


FIGURE A-3. Plot of  $G(o)$  as a Function of Temperature

A3.0 TEMPERATURE/POWER SLOPE BEHAVIOR WITH FIXED CONDUCTIVITY  
AND TEMPERATURE DEPENDENT CONDUCTANCE

In this section, we examine a case at the opposite extreme from the one just examined. We assume the change in fuel-to-coolant conductance to be very large throughout the power drop, relative to the change in effective conductivity,  $\bar{K}$ , and effective heat capacity. This approximation holds well for an open-gap rod with severely degraded gas conductivity for two reasons:

1. The fuel contraction/expansion causes a very large change in gap size and gap conductance even over a 20% power change; and
2. The fuel surface temperature holds fairly constant as a function of power because increasing conductance with power offsets increased heat flux, such that

$$\bar{K} = \int_{T_s}^{T_0} K dT \left( \frac{1}{T_0 - T_s} \right)$$

changes very little over a 20% power change. (a)

The particular dependence of conductance,  $H$ , on temperature which we will use is that  $H$  increases linearly with volume average temperature  $\bar{T}$ . This choice is based on GAPCON-3 runs, correlated to data from Rods 1 and 2 at high burnup, where it is evident that the effects of temperature-dependent gas and cladding conductivity, temperature jump distance and fuel expansion combine to produce a fairly linear dependence of  $H$  on  $\bar{T}$ . Since for constant  $K$ ,  $\bar{T}$  is given to be simply

$$\bar{T} = \frac{T(r=0,t) + T(r=R,t)}{2}$$

---

(a) The effective heat capacity,  $\bar{C}$ , also changes very little, and in any case its temperature dependence is small enough to have very little effect on quasi-steady-state behavior. Therefore, we take  $\bar{C}(t) = C$  (constant).

we write

$$H = L + M\bar{T} = L + \frac{M}{2} [T(0,t) + T(R,t)] \quad (\text{A3.1})$$

The applicable equation is

$$\frac{cd}{K} \frac{\partial T}{\partial t} = \frac{\partial^2 T}{\partial r^2} + \frac{1}{r} \frac{\partial T}{\partial r} + \frac{Q(t)}{K}$$

with boundary conditions

$$\frac{\partial T}{\partial r} = 0 \text{ at } r = 0 \quad (\text{A3.2a})$$

and

$$-K \left. \frac{\partial T}{\partial r} \right|_{r=R} = \left[ L + \frac{M}{2} [T(0,t) + T(R,t)] \right] [T(R,t) - T_\infty] \quad (\text{A3.2b})$$

Again we represent

$$\begin{aligned} Q(t) &= Q_0 - bt \\ T(r,t) &= T_0(r) + \Delta T(r,t) \end{aligned} \quad (\text{A3.3})$$

Now  $T_0(r)$  should be the solution to the steady-state equation,

$$0 = \frac{\partial^2 T_0}{\partial r^2} + \frac{1}{r} \frac{\partial T_0}{\partial r} + \frac{Q_0}{K}$$

with boundary conditions

$$\frac{\partial T_0}{\partial r} = 0 \text{ at } r = 0 \quad (\text{A3.4a})$$

and

$$-K \frac{\partial T_0}{\partial r} = \left[ L + \frac{M}{2} [T_0(0) + T_0(R)] \right] [T_0(R) - T_\infty] \text{ at } r = R \quad (\text{A3.4b})$$

Without loss of generality, let  $T_\infty = 0$ . This will simplify the subsequent algebra. Now, from Equation A1.4, we already know that, for constant  $K$ ,

$$T_0(0) = T_0(R) + \frac{Q_0 R^2}{4K}$$

Also, in steady-state, Fourier's law at the fuel surface gives

$$-K \left. \frac{\partial T}{\partial r} \right|_{r=R} = \frac{\pi Q R^2}{2\pi R} = \frac{QR}{2}$$

Substituting all this back into (A3.4b) we have

$$\frac{QR}{2} = \left[ L + \frac{M}{2} \left[ 2T_0(R) + \frac{QR^2}{4K} \right] \right] T_0(R)$$

or, rearranging to standard quadratic form

$$MT_s^2 + \left[ L + \frac{MQR^2}{8K} \right] T_s - \frac{QR}{2} = 0 \quad (\text{A3.5})$$

where

$$T_s = T_0(R)$$

Thus,  $T_0(R)$  is found as the solution to the above quadratic, and  $T_0(r)$  is the initial condition for (A3.1).

Now reducing the original equation to a transient equation is done exactly as before:

$$cd \frac{\partial \Delta T}{\partial t} = \frac{\partial^2 \Delta T}{\partial r^2} + \frac{1}{r} \frac{\partial \Delta T}{\partial r} - \frac{bt}{K} \quad (A3.6)$$

However, the outer boundary condition for (A3.6) is more complicated. First, the expanded condition for the original Equation (A3.1) is

$$\begin{aligned} -K \left. \frac{\partial T}{\partial r} \right|_{r=R} &= [L + M\bar{T}] T(R,t) = \left[ L + \frac{M}{2} T_0(0) + \Delta T(0,t) + T_0(R) + \Delta T(R,t) \right] \\ &\quad \times [T_0(R) + \Delta T(R,t)] \end{aligned}$$

If the above is written out and the steady-state terms (A3.4b) eliminated, we have left

$$\begin{aligned} -K \left. \frac{\partial \Delta T}{\partial r} \right|_{r=R} &= L\Delta T(R,t) + \frac{M}{2} \left[ 2T_0(R)\Delta T(R,t) + T_0(0)\Delta T(R,t) + T_0(R)\Delta T(0,t) \right] \\ &\quad + \frac{M}{2} \left[ \Delta T(R,t)^2 + \Delta T(0,t)\Delta T(R,t) \right] \end{aligned} \quad (A3.7)$$

This is the outer boundary condition for Equation (A3.6).

Now the terms  $\Delta T(R,t)^2$  and  $\Delta T(0,t)\Delta T(R,t)$  are quite small with respect to the other terms in (A3.7), as the reader can verify by examination of the numerical example at the end of this section. We will therefore ignore them. The resulting approximate (quasi-linear) boundary condition, rearranged slightly, is

$$-K \left. \frac{\partial \Delta T}{\partial r} \right|_{r=R} = E\Delta T(R,t) + F\Delta T(0,t) \quad (A3.8)$$

where

$$E = L + \frac{M}{2} [2T_0(R)] + T_0(0)$$

$$F = \frac{M}{2} (T_0(R))$$

Now to solve Equation (A3.6) we proceed just as with Equation (A1.5). We normalize  $r$  and  $t$ , transform to the LaPlace range, and obtain a solution in the LaPlace range identical to (A1.9):

$$\Delta T^* = AI_0(qy) \frac{-bR^4}{\alpha K \sigma^3} \quad (A3.9)$$

The normalized and transformed outer boundary condition (A3.8) is just

$$\frac{-K}{R} \Delta T^*(1, \sigma) = E \Delta T^*(1, \sigma) + F \Delta T^*(0, \sigma)$$

Substituting (A3.9) into (A3.8), we have

$$\frac{-K}{R} [AqI_1] = E AI_0(q) + FA \frac{-bR^4(E + F)}{\alpha K \sigma^3}$$

or

$$A \left[ ZqI_1 + EI_0 + F \right] = \frac{bR^4(E + F)}{\alpha K \sigma^3}, \quad Z = K/R$$

such that

$$\Delta T^* = \frac{bR^4}{\alpha K \sigma^3} \left[ \frac{I_0 q(y)(E + F)}{ZqI_1(q) + EI_0(q) + F} - 1 \right]$$

Now let  $B = \frac{bR^4}{\alpha K}$ . Also realize that we seek only

$$D(\tau) = \frac{\partial \Delta T(0, \tau)}{\partial \tau}$$

so that

$$D^*(\sigma) = \sigma \Delta T^*(0, \sigma)$$

Thus,

$$D^*(\sigma) = \frac{B}{\sigma^2} \left[ \frac{E + F}{ZqI_1 + EI_0 + F} - 1 \right]$$

and again, we are only interested in

$$D_\infty(\tau) = \lim_{\tau \rightarrow \infty} \frac{d\Delta T(0, \tau)}{d\tau}$$

which is given by the sum of residues of

$$e^{\sigma\tau} D^*(\sigma) \text{ at } \sigma = 0:$$

Applying the double pole formula, we have

$$\begin{aligned} D_\infty(\tau) &= B \left[ \lim_{q \rightarrow 0} (E + F) e^{\sigma\tau} (ZqI_1 + EI_0 + F)^{-1} + \lim_{q \rightarrow 0} (E + F) e^{\sigma\tau} \frac{d}{d\sigma} (ZqI_1 \right. \\ &\quad \left. + EI_0 + F)^{-1} \right] \\ &= B \left[ \frac{(E + F)\tau}{(E + F)} e^{-\tau} + \lim_{q \rightarrow 0} \frac{-(E + F)}{2q} (ZqI_0 + EI_1)(ZqI_1 + EI_0 + F)^{-2} e^{\sigma\tau} \right] \end{aligned}$$

$$= -B(E + F) \left[ \frac{Z}{2(E + F)^2} + \frac{E}{4(E + F)^2} \right]$$

$$= \frac{-bR^2}{\alpha K(E + F)} \left[ \frac{Z}{2} + \frac{E}{4} \right]$$

In real time,  $t$ ,

$$D_{\infty} = \frac{-bR^2}{K(E + F)} \left[ \frac{Z}{2} + \frac{E}{4} \right]$$

It is possible to show that the above result implies that  $|D_{N_{\infty}}| < |b_N|$  for any  $M$  in (A3.1) greater than zero. First, we define  $D_{N_{\infty}}$  to be

$$D_{N_{\infty}} = \frac{D_{\infty}(t)}{T_0(0) - 0} = \frac{bR^2}{K(E + F) T_0(0)} \left[ \frac{K}{2R} + \frac{E}{4} \right]$$

Now  $T_0(0)$  is given by

$$T_0(0) = \frac{Q_0 R^2}{4K} + \frac{-y^2 + \sqrt{y^2 - 4xz}}{zx}$$

where

$$x = M$$

$$y = L + \frac{M}{8} \left( \frac{QR^2}{4K} \right)$$

$$z = Q_0 R/2$$

Now suppose  $M$  is barely significant, such that  $y^2 \gg 4xz$ , and the radical can be approximated as

$$\sqrt{y^2 - 4xz} = y - \frac{1}{2} \frac{4xz}{y}$$

Then  $T_0(0)$  is given by

$$T_0 = \frac{Q_0 R^2}{4K} + \left[ \frac{-y + y \frac{-1}{2} \frac{4xz}{y}}{2x} \right] = \frac{-z}{y} + \frac{Q_0 R^2}{4K}$$

or

$$T_0 = Q_0 \left[ \frac{R^2}{4K} + \frac{R}{2} \left[ L + \frac{MQR^2}{8K} \right]^{-1} \right]$$

So that

$$D_{N_\infty} = b_N \left[ \frac{\frac{R^2}{4K} \left( \frac{E}{E+F} \right) + \frac{R}{2} \left[ \frac{1}{E+F} \right]}{\frac{R^2}{4K} + \frac{R}{2} \left[ L + \frac{MQR^2}{8K} \right]^{-1}} \right]$$

Now the two terms of the numerator are both *separately* less than the corresponding terms of the denominator, such that the whole fraction is less than 1.0:

$$1 < \frac{E}{E+F} \text{ for } M > 0$$

and

$$(E+F)^{-1} < \left[ L + \frac{MQR^2}{8K} \right]^{-1}$$

if

$$E+F > L + \frac{MQR^2}{8K}$$

But

$$E + F = L + \frac{M}{2} \left[ 3T_0(R) + T_0(0) \right] > \frac{MQR^2}{8K} + L$$

for  $M > 0$ , since

$$3T_0(R) + T_0(0) > \left[ \frac{QR^2}{4K} = T_0(0) - T_0(R) \right],$$

since

$$4T_0(R) > 0.$$

Therefore,  $|D_{N_\infty}| < b_N$

For larger  $M$ , the discrepancy in the terms becomes even larger, and the fraction even smaller.

This confirms the trend that the steeper the negative slope of  $R$  vs.  $P$ , the smaller the temperature/power slope ratio.

#### Numerical Example

Consider a fuel rod with solid pellets of radius 0.00534 m, operating at  $3.0 \times 10^4$  W/m, such that  $Q = 3.35 \times 10^8$  W/m<sup>3</sup>. Let the conductivity  $K$  be fixed at 3.0 W/m and the fuel surface-to-coolant conductance to be given by

$$H = -2.8 \times 10^4 + 50 \bar{T}, \text{ W/m}^2\text{°C}$$

so " $L$ " =  $-2.8 \times 10^4$  and  $M = 50$ . Solving the quadratic for initial fuel surface temperature, we have  $T_s = 237.3^\circ\text{C}$ , and hence  $T_0(0) = 1033.3^\circ\text{C}$ . From this,

$\bar{T} = 635.3^{\circ}\text{C}$ , and  $H = 3.766 \times 10^4$ . The constants E and F are  $0.96975 \times 10^4$  and  $0.5932 \times 10^4$ , respectively. Thus, for  $b_N = 0.5\%/sec$ , we have  $b = -1.675 \times 10^6$   $\text{W/m}^3\text{-sec}$  and

$$D_{\infty} = \frac{1.675 \times 10^6 \times (0.00534)^2}{3 \times (0.96975 + 0.5932) \times 10^4} \left[ \frac{3}{(0.00534)^2} + \frac{0.96975 \times 10^4}{4} \right]$$

$$= 2.76^{\circ}\text{C/sec}$$

$$\frac{\partial T_{N_{\infty}}}{\partial t} = \frac{2.76}{1033} = 0.267\%/sec$$

$$\text{Slope ratio} = \frac{0.267}{0.50} = \underline{0.533}$$

A more exact numerical calculation of the sort described in Appendix B resulted in a slope ratio of 0.51.

#### A4.0 APPLICATION OF THE CORRELATION TO DETECTING ERRORS IN POWER AND TEMPERATURE ESTIMATES

To the degree that one can divine the split in resistance between fuel and conductance from R-P plots, and to the degree that one can obtain quasi-steady-state linear data from reactor power decreases, one should be able to predict the temperature/power slope ratios. If these estimates begin to vary from the data to a statistically significant degree, and if one has enough prior experience with the particular rod to believe the calculational procedures are adequate, then errors in the steady-state power or temperature estimates may well be suspected. The reason the temperature/power slope ratio may be useful in detecting and quantifying such errors is given in the following paragraph.

Those slope ratios are the ratios of variation of *normalized relative values* with respect to time. They depend on the *small* change of temperature in response to a *small* change in power. However, the normalization factors are the *absolute* values of power and temperature. But if the absolute values are in error, the observed relative changes, normalized to those erroneous values) will certainly not match predictions for the normalized response.

More work has yet to be done in refining R-P plots, and tracing the propagation of uncertainties in data and models as one goes from an R-P data plot through a code like GAPCON-3 to a slope ratio prediction. Only then can the detection limits of power or temperature error be quantified. But it should be clear that the correlation of R-P plots with temperature/power slope ratios holds the promise of defining error limits.

In particular, consider the problem of thermocouple decalibration. The transmutation formation of osmium in tungsten-rhenium thermocouples certainly will affect the translation of millivolts into temperature. This translation is currently done on the basis of standard curves, such as in Figure A-4. Irradiation might be expected to make a *nonuniform* shift in such a curve. In that case, it should be clear that the relative and absolute predictions of temperature will not be the same as for the unshifted (now erroneous) curve. So the use of the unshifted curve will result in erroneous absolute temperatures, and this may be detectable by the methods just outlined.

Similarly, drifts in neutron detector readings at constant flux (and the inevitable drift in flux to power ratio due to fuel depletion) may be better quantified by the methods outlined in this report.

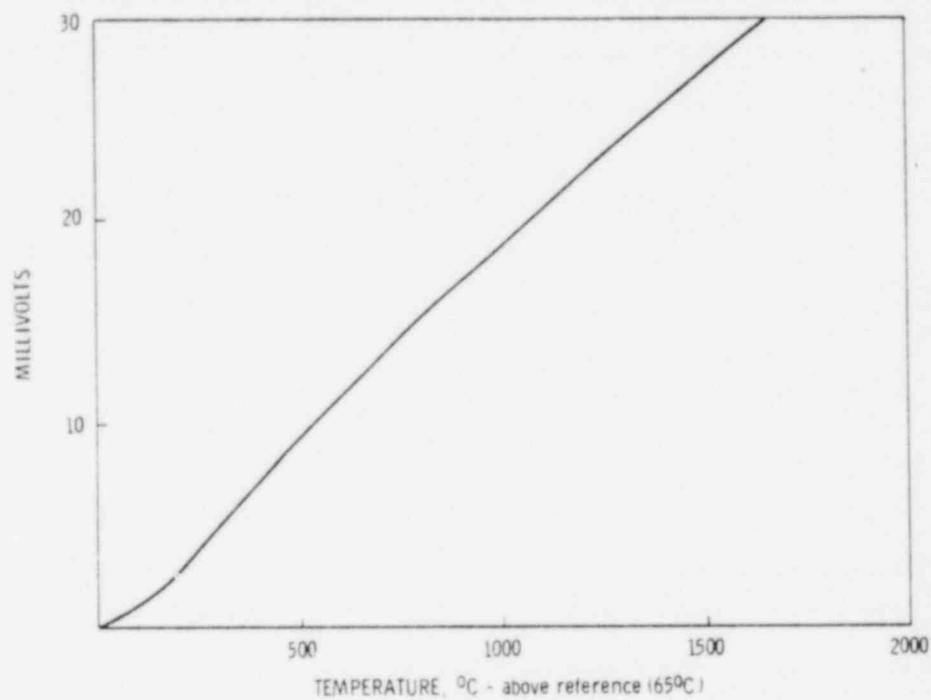


FIGURE A-4. Calibration Curve for a W-26% Re/W-5% Re Thermocouple

## APPENDIX B

### CALCULATIONAL PROCEDURES FOR PRODUCING TEMPERATURE/POWER SLOPE ESTIMATES FROM CALCULATED R-P CURVES

In the main report, calculated curves of resistance versus power are compared to steady-state data (R-P curves). Corresponding quasi-steady-state temperature/power slope ratios were also calculated, and compared to time-varying thermocouple data at comparable burnup. Conclusions were drawn on the fission gas content and fuel relocation and conductivity, based on both comparisons.

In this appendix, we outline the procedure by which the expected temperature/power slope ratios were derived from the calculations for the R-P curves.

#### GENERAL PROCEDURE

The tool used to calculate the transient temperatures was MWRAM, a modification of subroutine DDLR from GAPCON-3. This subroutine is described in the next section; it applies the collocation technique to solve the nonlinear radial transient heat transfer equations.

The steps taken to obtain calculated temperature/power slopes are the following:

1. Input between GAPCON-3 and MWRAM is matched, to produce initial conditions which are matched. This input includes such things as geometry enrichment, coolant temperature and converged gap conductance.
2. The same GAPCON-3 run used to make the R-P plot is used to develop a linear fit of gap gas conductivity,  $K_{\text{gas}}$  on gap temperature and a linear fit of effective gap size,  $d_{\text{gap}}$  (including temperature jump distance), on fuel volume average temperature.
3. During the successive steps of the transient, the gap conductance is given by

$$h_{\text{gap}} = \frac{k_{\text{gas}}}{d_{\text{gap}}} + h_{\text{rad}}$$

where  $h_{\text{rad}}$  is a standard calculation of radiation heat transfer, and for the cases of interest never exceeds 5% of the total conductance. For each time step,  $h_{\text{gap}}$  was evaluated using the temperatures from the previous time step.

4. The power history is input as interpolation between the normalized cobalt detector signals given once every 1 to 3 seconds during the 20% power decrease.
5. As with the temperature and power data, the quasi-steady-state slope of the normalized calculated temperatures is taken as the least-squares fit through the most linear variation with time.<sup>(a)</sup>

The reason for taking the above procedure, as opposed to running GAPCON-3 itself, is one of economics. The MWRAM run takes an execution time factor of 30 less on the CDC 6600 computer, and produces answers nearly identical to a full GAPCON-3 run.

#### THE SOLUTION ROUTINE MWRAM

In Appendix A, where we sought to present analytical solutions for the nonlinear behavior of the fuel rod, a considerable number of approximations had to be made in order to arrive at a form of the radial heat transfer equation and its boundary conditions which we could solve. In the computer solution, most of these approximations need not be made.

Solutions for both the steady-state and transient equations, based on the collocation technique of the method of weighted residuals (MWR) was formulated for GAPCON-3. The specific steps are a slight variation of that proposed by B. A. Finlayson.<sup>(11)</sup> The details of the formulation are found in the GAPCON-3

---

(a) The extent of this range is judged by visual inspection of plots of normalized data vs. time. By choosing the same range for both the data and calculated values, we seek to minimize whatever bias may be introduced.

code description,<sup>(1)</sup> which the reader may consult. In brief, the appropriate heat transfer equations for the fuel and cladding are forced to be satisfied at specific points. That condition, plus the boundary conditions generate a number of simultaneous equations which can be solved for unknown coefficients of the trial functions,

$$T_f = \sum_{j=1} d_j r^{j-1} \text{ for the fuel}$$

$$T_c = \sum_{j=1} c_j r^{j-1} \text{ for the cladding}$$

A small number of evaluation points (called "collocation" points) is sufficient to generate very accurate approximations to the nonlinear, coupled transient and steady-state radial heat transfer equations for fuel and cladding. The coupling occurs in the gap condition, and is temperature dependent, since the gap conductance is temperature dependent.

In steady-state, GAPCON-3 does "gap conductance iterations" to account for the temperature-dependent feedback between temperatures and gap conductance, that occurs because of fuel and cladding thermal expansion. Each iteration implies a solution of the coupled equations, for the current estimate of gap conductance. The converged temperature distribution and gap conductance from the GAPCON run are taken as the initial conditions for the MWRAM transient calculation.

In transient operation, GAPCON-3 and MWRAM both evaluate the gap conductance in the current time step based on the temperatures from the previous time step. Thus, in order to follow the nonlinear and path-dependent temperature response, the time steps have to be kept small relative to the time span of, say, 5% relative change in power.<sup>(a)</sup> The dependence of gap conductance on temperature is fed to MWRAM from GAPCON runs, as described. The power

---

(a) For the transients we are examining, it has been found that time steps of 0.1 seconds are definitely small enough. This has been concluded by testing the routine against idealized situations for which analytical solutions exist.

history is interpolated between 1 to 3 second normalized cobalt detector data points, and the calculated temperatures are normalized and plotted.

The effects of flux depression, central (thermocouple) hole, temperature dependence of cladding and fuel thermal properties, and energy storage in the cladding are all included in the MWRAM solution. Also included are the effects of temperature dependent gap conductance (as noted) and power-dependent film coefficient (Jens-Lottes correlation). It has been concluded from prior experience in the GAPCON-3 verification that for smooth variations of the thermal properties, the calculated temperatures are accurate within 5°C.

This is considerably closer than the fuel temperatures can be measured in-reactor, and much less than the calculational uncertainties due to uncertainties in the thermal properties and gap conductance models. Thus, we feel the solution routine itself (divorced from models) is adequate.

## REFERENCES

1. D. D. Lanning, F. E. Panisko, C. L. Mohr and K. B. Stewart, GAPCON-THERMAL-3 Code Description, PNL-2434, 1978.
2. C. R. Hann, D. D. Lanning, R. K. Marshall, A. R. Olsen and R. E. Williford, A Method for Determining the Uncertainty of Gap Conductance Deduced from Measured Centerline Temperatures, BNWL-2901, 1977.
3. M. F. Lyons et al., UO<sub>2</sub> Pellet Thermal Conductivity from Irradiation with Central Melting, GEAP-4624, 1964.
4. C. R. Hann, E. R. Bradley, M. E. Cunningham, D. D. Lanning, R. K. Marshall, R. E. Williford, Data Report for the NRC/PNL Halden Assembly IFA-432, PNL-2673, 1978.
5. C. R. Hann et al., Test Design, Precharacterization and Fuel Assembly Fabrication for Instrumented Fuel Assemblies IFA-431 and IFA-432, NUREG/CR-0332 BNWL-1988, 1978.
6. R. E. Williford and C. R. Hann, Effects of Fill Gas Composition and Pellet Eccentricity, BNWL-2585, 1977.
7. S. Glasstone and A. Sesonske, Nuclear Reactor Engineering, pp. 358-359, D. Van Nostrand and Co., Princeton, NJ, 1967.
8. G. E. Myers, Analytical Methods in Conduction Heat Transfer, McGraw Hill Co., New York, NY, 1971.
9. A. V. Liukov, Analytical Heat Diffusion Theory, Academic Press, New York, NY, 1968.
10. J. F. Kerrisk and D. G. Clifton, "Smoothed Values of the Enthalpy and Heat Capacity of UO<sub>2</sub>," Nuclear Technology, Volume 16, 1972.
11. B. Finlayson, The Method of Weighted Residuals and Variational Principles, Academic Press, New York, NY, 1972.

DISTRIBUTION

No. of  
Copies

No. of  
Copies

OFFSITE

10	Chief, Fuel Behavior Research Branch Division of Reactor Safety Research U.S. Nuclear Regulatory Commission Washington, D.C. 20555		J. T. A. Roberts Electric Power Research Institute 3412 Hillview Avenue Palo Alto, CA 94304
	Librarian, Technical Lib. Argonne National Laboratory 9700 South Cass Avenue Argonne, IL 60439		Manager Fuel Technology Exxon Nuclear Company, Inc. 2955 George Washington Way Richland, WA 99352
	Manager, Product Developmt. Division Babcock & Wilcox Company P.O. Box 1260 Lynchburg, VA 24505		Manager Program Development & Evaluation Thermal Fuel Behavior Div. EG&G Idaho, Inc. P.O. Box 1625 Idaho Falls, ID 83401
	R. Duncan Vice-President - Developmt. Nuclear Power Systems Combustion Engineering, Inc. P.O. Box 500 Windsor, CT 06095		Director Nuclear Safety & Anal. Development Electric Power Research Institute 3412 Hillview Avenue Palo Alto, CA 94304
	Manager Code Veriication & Appl. Br. EG&G Idaho, Inc. P.O. Box 1625 Idaho Falls, ID 83401		Manager Reactor Systems Safety Development General Electric Company 175 Curtner Avenue San Jose, CA 95125
2	DOE Technical Information Center		
	A. A. Churm DOE Patent Division 9800 S. Cass Ave. Argonne, IL 60439	25	NTIS

No. of  
Copies

No. of  
Copies

OFFSITE

ONSITE

	Joel R. Buchanan Assistant Director Nuclear Safety Information Center P.O. Box Y Oak Ridge, TN 37830	35	<u>Pacific Northwest Laboratory</u> B. O. Barnes J. O. Barner E. R. Bradley E. L. Courtright M. E. Cunningham R. L. Goodman R. J. Guenther C. M. Hagen C. R. Hann K. A. Hsieh D. D. Lanning (10) R. K. Marshall R. P. Marshall C. L. Mohr C. Neally F. E. Panisko S. R. Wagoner R. E. Williford C. L. Wilson Tech. Info. Files (5) Publishing Coordination (2)
40	NRC Safety Research Exchange ORNL Laboratory Records Nuclear Safety Information Ctr. P.O. Box X, Bldg. 4500 Oak Ridge, TN 37830  Executive Director ACRS US NRC H1016 Washington, D.C. 20555  Robert Ritzmann Science Applications, Inc. 2680 Hanover Street Palo Alto, CA 94303		
40	Adm. Dist. Serv. Branch - Shelf US NRC Washington, D.C. 20555  Engineering Manager Nuclear Fuel Division Westinghouse Electric Corp. P.O. Box 355 Pittsburgh, PA 15230  Branch Chief NRC Core Performance Branch US NRC P-1114 Washington, D.C. 20555		